35

NOLTR 67-178

AD669447

MEDIUM STRAIN RATE, COMPRESSION TESTING OF SELECTED PLASTIC MATERIALS

23 DECEMBER 1967

NOL

UNITED STATES NAVAL ORDNANCE LABORATORY, WHITE OAK, MARYLAND

NOLTR 67-178

DDC
RECEIVED
MAY 24 1968
C

Distribution of this document is unlimited.

105

DISCLAIMER NOTICE

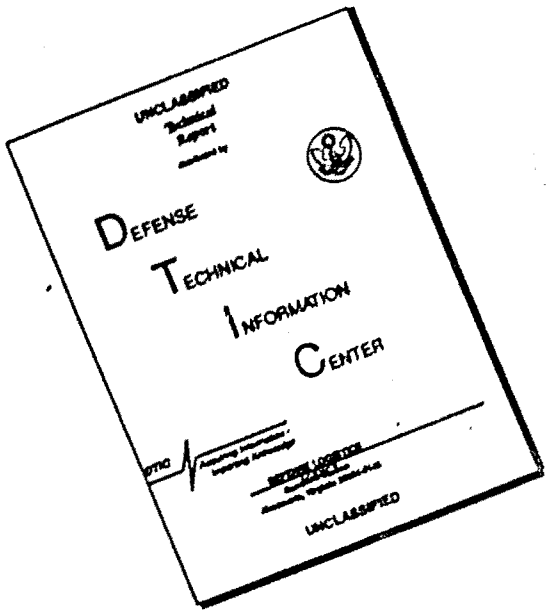

THIS DOCUMENT IS BEST QUALITY AVAILABLE. THE COPY FURNISHED TO DTIC CONTAINED A SIGNIFICANT NUMBER OF PAGES WHICH DO NOT REPRODUCE LEGIBLY.

MEDIUM STRAIN RATE, COMPRESSION TESTING OF SELECTED PLASTIC MATERIALS

Prepared by:
William M. Hinckley and Frederick P. Stecher

ABSTRACT: Stress-strain relations have been obtained in compression at medium strain rates for selected plastic materials suitable for shock mitigation. Data have been acquired at room temperature, and at 200° F and 350° F for those materials capable of withstanding the elevated temperatures. Rates of strain between 0.004 in/in/sec and 60 in/in/sec have been obtained using a conventional high-speed testing machine. Most of the materials investigated have exhibited strain rate sensitivity over the range tested.

U. S. NAVAL ORDNANCE LABORATORY
WHITE OAK, MARYLAND

NOLTR 67-178 23 December 1967

MEDIUM STRAIN RATE, COMPRESSION TESTING OF SELECTED PLASTIC MATERIALS

This report is part of the continuing effort of the U. S. Naval Ordnance Laboratory in the determination of dynamic properties of materials.

The authors wish to express their appreciation to the many individuals who assisted in this undertaking, especially Mrs. Louise Brown for her able assistance in the reduction of data.

E. F. SCHREITER
Captain, USN
Commander

A. E. Seigel
A. E. SEIGEL
By direction

CONTENTS

ILLUSTRATIONS

INTRODUCTION

The purpose of this report is to bridge the gap between the "static" and the "dynamic" stress-strain data presented in reference 1. These data are for compression tests at room temperature. The scope of the data in this report has been expanded to include compression results at elevated temperatures. Data at 200° F and 350° F are presented for those materials which maintained rigidity.

EXPERIMENTAL APPARATUS

The tests were performed with a high-speed testing machine - a modified Plastechon Model 581 shown in figure 1. A high-pressure gas source activated the driver while a hydraulic system provided the speed control. A schematic of the machine hardware is shown in figure 2. Gas was supplied to the high-pressure section at constant pressure forcing the driving piston down. The piston in turn forced the oil through the hydraulic system into the accumulator. The restriction of the oil flow through the variable orifices provided the control for the flow rate and, hence, the crosshead velocity. The oil was precompressed before each test by applying the gas pressure to the system while blocking the flow of oil with the solenoid valve. This valve was then rapidly opened to start the test. A slack adapter was coupled between the compression cage and the crosshead to allow the crosshead to accelerate to a constant velocity before engaging the specimen.

As delivered, this machine was equipped with a Schavitz-Bytrex Model PL 2500 load cell for sensing the applied load and a slide wire potentiometer for sensing the crosshead displacement. The voltage outputs from these two transducers were simultaneously fed to a Tektronix Type 502A dual beam oscilloscope. The horizontal sweep was disconnected and the upper beam amplifier was switched to serve as the horizontal deflection drive for the lower beam. With the load cell output displayed on the vertical axis and the potentiometer output displayed on the horizontal axis, a load versus displacement plot was presented directly on the face of the oscilloscope. The trace was photographically recorded with a Polaroid camera. A Hewlett-Packard oscillator was connected to the z-axis of the oscilloscope to modulate the beam intensity by chopping the beam at a known frequency. The load-displacement curve was presented as a series of dots. The strain rate was then determined by counting the dots and working out the appropriate mathematics using the corresponding displacement, the original specimen length, and the chopping frequency of the oscillator. The curve represented by the dots was not distinct in regions of rapidly changing the load. Thus, this technique of data display was abandoned in favor of simple load-time and displacement-time records.

Further investigation of the recording technique revealed that crosshead displacement was not a good representation of specimen deformation. Machine stretch was introducing considerable error. An attempt was made to compensate for this stretch in the data reduction but it was felt to be unreliable. An Optron Model 680AX electro-optical extensometer was then installed to measure deformation. Basically, it consisted of two optical trackers which followed the movements of color contrasted targets and converted their movements to corresponding voltage outputs. When used as a pair, the differential output was proportional to the relative motion of the two targets. The targets were attached to the upper and lower plates of the compression cage (fig. 3) immediately adjacent to the specimen. Machine stretch was eliminated from the measurement. Only the deflection of the plates needed to be considered, and a calculation showed this to be negligible.

A lightweight compression cage was designed to replace the massive steel one provided by the manufacturer. The cage consisted of a capped cylinder (fig. 3) with a piston inside. The specimen was compressed between the piston and the capped end. This design afforded an improvement in maintaining parallelism between the test faces. Ball joints were installed on both ends to prevent binding of the sliding surfaces of the cage due to machine misalignment.

A thermal isolator (fig. 4) was required to protect the load cell when working at the elevated temperatures since the manufacturer only claimed temperature compensation up to 115° F. The isolator consisted of a tube placed between the compression cage and the load cell. A flow of water was run continuously through the tube to remove the heat being conducted to the cell.

The high-speed capability of the machine could not be used to full advantage. The natural frequency of the load cell system was so low as to reduce the effective use of the machine to a speed of 50 in/sec. A natural frequency of 292 Hertz was calculated by using a spring mass approximation as shown in Appendix A. A natural frequency of 475 Hertz was determined experimentally.

EXPERIMENTAL TECHNIQUE

The experimental objective was to test each material at three rates of strain, an order of magnitude apart. Since the testing machine was not servo-controlled, the piston velocity was influenced by the varying load carrying capability of the deforming specimen. Nonuniform rates of strain resulted. Usually, an abrupt change in speed was observed when the material yielded giving rise to two distinct rates. This abrupt change in rate is illustrated in picture a. The rubbers and weaker polymers were not so affected, as shown in picture b, because the loads involved were not great enough to tax the capability of the machine.

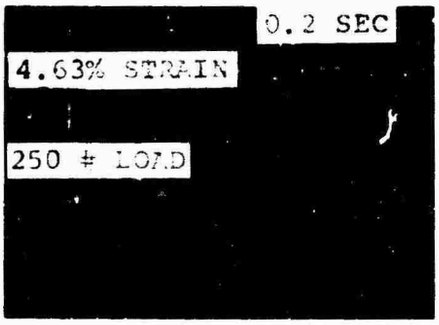

a. Data Showing Abrupt Change in Strain Rate

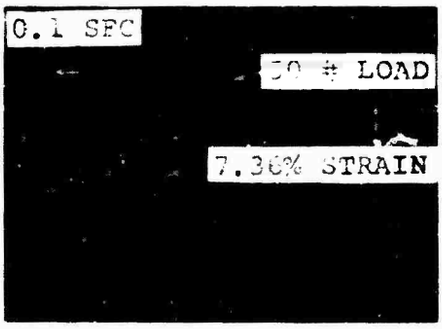

b. Data Showing Constant Strain Rate

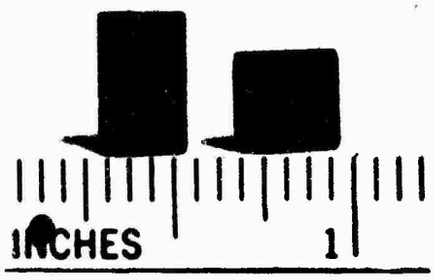

c. Typical Specimen Before and After Test

The limited load capacity (1,000 lbs) of the modified testing machine necessitated the use of small cylindrical specimens (0.5-inch diameter for the rubbers and 0.25-inch diameter for the polymers). To avoid buckling and distortion of the specimen, the length to diameter ratio was held between 1.0 and 1.5. Lubricants were applied to the ends of the specimens to enhance radial slippage at the faces and thereby eliminate or reduce the bulging of the specimens. This lubrication was effective and no significant bulging was encountered at strains of less than 25 percent. A typical test specimen is shown in picture c before and after loading.

MATERIALS TESTED

The majority of the materials tested are the same shock mitigating materials as presented in reference 1. A few materials were eliminated due to unavailability and several comparable new ones were added. The high-pressure molded thermosetting compounds were eliminated due to brittleness. The four remaining material categories are:

I - Casting Resins - Thermally Stable

II - Rubber Compositions

III - High-Pressure Molded Thermoplastics

IV - Casting Resins

A list of the materials tested is given in Table 1. The compositions, suppliers, and specific gravities of the new materials are given in Table 2. For the other materials, these details are given in reference 1.

DATA ANALYSIS

Stress is defined as the "engineering stress"; that is, the ratio of the axial load to the original area of the cross section. The strain is the axial strain associated with the engineering stress and is defined as the ratio of the axial deformation to the original gage length of the test specimen. Strain rate is defined as the change in strain per unit time. These definitions were used in reducing the experimental observables, load and deformation, to final values of stress and strain.

To actually convert the experimental observables to stress and strain, the load-time and deformation-time records were read on a Universal Telereader Type 17A. Pairs of points were read at various instants of time and automatically punched on computer cards. A data reduction computer code was used to convert these values to stress and strain and generate a tape for plotting on a Calcomp plotter.

Error in the stress-strain results was encountered from instrumentation and data reduction. The instrumentation included a load cell transducer, an electro-optical extensometer, a dual beam oscilloscope with camera, and a strain gage type temperature sensor with Wheatstone bridge circuitry. The data reduction involved the optical reading of the oscilloscope traces, conversion of these readings to stress, strain, and strain rate through use of a computer code, and final plotting of the results.

The instrumentation was statically calibrated prior to testing. The load cell electronic circuitry incorporated two calibration resistors to simulate various loadings. Once these resistors were set to match the output of the load cell, they were used to calibrate the oscilloscope each day. These resistors were adjusted to simulate 500 and 1,000-pound loads. A dead weight of 13.4 pounds was then hung from the load cell to check the calibration at the low loads. The manufacturer quoted the electro-optical extensometer as having a resolution of 0.025 percent of full scale and a linearity better than 1 percent over a range from 0 to 0.2-inch deformation. The deformation of the specimens was well within this range. The oscilloscope manufacturer quoted that device as having a vertical deflection system accurate within 3 percent and a horizontal deflection system typically accurate within 1 percent and, in all cases, accurate within 3 percent of full scale. The error due to the distortion of the photograph taken with the oscilloscope camera was determined to be 3 percent.

Optical reading error was introduced with the telereader. This error was less than 1 percent. The numerical calculations were performed on an IBM 7090 computer and the plotting was done on a Calcomp plotter. The computer and the plotter introduced negligible errors.

The cumulative error of both the instrumentation and the data reduction was 8 percent for the stress-strain results and 10 percent for the strain rates.

TABLE 1

MATERIALS TESTED

	FIGURES
Category I - Casting Resins--Thermally Stable	
RDR-701+NMA	5
RDR-701+NMA+20% filler	6
RDR-70[illegible]+NMA+20% filler	7
DEN-438+NMA+20% filler	8
DEN-438+DADPS+20% filler	9
KOPOX 159+DADPS+20% filler	10
KOPOX 159+NMA+20% filler	11
KOPOX 997A+NMA+20% filler	12
ERLA-0400+MPDA+20% filler	13
Ironsides DP4-88S	14
Category II - Rubber Compositions	
WS-4863	15
WS-2822	16
UA-35	17
SC-620	18
PS-3	19
GRI-218	20
FM-1	21
Category III - High-Pressure Molded Thermoplastics	
Alathon-A7020	22
Tenite 265A-37200S	23
Cycolac T-1000	24
Delrin-500	25
Ethocel-Q303.4	26
Ethyl Cellulose	27
KEL-F	28
Lexan 101-112	29
Marlex-5005	30
Plexiglas VS	31
Polyethylene DYLT	32
Polypropylene 1014	33
PPO	34
Teflon-FEP100	35
Teflon-TFE	36
Category IV - Casting Resins	
Adiprene L-315	37
Conathane 2000	38
Scotchcast 221	39
Sylgard 187	40

TABLE 2

COMPOSITIONS AND PROPERTIES OF ADDITIONAL MATERIALS

III. HIGH-PRESSURE MOLDED THERMOPLASTICS

Material	Type	Supplier	Sp. Gr.
Delrin 500	Acetal	E. I. duPont	1.425
PPO	Polyphenylene Oxide	General Electric Co.	1.06

IV. CASTING RESINS

Material	Type	Supplier	Sp. Gr.	Cure
Conathane 2000	Polyurethane (unfilled)	Conap Corp.	1.05	6 hrs. at 60° C
Scotchcast 221	Polyurethane (unfilled)	3M Co.	1.06	12 hrs. at room temp.
Sylgard 187	Silicone	Dow Corning Corp.	1.12	15 mins at 300° F

The oven was equipped with a thermocouple for both temperature recording and automatic thermostatic control. But the air temperature was not representative of the specimen temperature. A Micro-Measurements STG-50 temperature sensor was mounted on the compression cage piston opposite the specimen (fig. 3). A test was made to determine the time necessary for a specimen to reach a steady state temperature. The temperature at the center of the specimen, which was measured with an iron constantan thermocouple, and at the top of the piston was monitored every minute for 30 minutes. The specimen and the piston reached steady state in 14 minutes for the 200° F test and 17 minutes for the 350° F test. The temperature at the center of the specimen was 6° F and 11° F higher than the piston temperature for the 200° F and 350° F tests, respectively. For all data presented, the temperature of the specimen was within 5 percent of the stated temperature.

DATA PRESENTATION

The plots of stress versus strain at various strain rates and temperatures are presented in figures 5 through 40. The strain rates are presented on each figure as a table with two columns of values. The columns are labeled $\dot{\epsilon}_E$ and $\dot{\epsilon}_P$. $\dot{\epsilon}_E$ and $\dot{\epsilon}_P$ refer to the average rate of straining in the elastic and plastic regions of the stress-strain curve, respectively. For some curves, only elastic strain rates are shown since plastic strain rates could not be determined. For each material, results are given for room temperature in the "a" figure, for 200° F in the "b" figure and for 350° F in the "c" figure.

Each stress-strain curve is the result of a single test. Figure 41 shows the variation in the stress-strain curves for a series of six tests of WS 2822 rubber at the same strain rate and temperature. The repeatability of these tests gives support to the assumption that the single test results are representative of the materials.

GENERAL OBSERVATIONS

Strain rate sensitivity has been noted in most of the materials tested. Increases in yield stress have been observed with increase in the rate of straining. Variations in the modulus of elasticity have also been observed. The accuracy of the modulus is of the order of 11 percent and could account for some of these variations. In general, the trend is for the elastic modulus to increase with increasing rate of straining. Many of these modulus increases are in excess of the amount attributable to the error.

Strain rate sensitivity is still prevalent at the elevated temperatures. Heating of the materials lowers the yield stress but for any given temperature an increase in strain rate will produce an increase in yield stress.

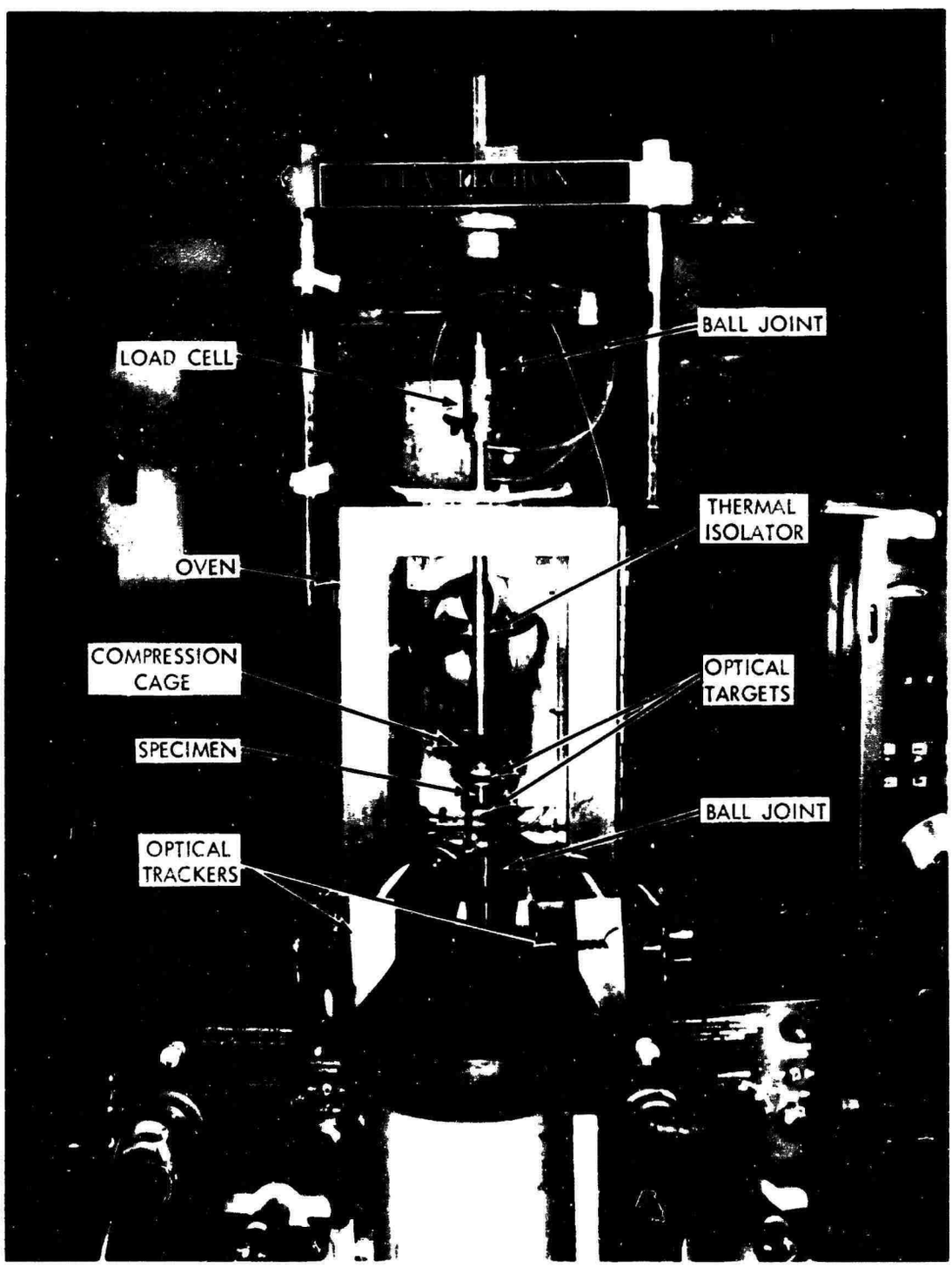

FIG. 1 HIGH-SPEED TESTING APPARATUS

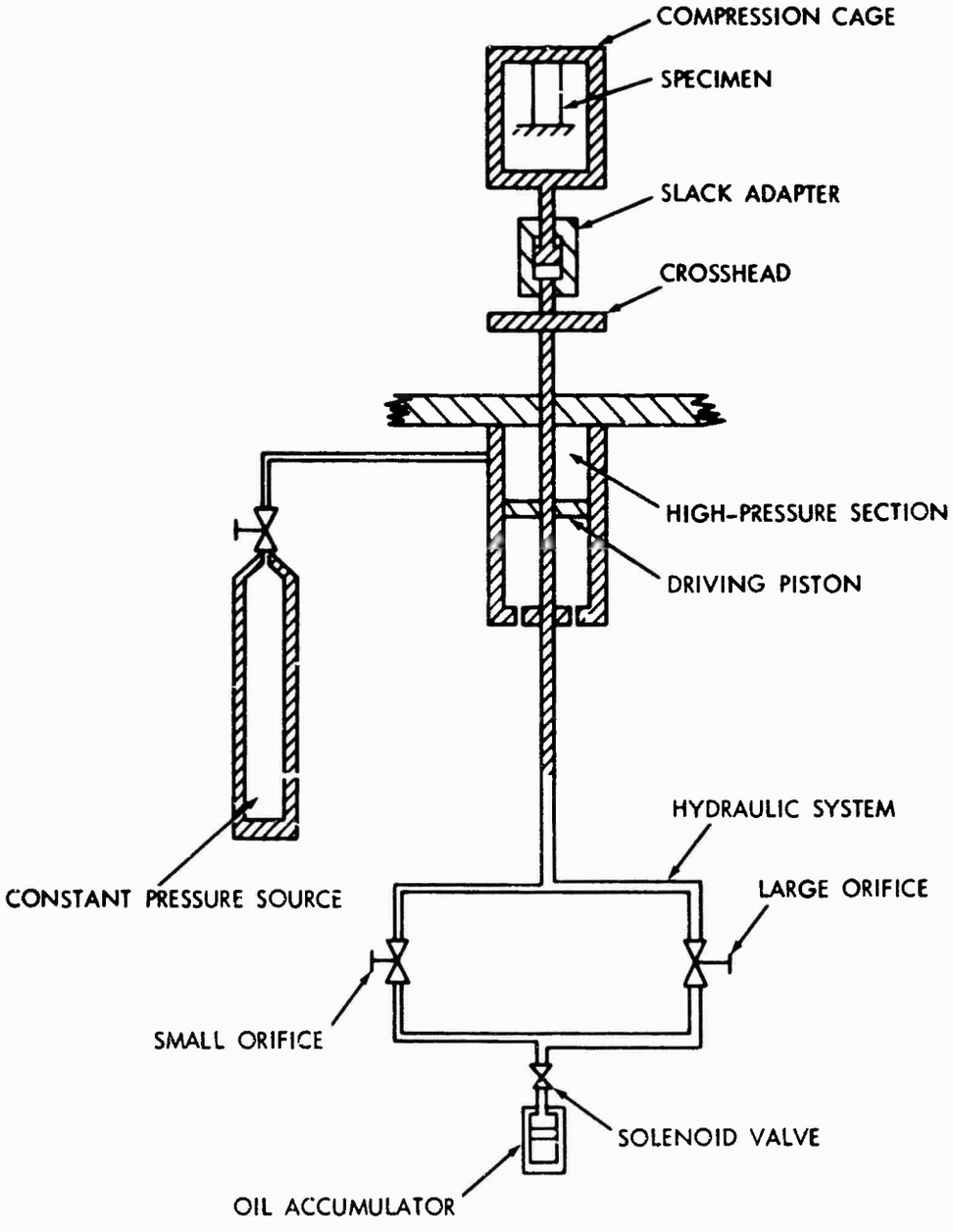

FIG. 2 SCHEMATIC DIAGRAM OF HIGH-SPEED TESTING APPARATUS

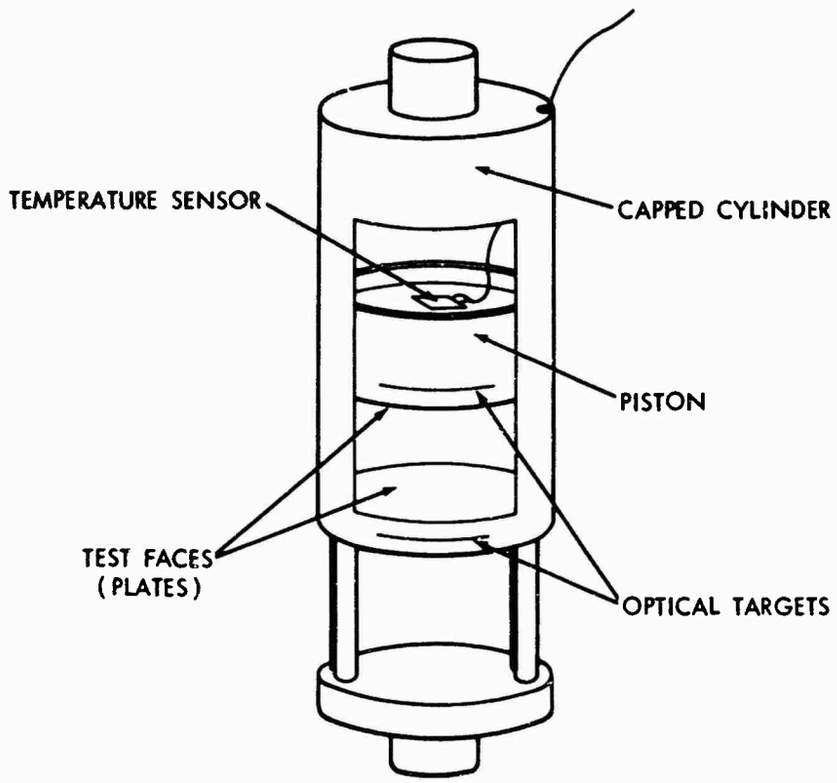

FIG. 3 LIGHTWEIGHT COMPRESSION CAGE

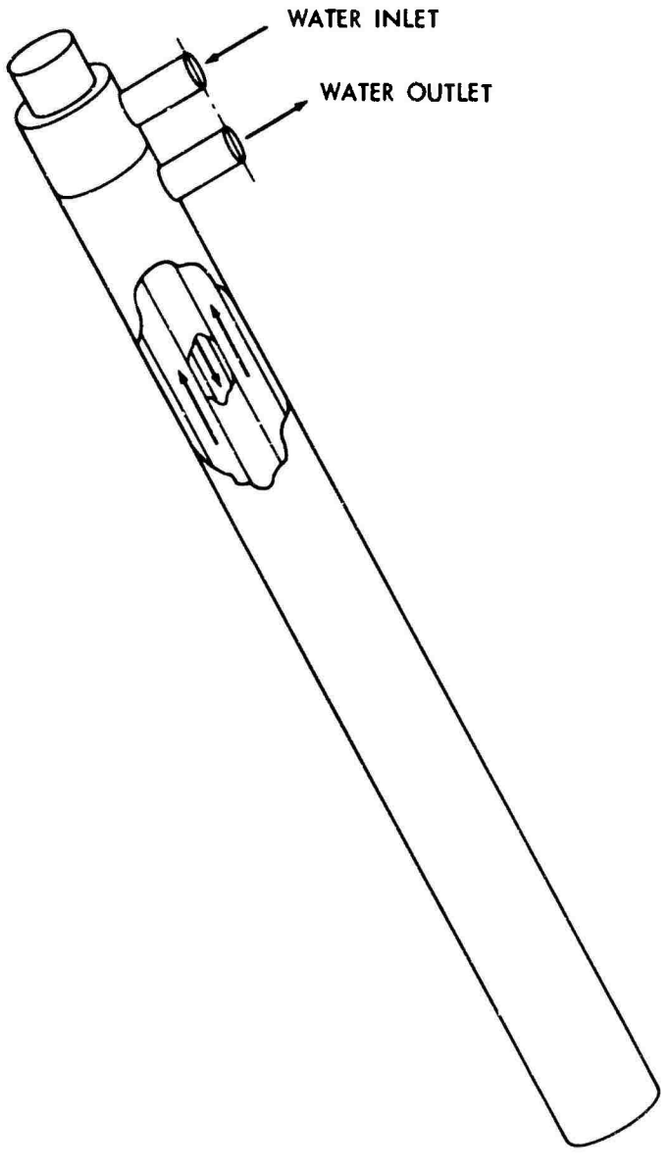

FIG. 4 THERMAL ISOLATION

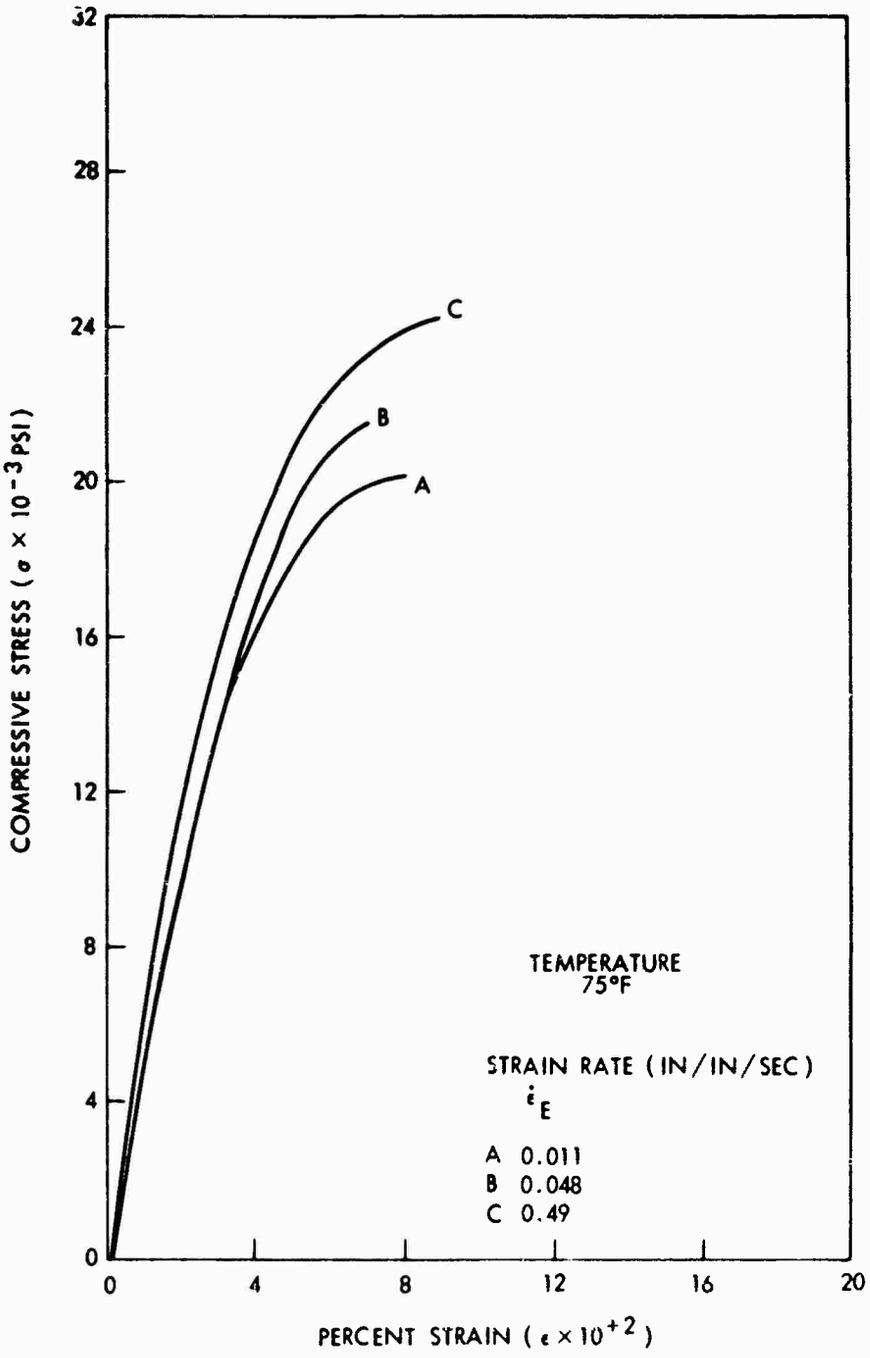

FIG. 5-a DYNAMIC STRESS-STRAIN RELATION OF RDR-701 + NMA

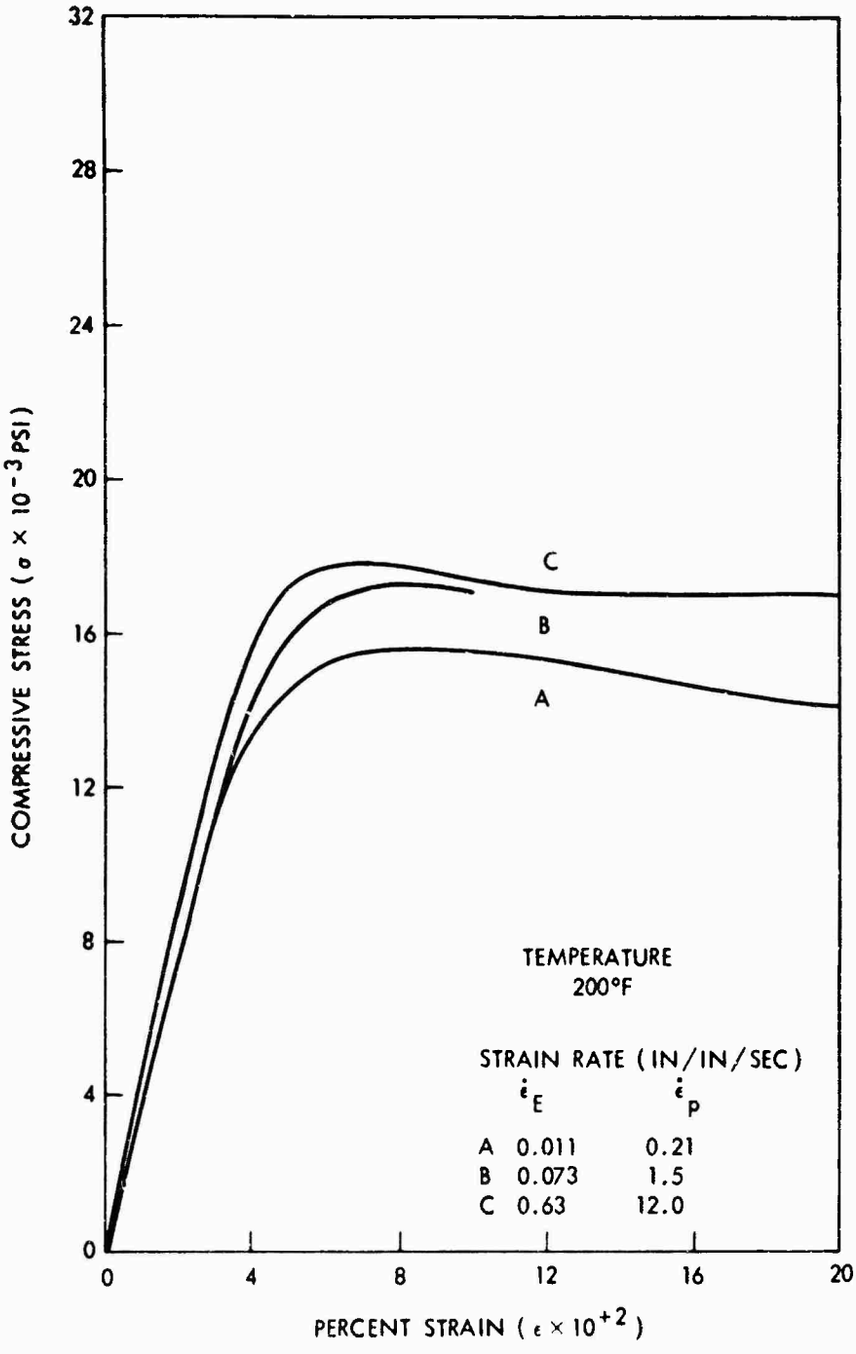

FIG. 5-b DYNAMIC STRESS-STRAIN RELATION OF RDR-701 + NMA

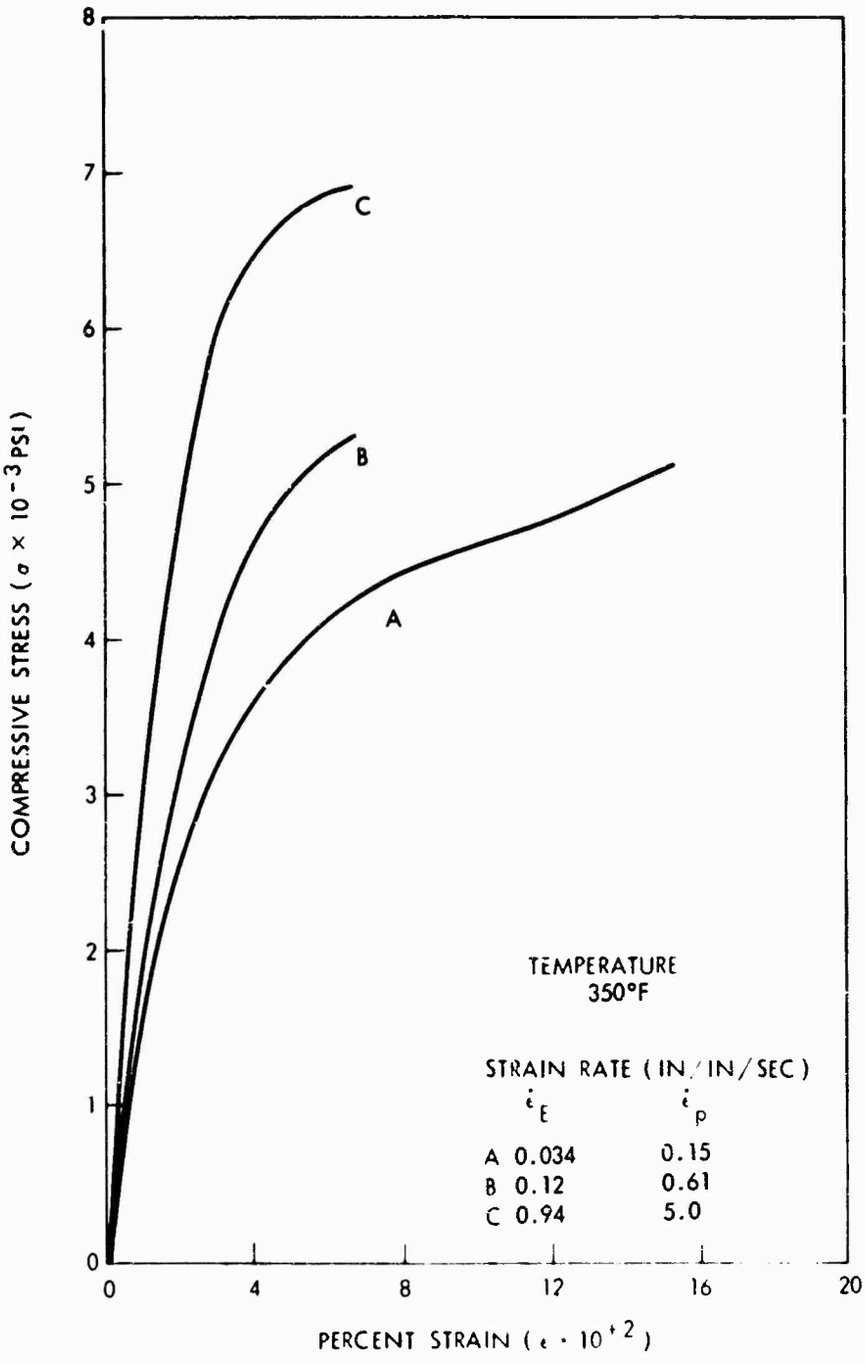

FIG. 5-c DYNAMIC STRESS-STRAIN RELATION OF RDR-701+ NMA

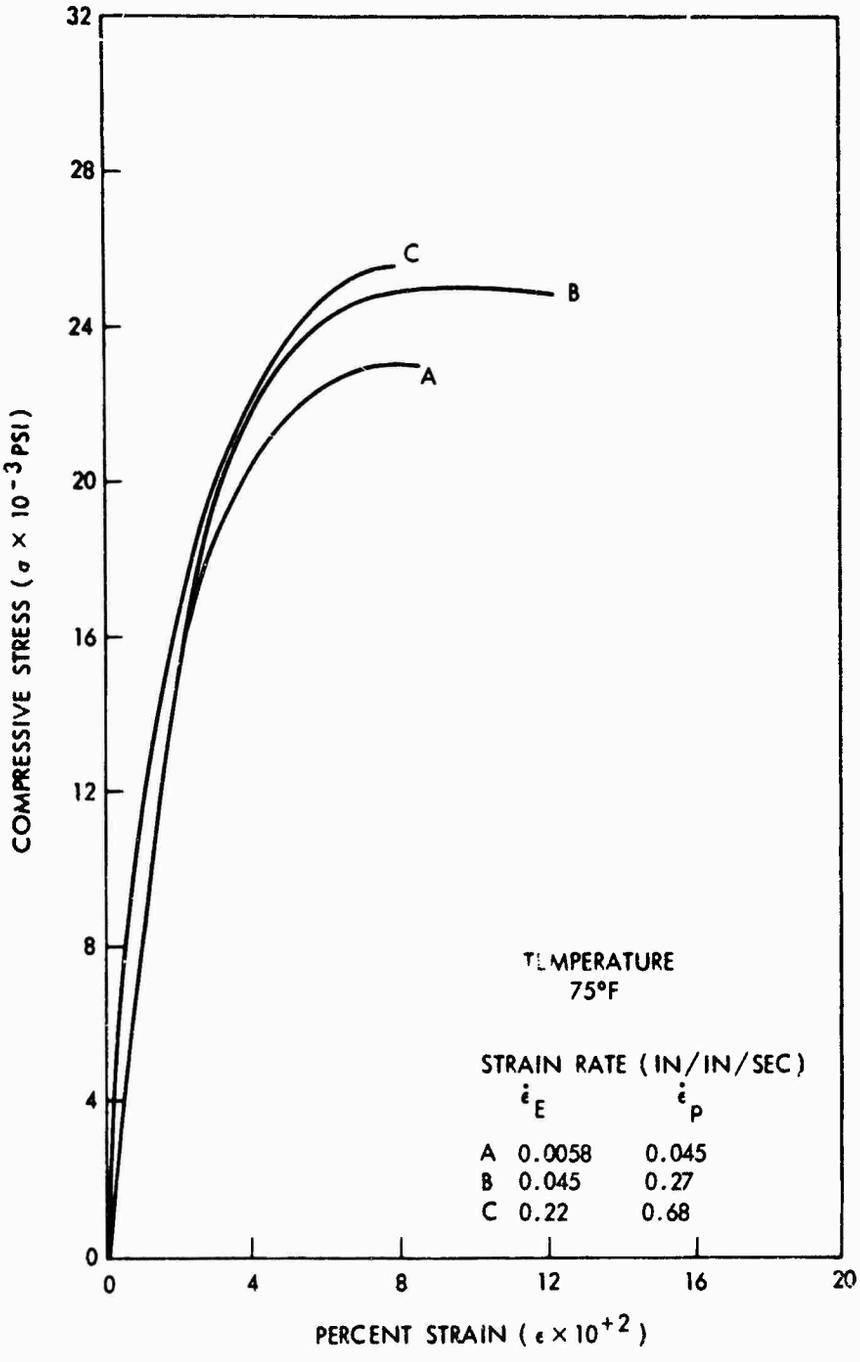

FIG. 6-a DYNAMIC STRESS-STRAIN RELATION OF RDR-701 + NMA + 20% FILLER

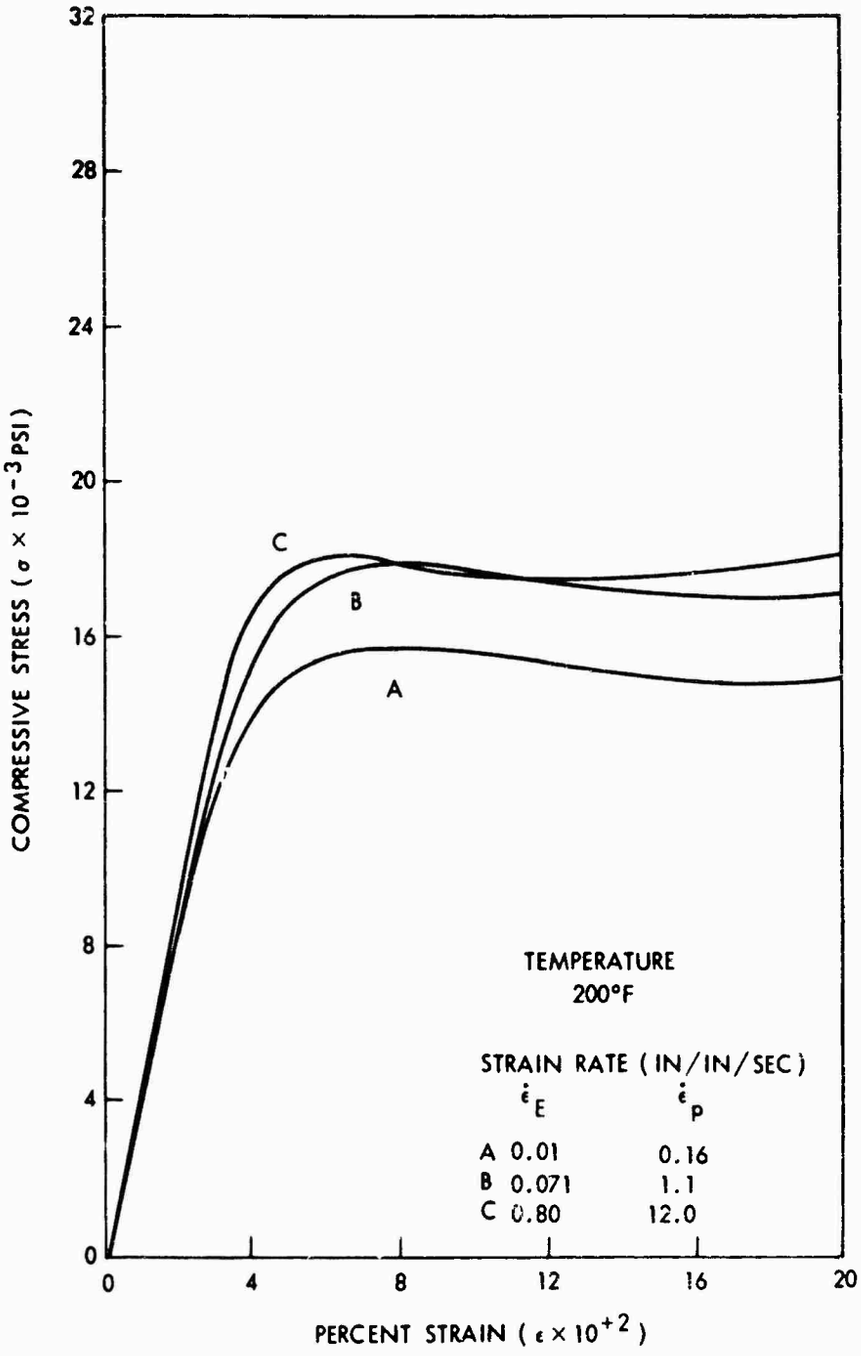

FIG. 6-b DYNAMIC STRESS-STRAIN RELATION OF RDR-701 + NMA + 20% FILLER

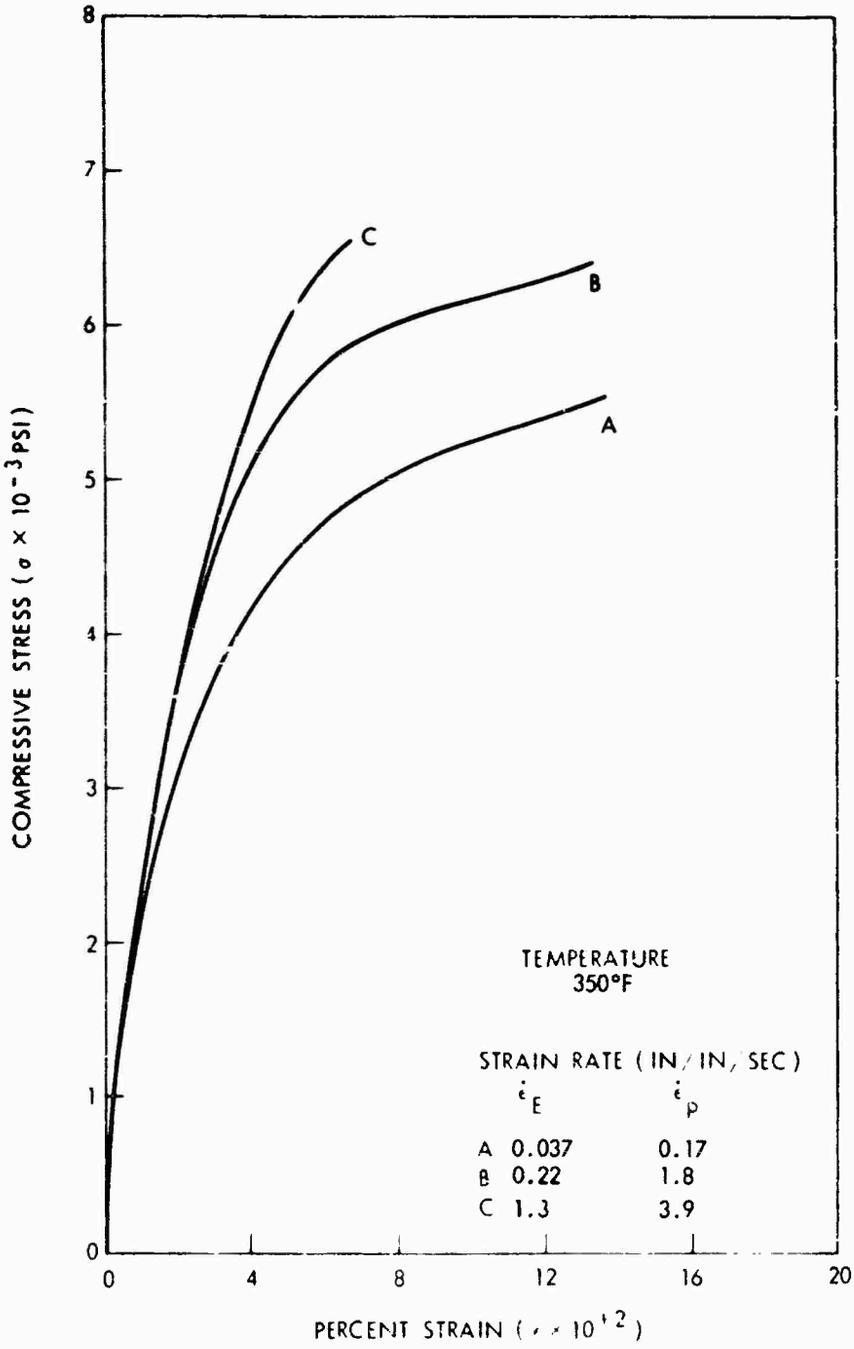

FIG. 6-c DYNAMIC STRESS-STRAIN RELATION OF RDR-701 + NMA + 20% FILLER

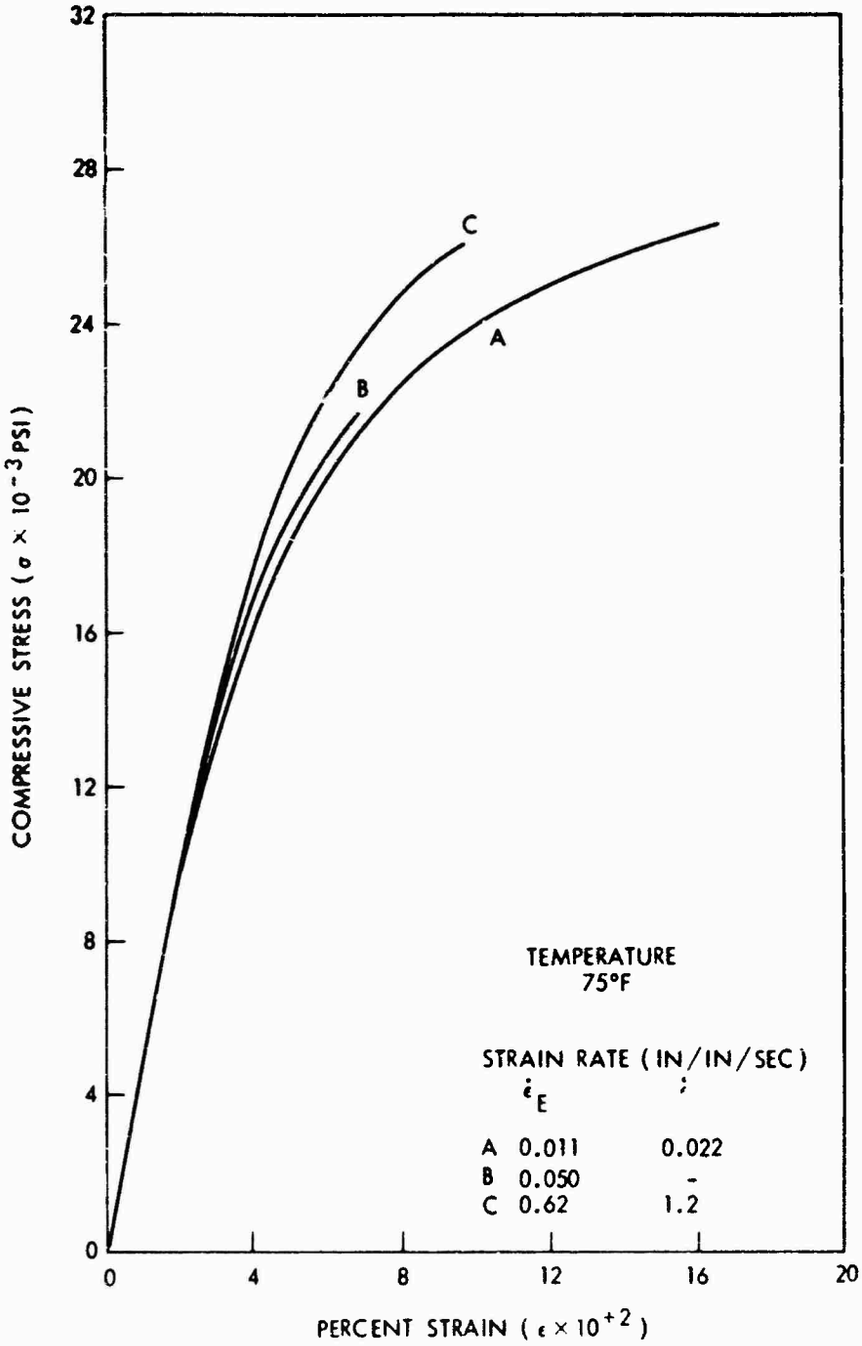

FIG. 7-a DYNAMIC STRESS-STRAIN RELATION OF RDR-700 + NMA + 20% FILLER

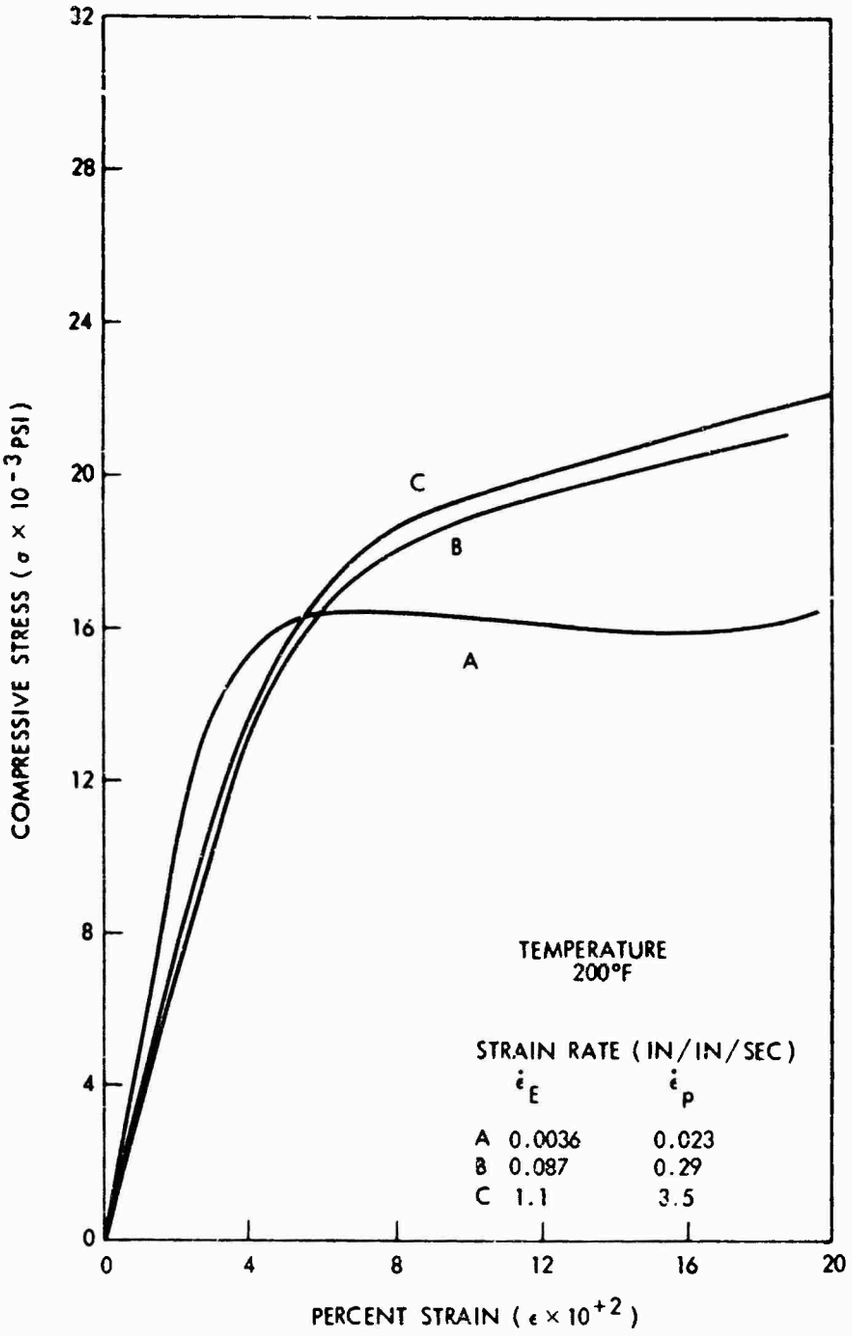

FIG. 7-b DYNAMIC STRESS-STRAIN RELATION OF RDR-700 + NMA + 20% FILLER

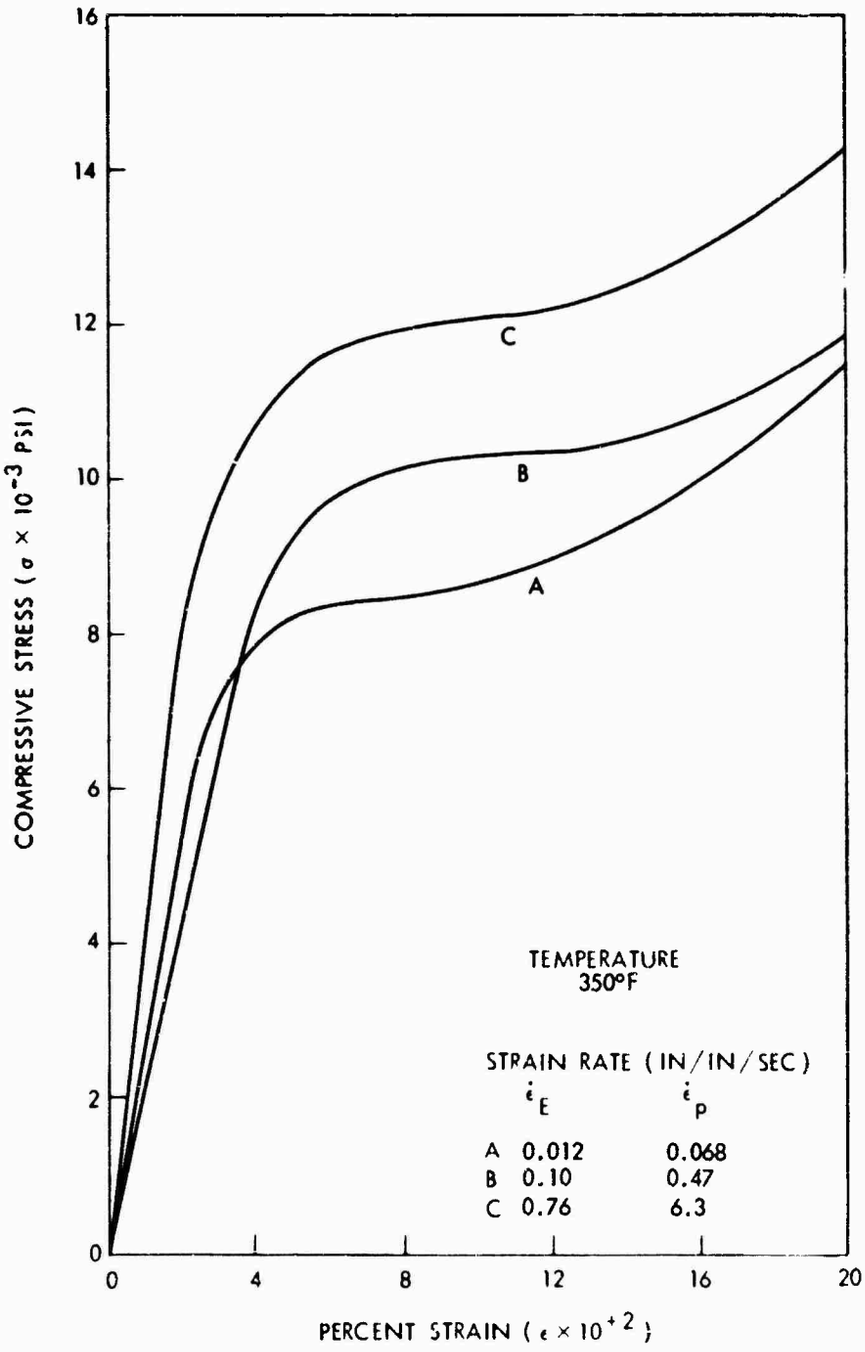

FIG. 7-c DYNAMIC STRESS-STRAIN RELATION OF RDR-700 + NMA + 20% FILLER

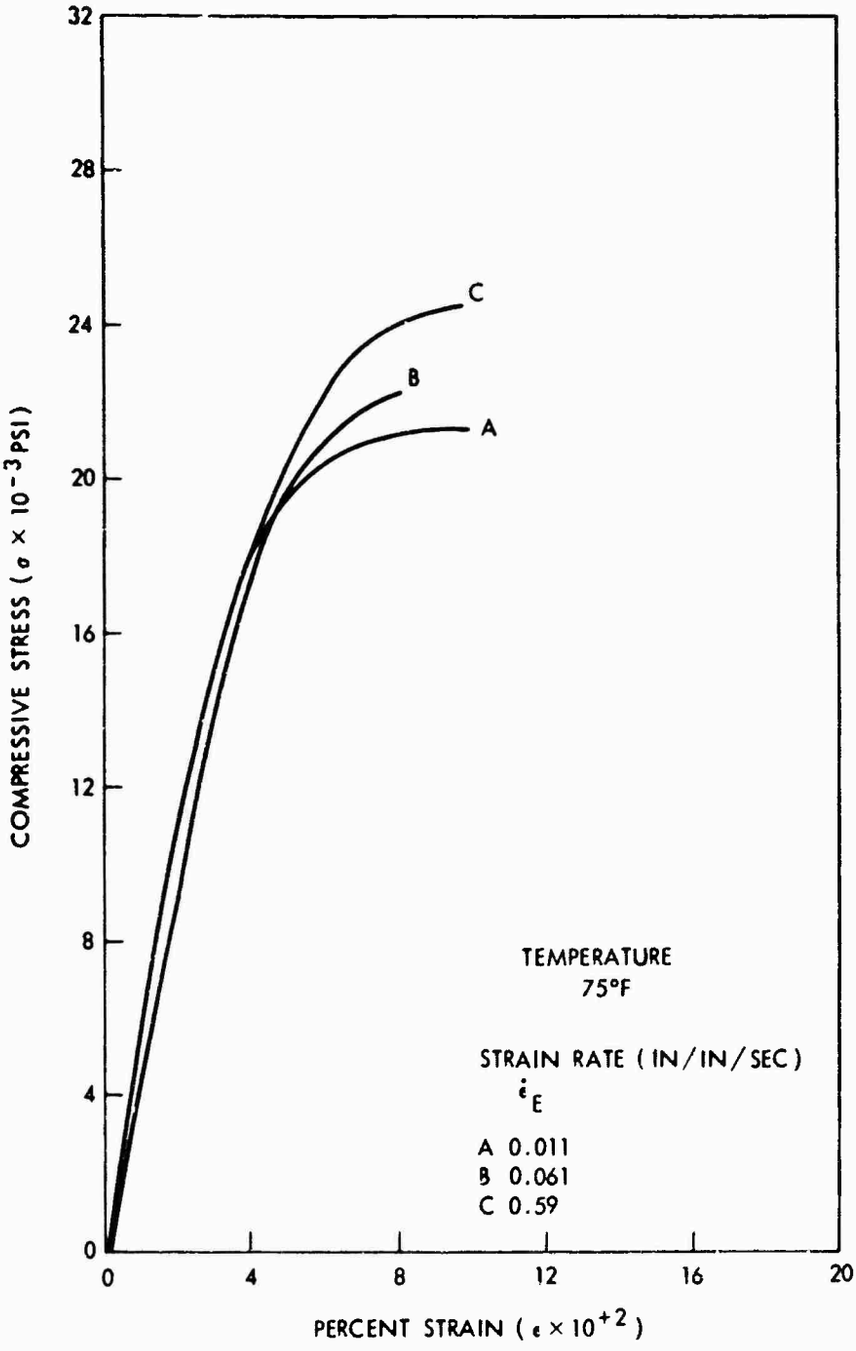

FIG. 8-a DYNAMIC STRESS-STRAIN RELATION OF DEN-438 + NMA +20% FILLER

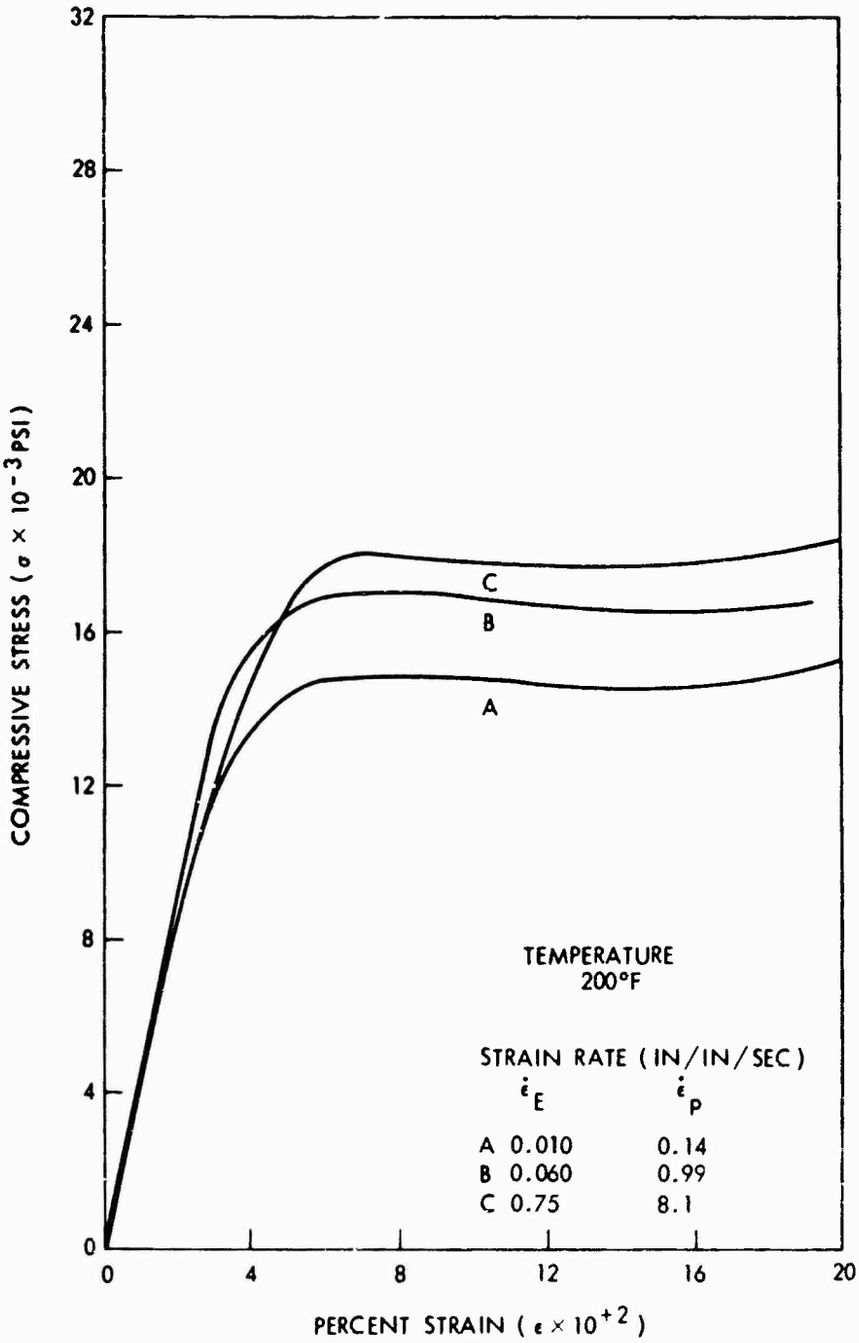

FIG. 8-b DYNAMIC STRESS-STRAIN RELATION OF DEN-438 + NMA + 20% FILLER

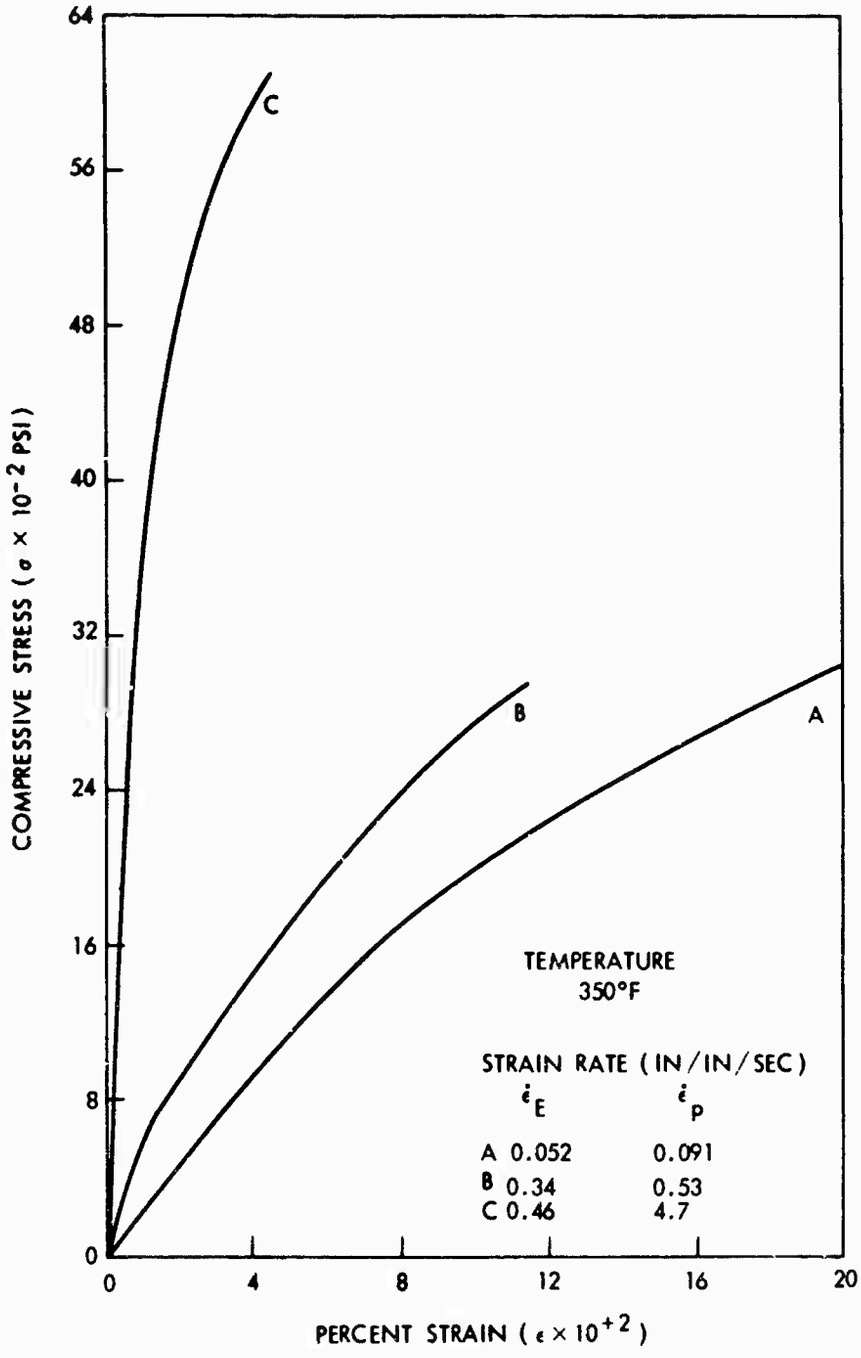

FIG. 8-c DYNAMIC STRESS-STRAIN RELATION OF DEN-438 + NMA + 20% FILLER

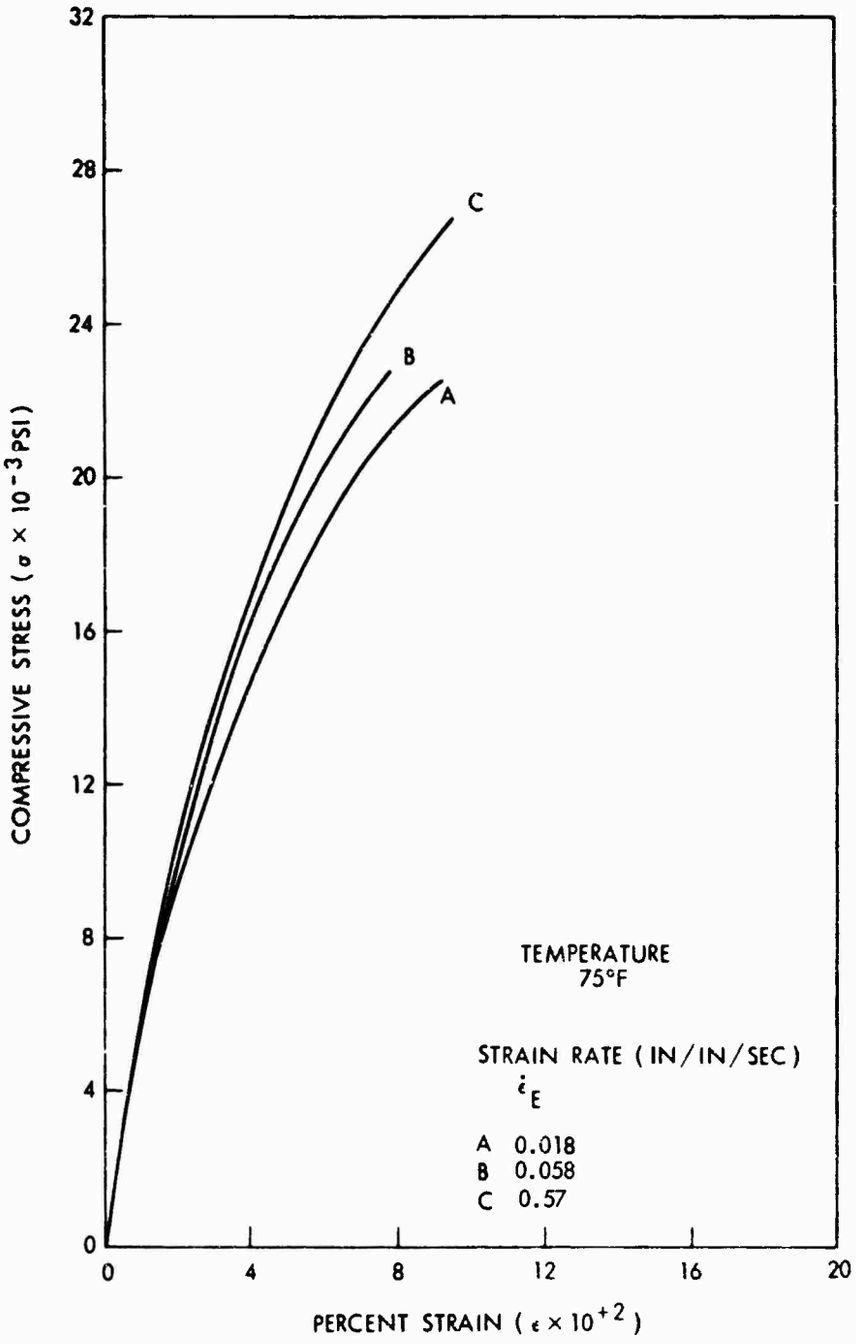

FIG. 9-a DYNAMIC STRESS-STRAIN RELATION OF DEN-438 + DADPS + 20% FILLER

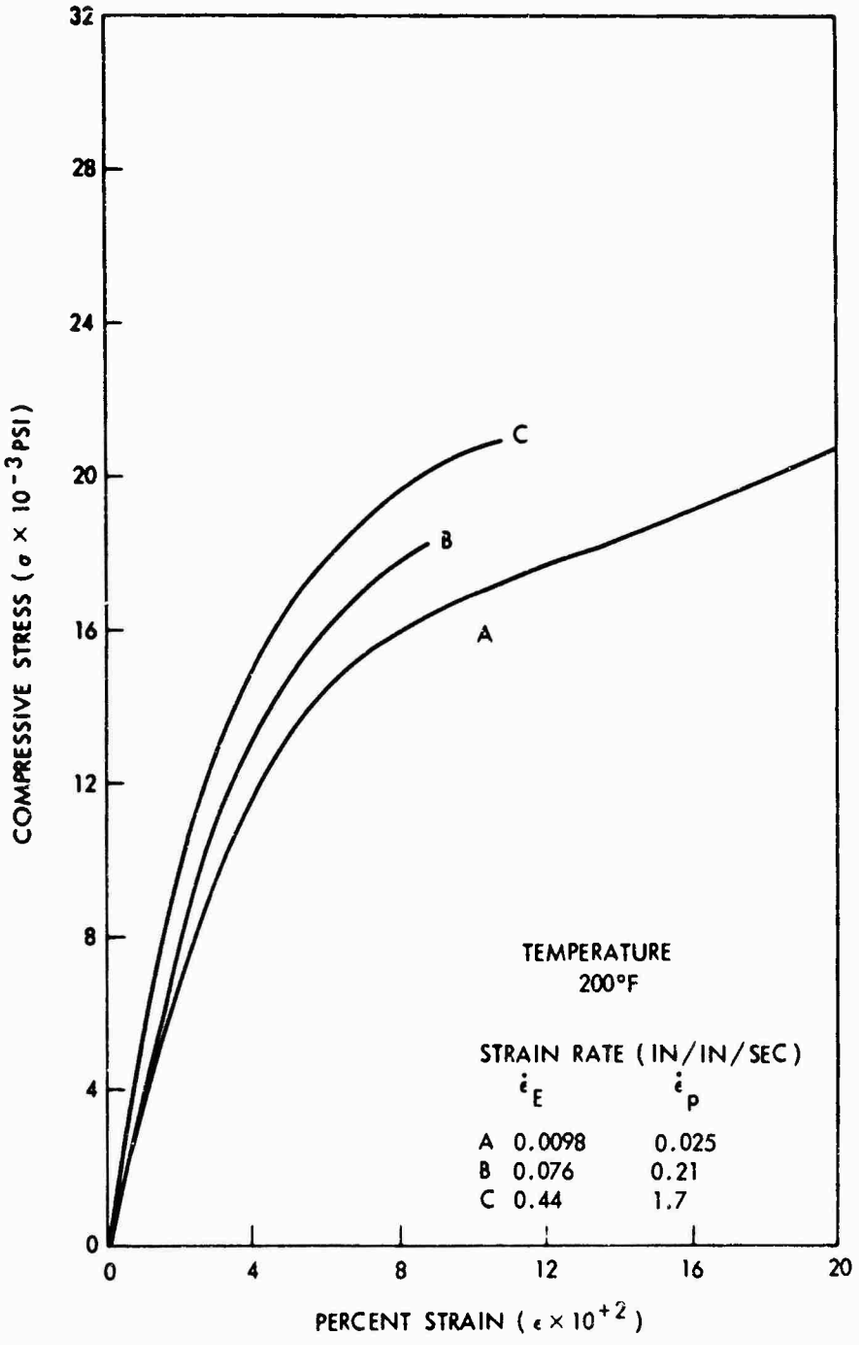

FIG. 9-b DYNAMIC STRESS-STRAIN RELATION OF DEN-438 + DADPS + 20% FILLER

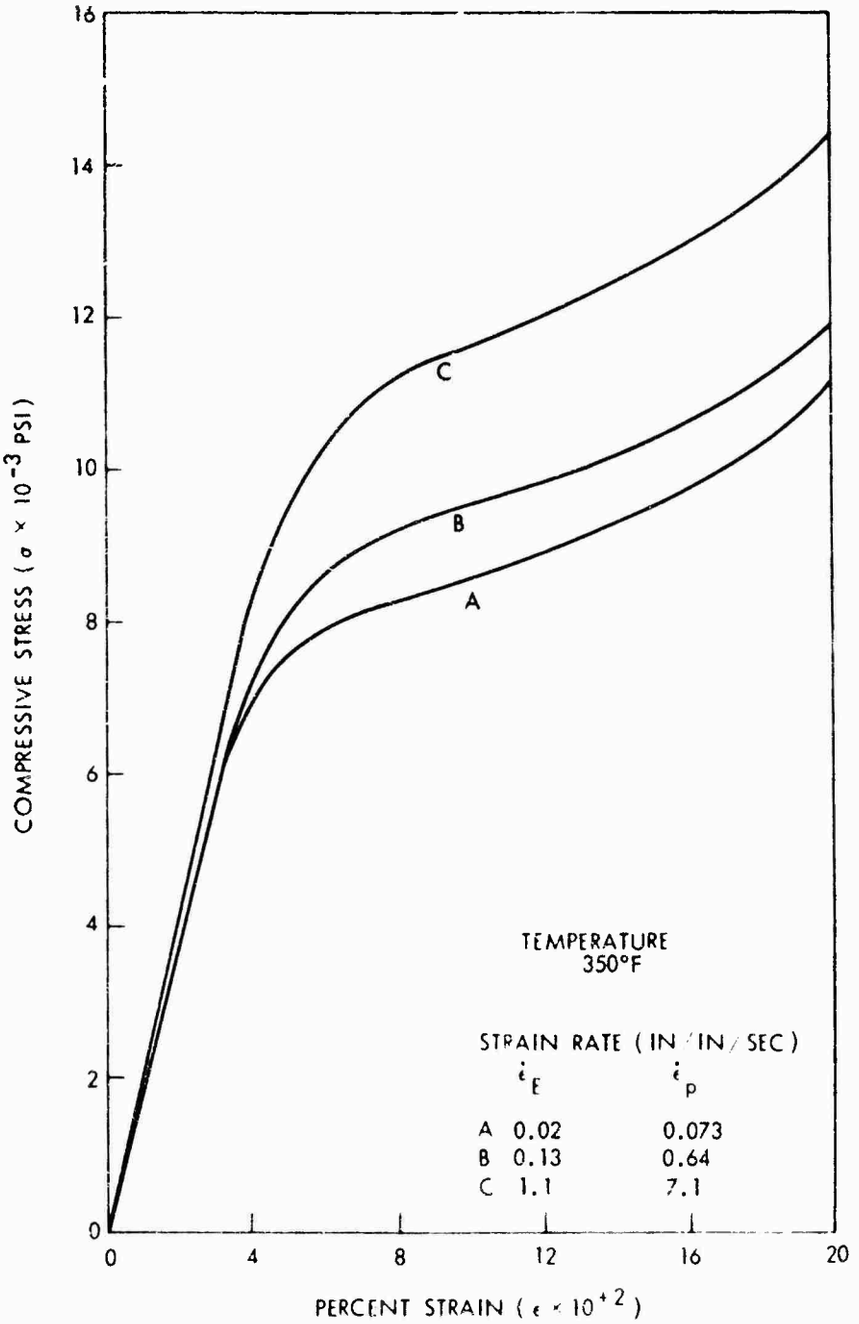

FIG. 9-c DYNAMIC STRESS-STRAIN RELATION OF DEN-438 + DADPS + 20% FILLER

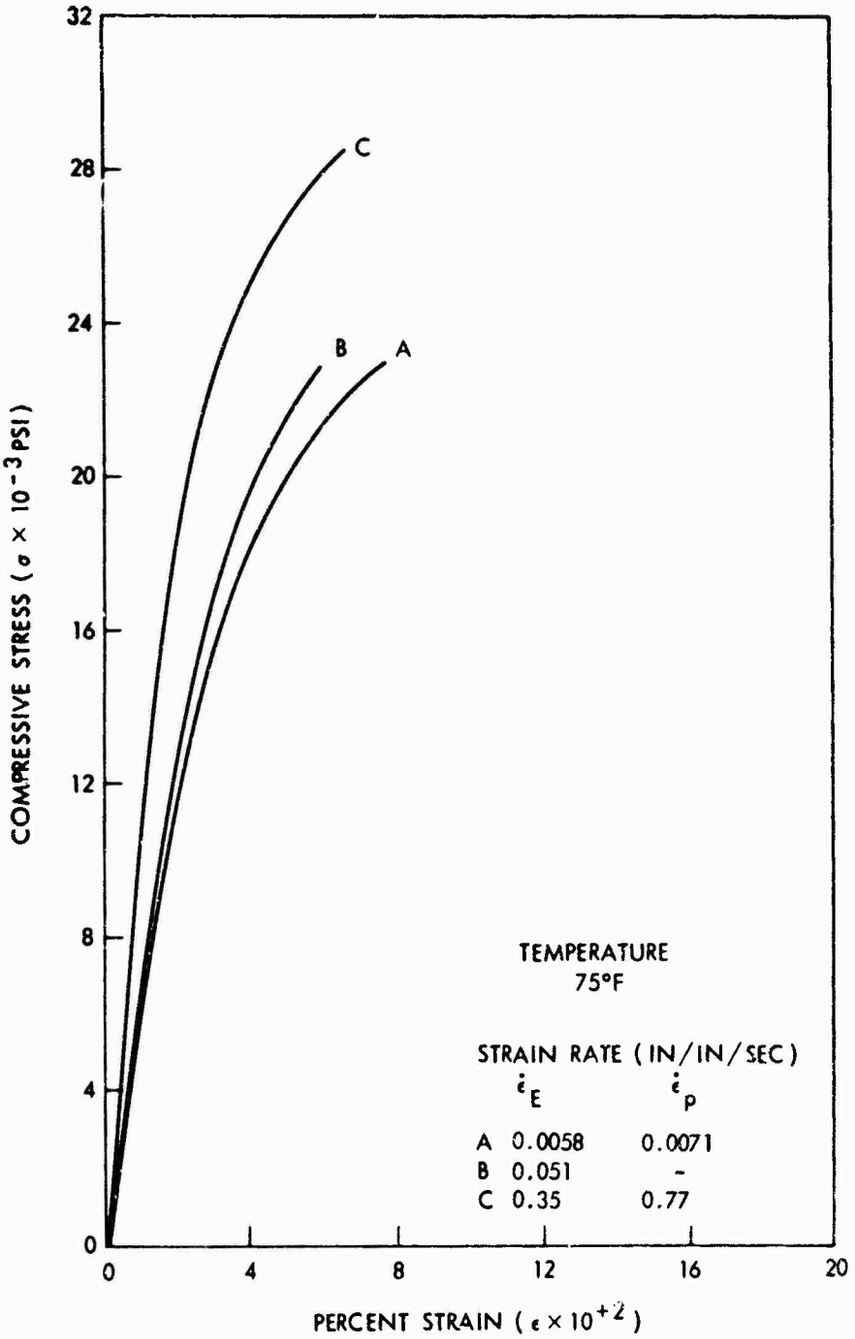

FIG. 10-a DYNAMIC STRESS-STRAIN RELATION OF KOPOX 159 + DADPS + 20% FILLER

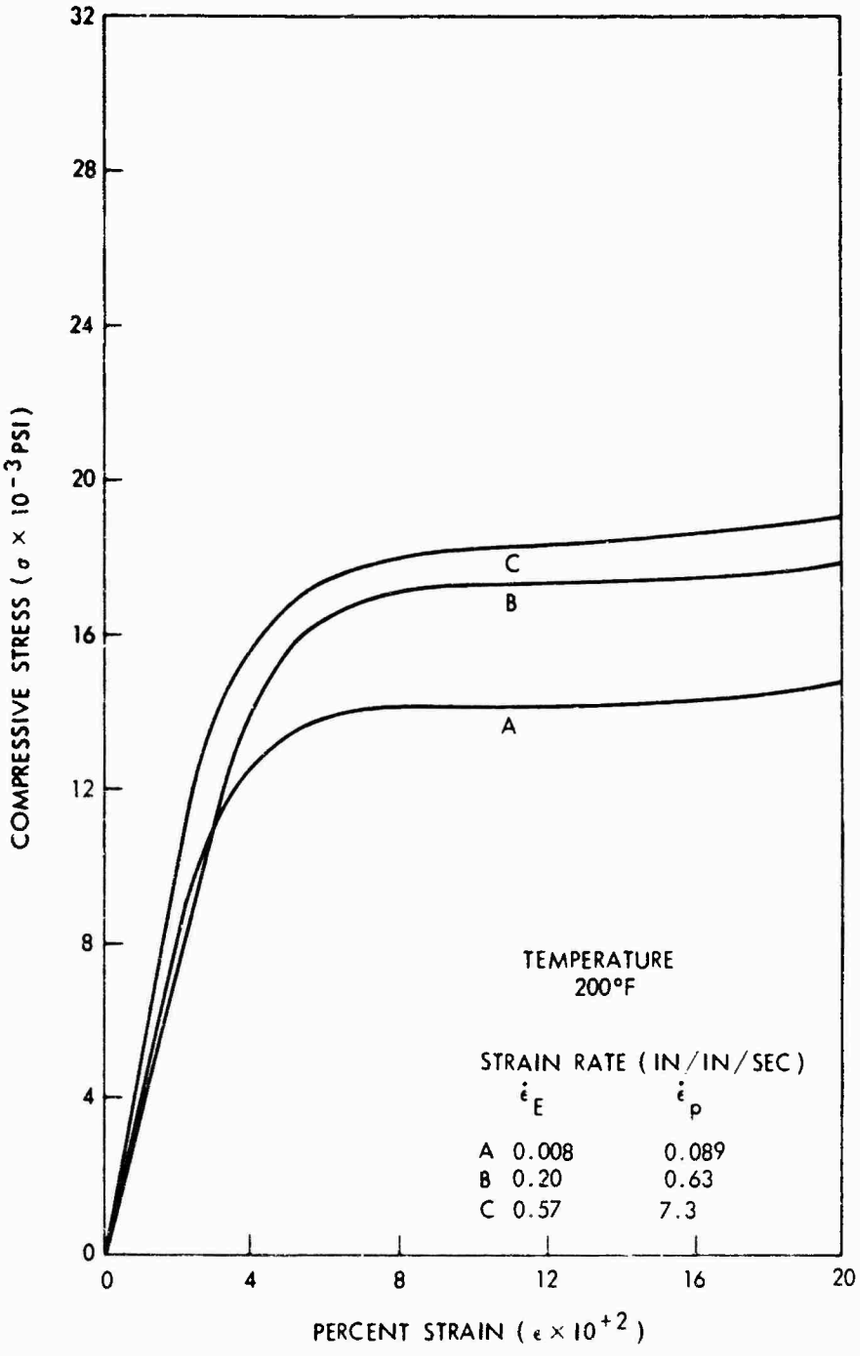

FIG. 10-b DYNAMIC STRESS-STRAIN RELATION OF KOPOX 159 + DADPS + 20% FILLER

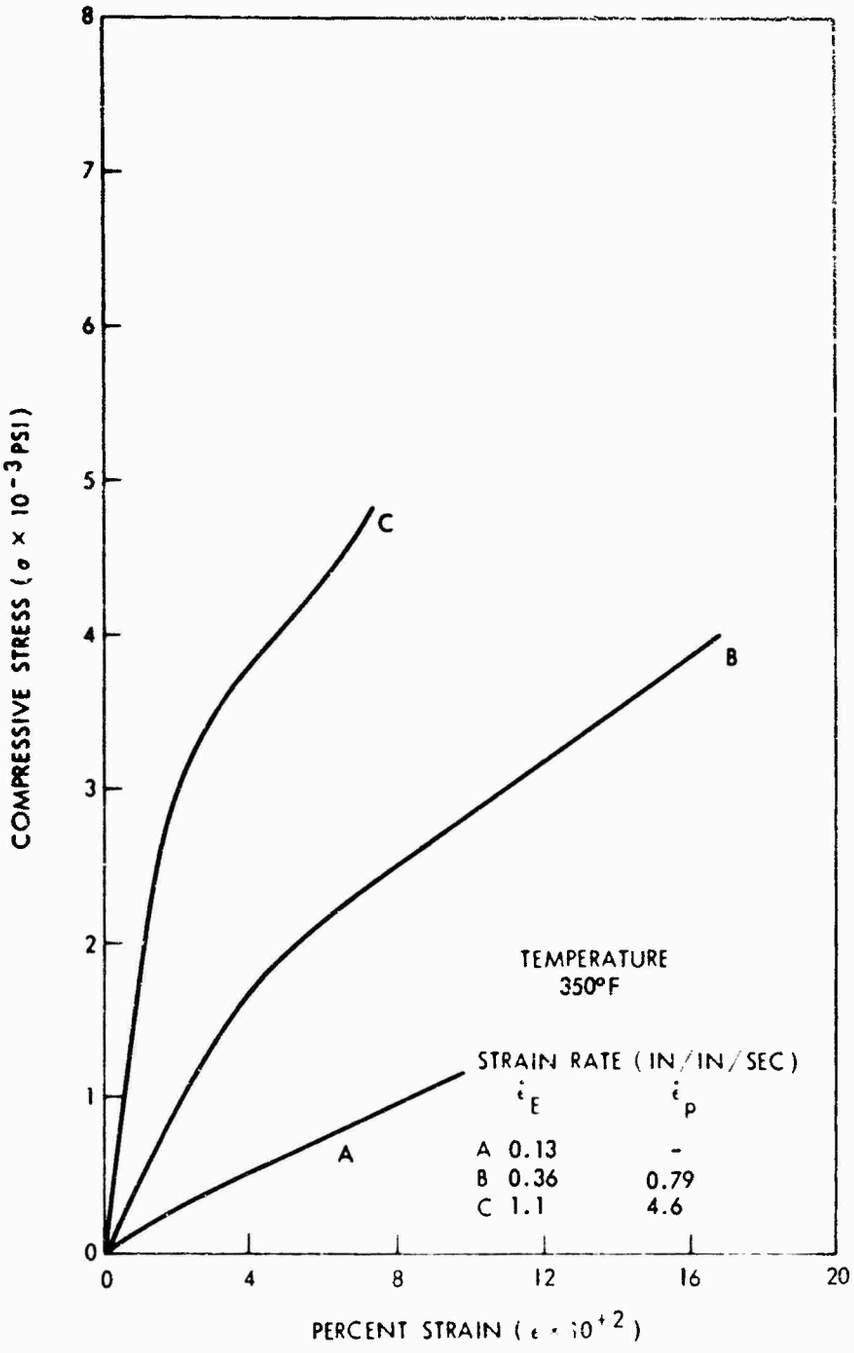

FIG. 10-c DYNAMIC STRESS-STRAIN RELATION OF KOPOX 159 + DADPS + 20% FILLER

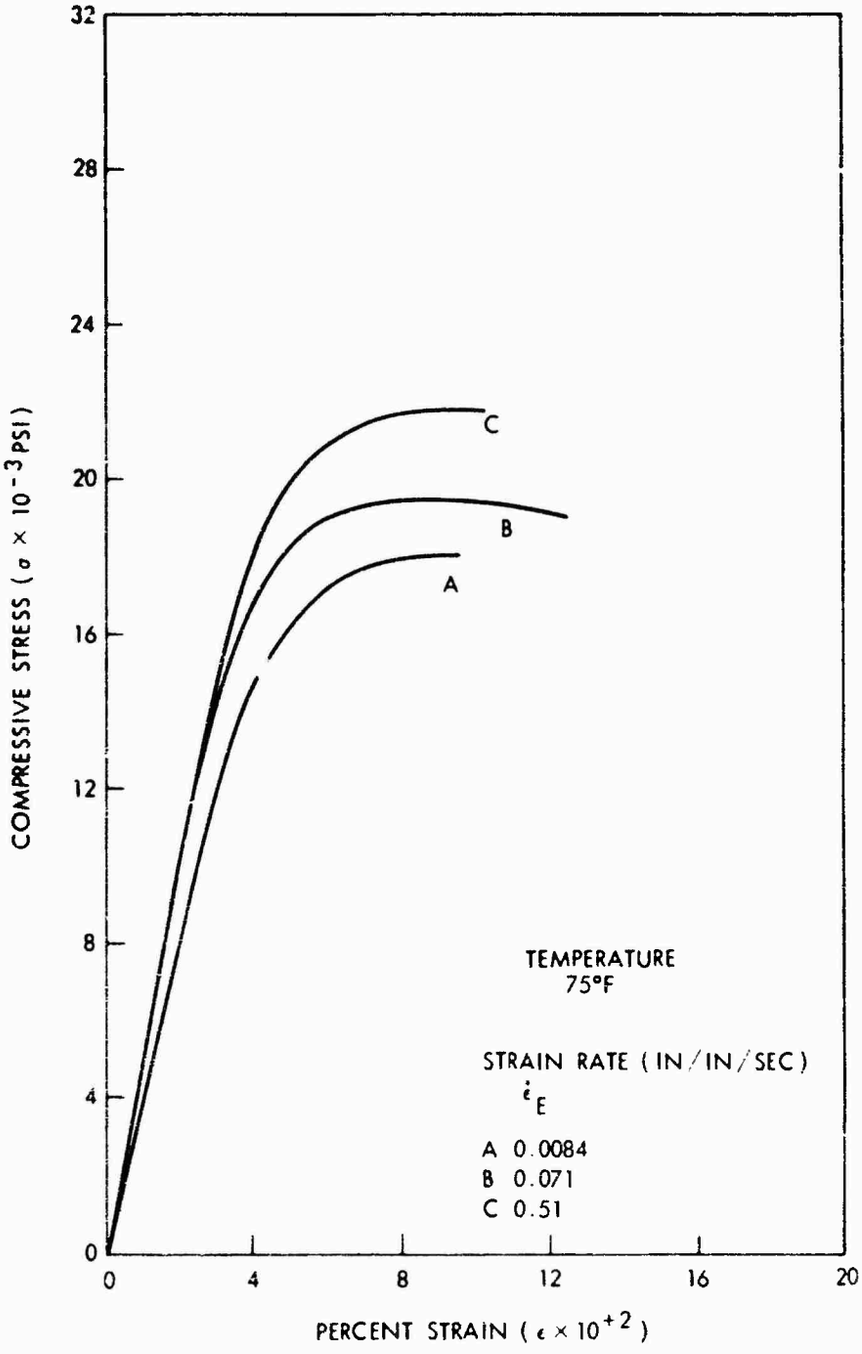

FIG. 11-a DYNAMIC STRESS-STRAIN RELATION OF KOPOX 159 + NMA + 20% FILLER

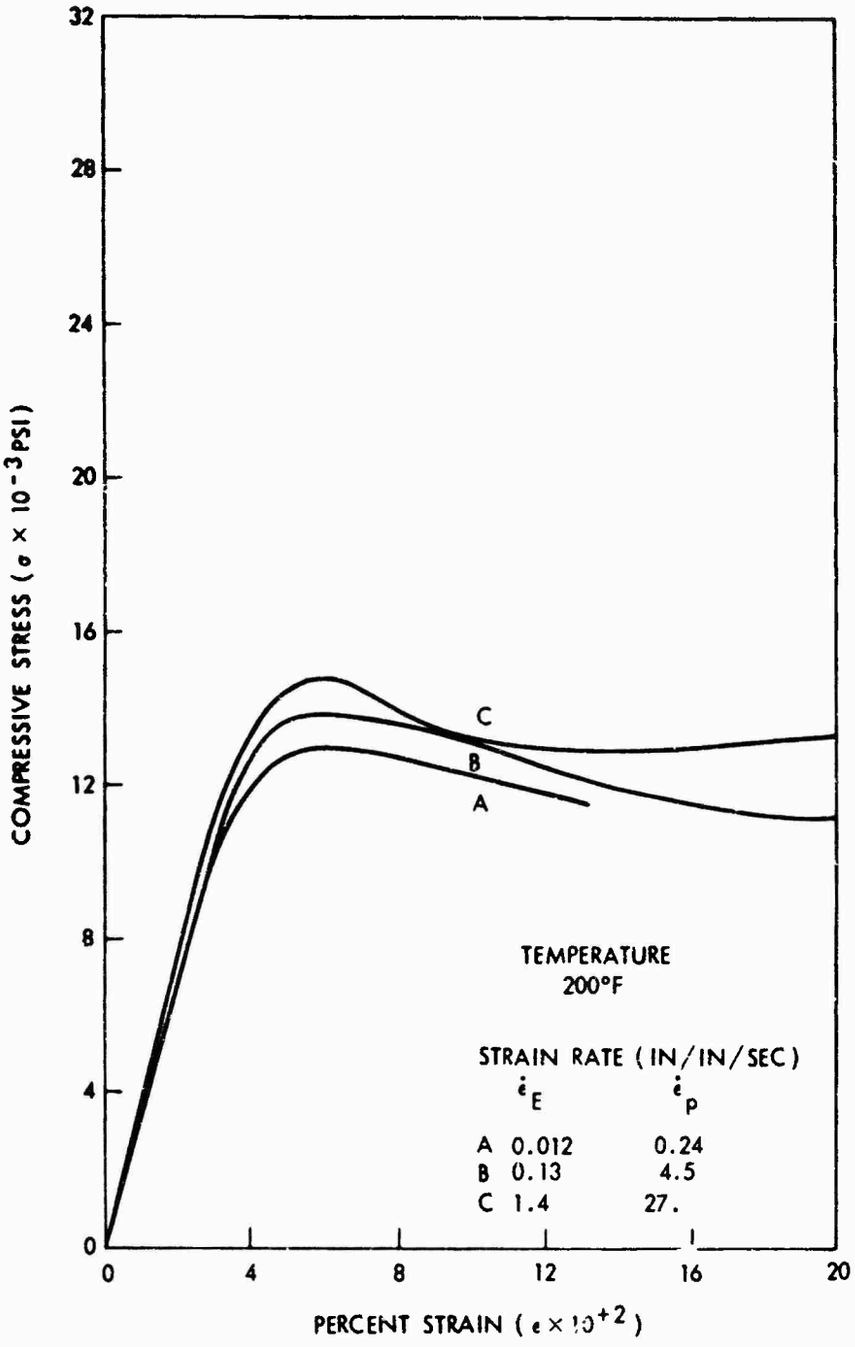

FIG. 11-b DYNAMIC STRESS-STRAIN RELATION OF KOPOX 159 + NMA + 20% FILLER

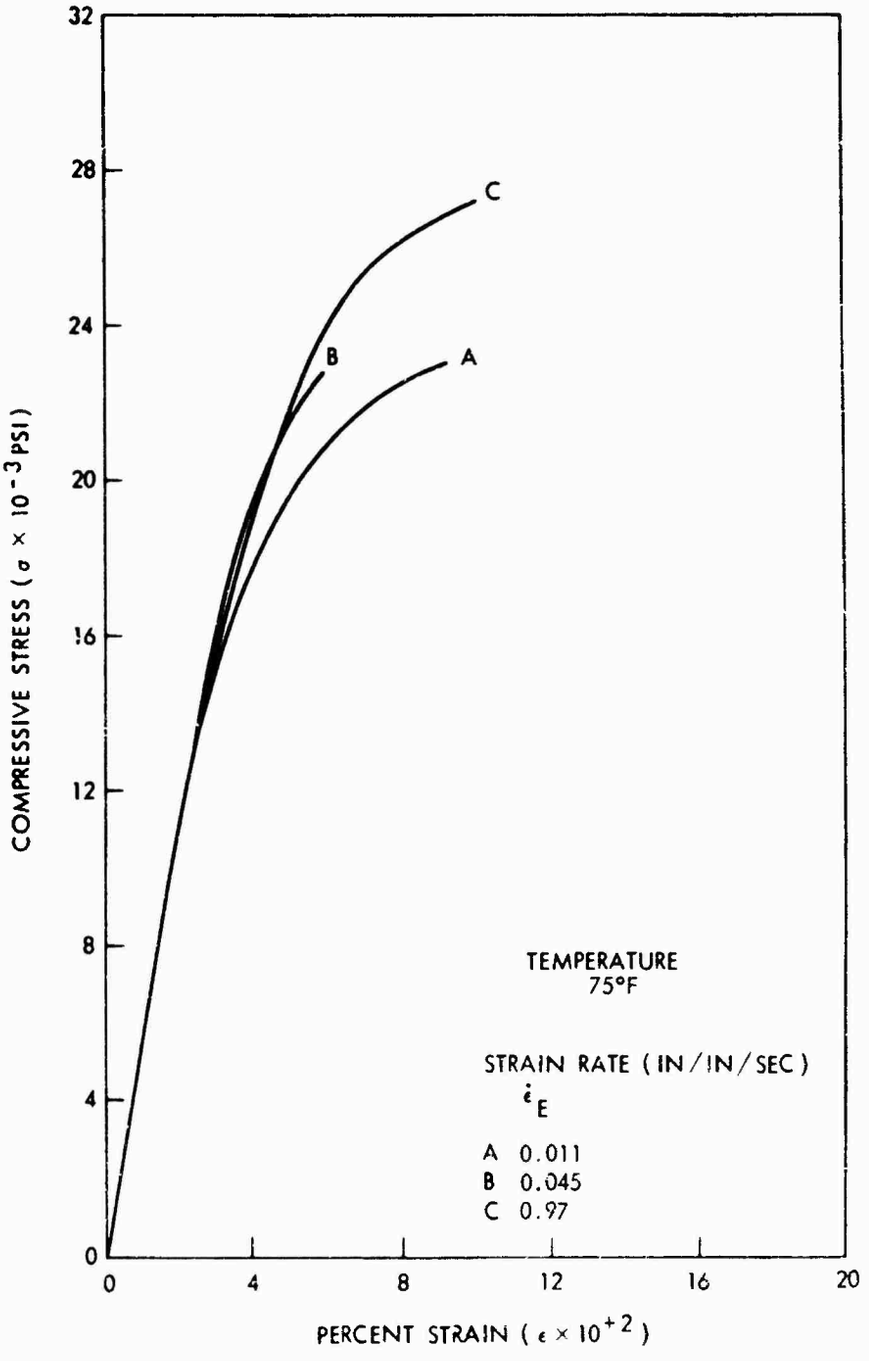

FIG. 12-a DYNAMIC STRESS-STRAIN RELATION OF KOPOX 997A + NMA + 20% FILLER

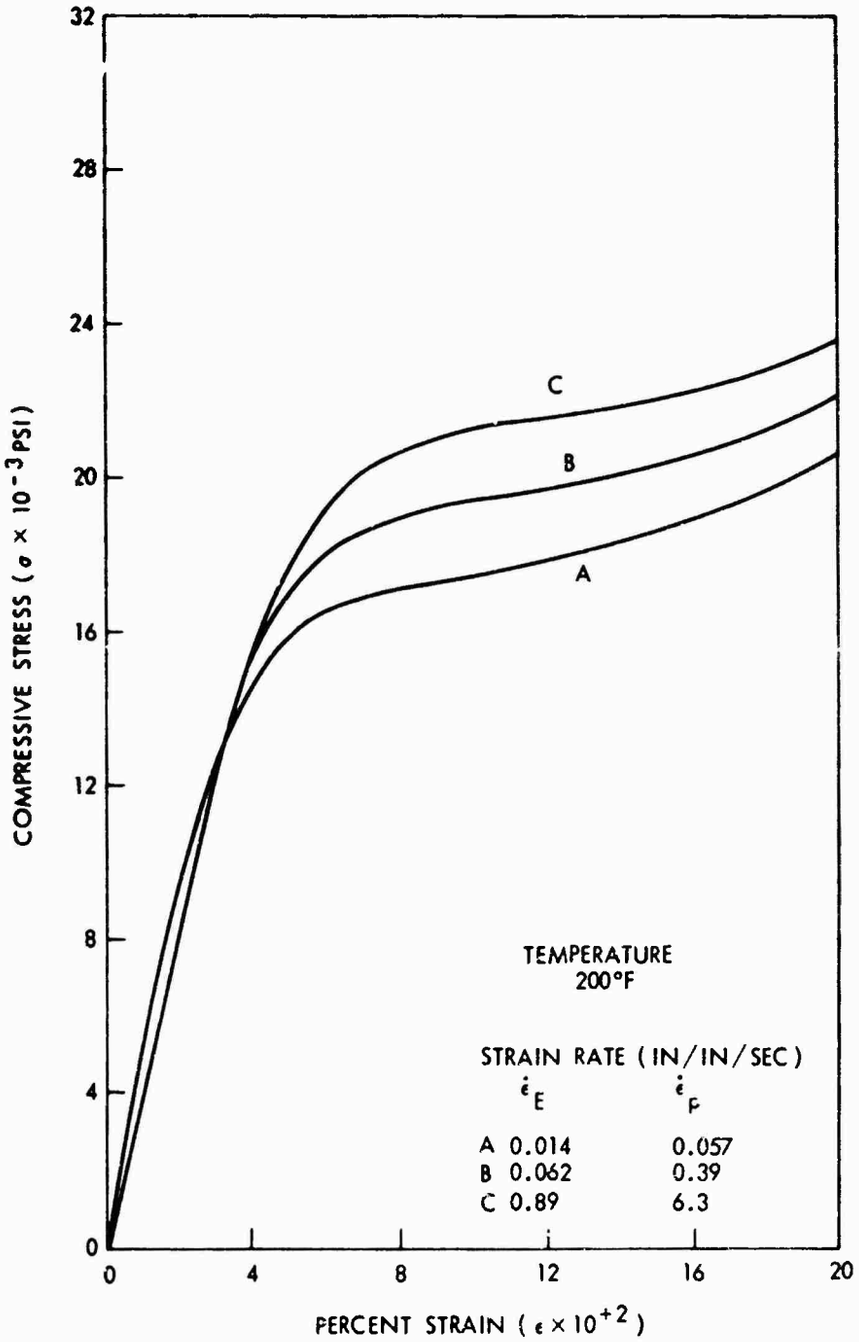

FIG. 12-b DYNAMIC STRESS-STRAIN RELATION OF KOPOX 997A + NMA + 20% FILLER

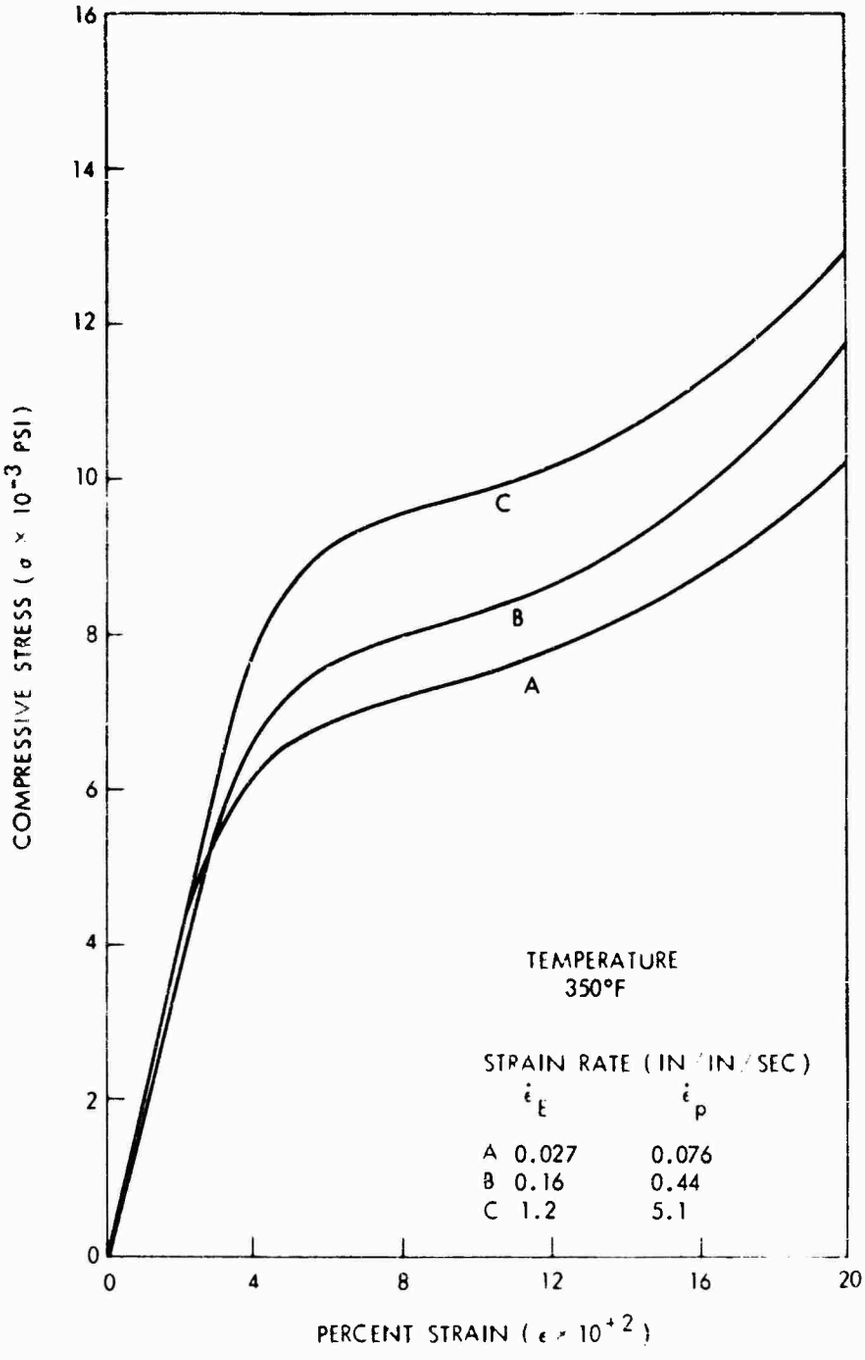

FIG. 12-c DYNAMIC STRESS-STRAIN RELATION OF KOPOX 997A + NMA + 20% FILLER

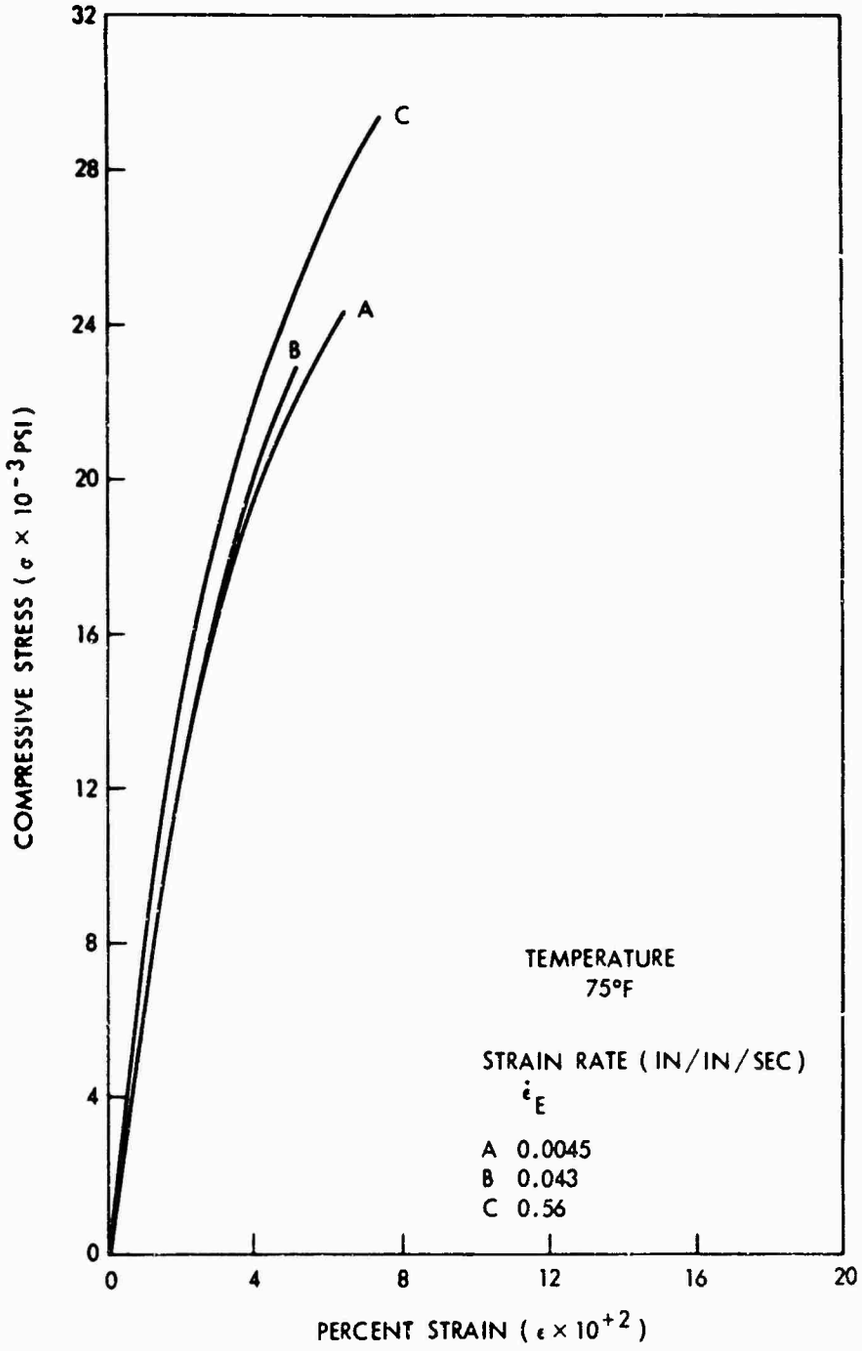

FIG. 13-a DYNAMIC STRESS-STRAIN RELATION OF ERLA-0400 + MPDA + 20% FILLER

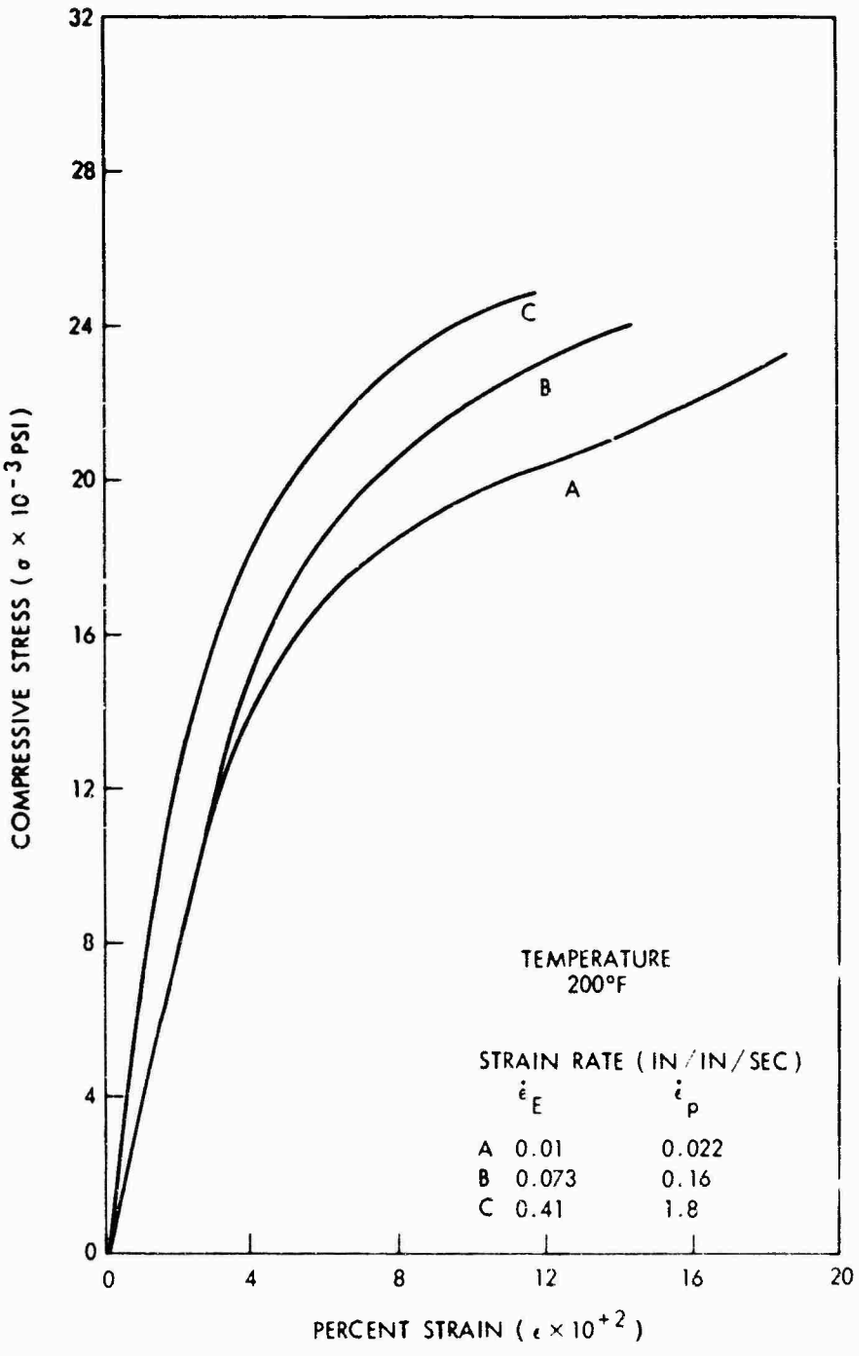

FIG. 13-b DYNAMIC STRESS-STRAIN RELATION OF ERLA-0400 + MPDA + 20% FILLER

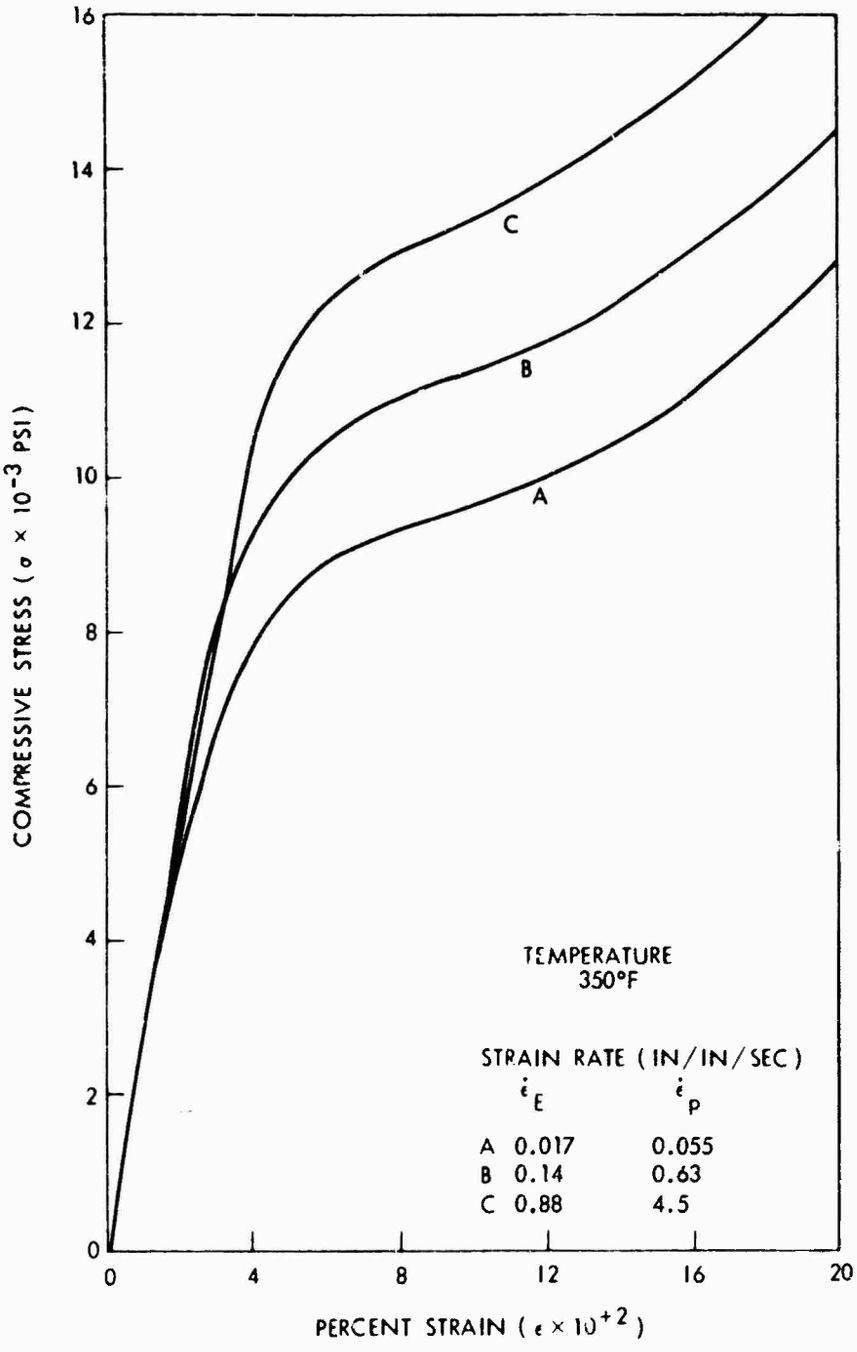

FIG. 13-c DYNAMIC STRESS-STRAIN RELATION OF ERLA-0400 + MPDA + 20% FILLER

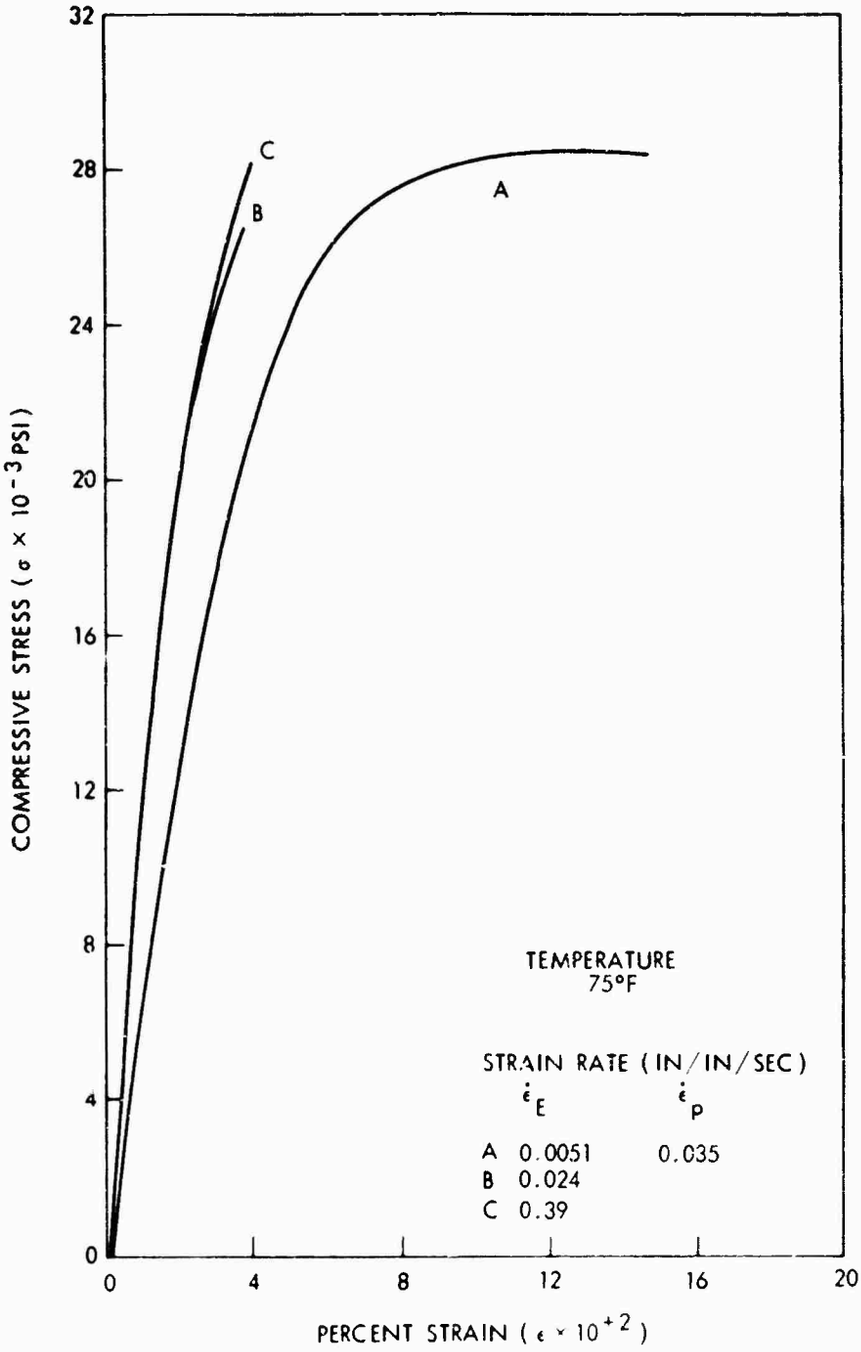

FIG. 14-a DYNAMIC STRESS-STRAIN RELATION OF IRONSIDES DP4-88S

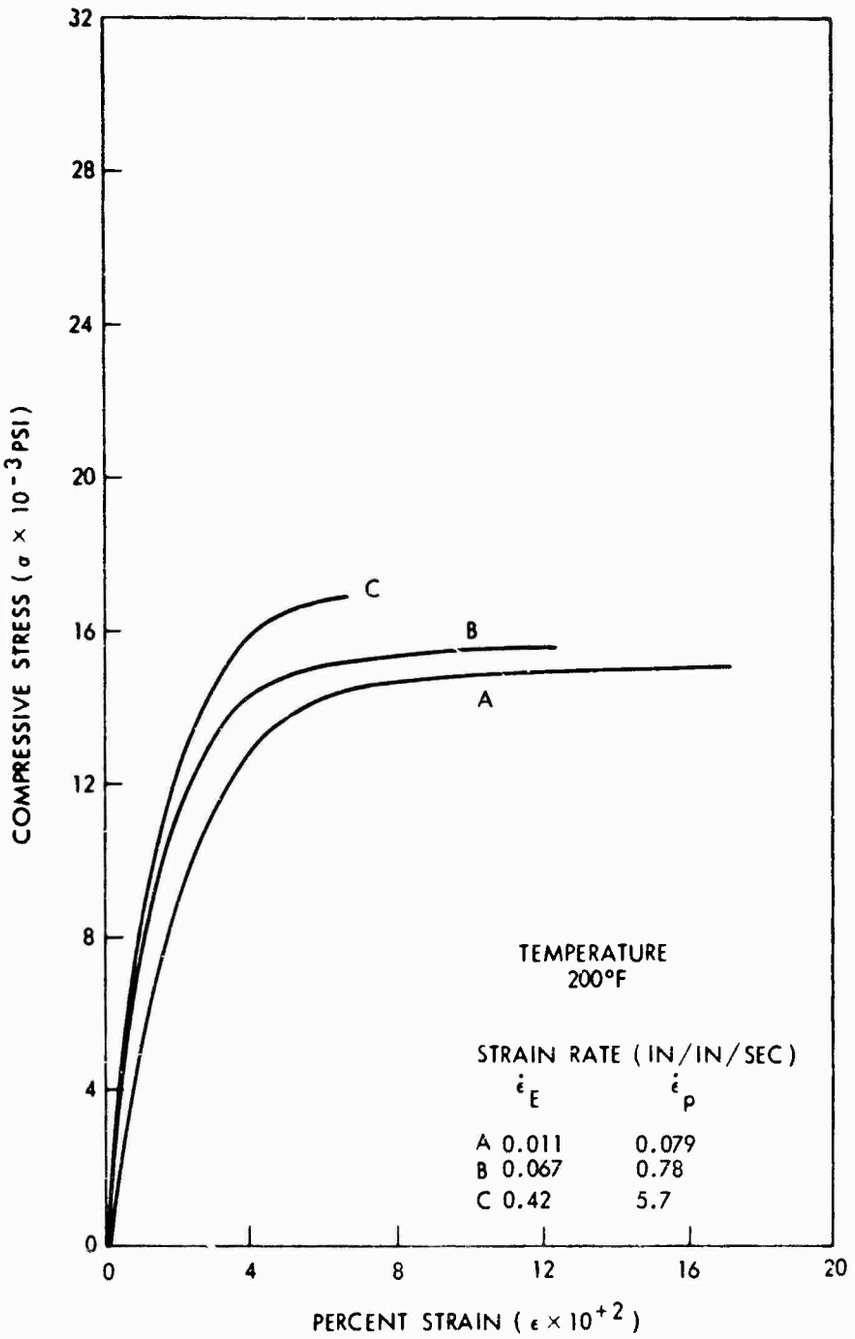

FIG. 14-b DYNAMIC STRESS-STRAIN RELATION OF IRONSIDES DP4-88S

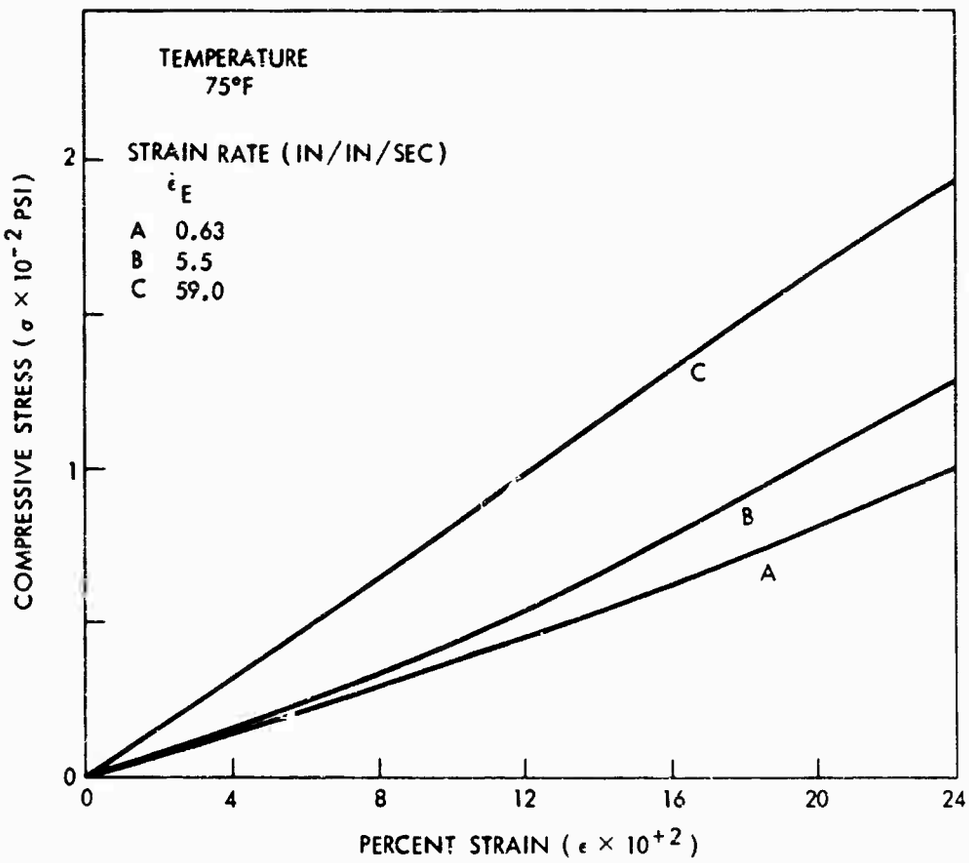

FIG. 15-a DYNAMIC STRESS-STRAIN RELATION OF RUBBER COMPOSITION WS-4863

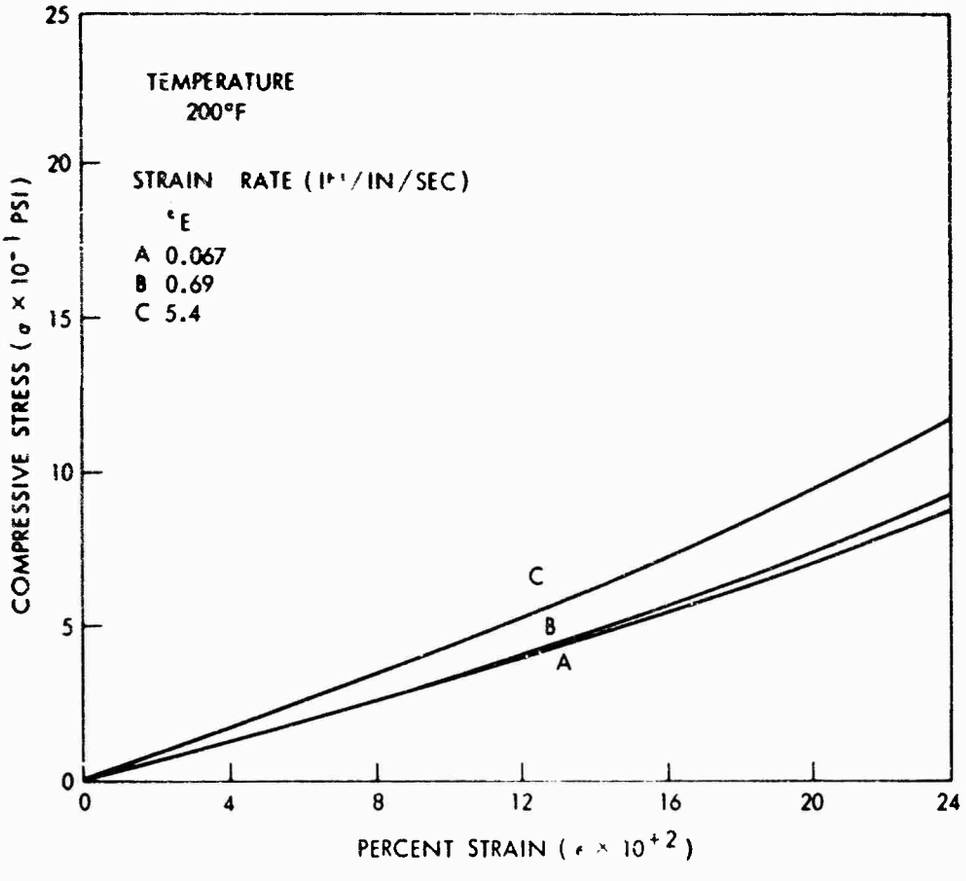

FIG. 15-b DYNAMIC STRESS-STRAIN RELATION OF RUBBER COMPOSITION WS-4863

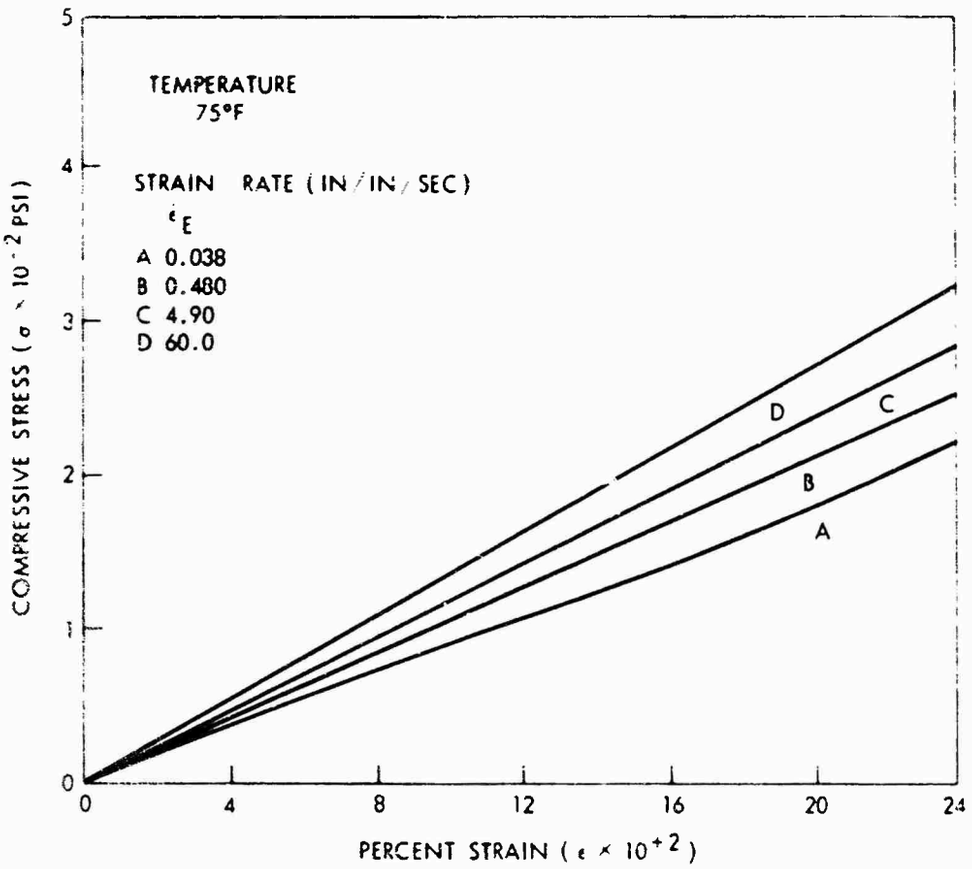

FIG. 16-a DYNAMIC STRESS-STRAIN RELATION OF RUBBER COMPOSITION WS-2822

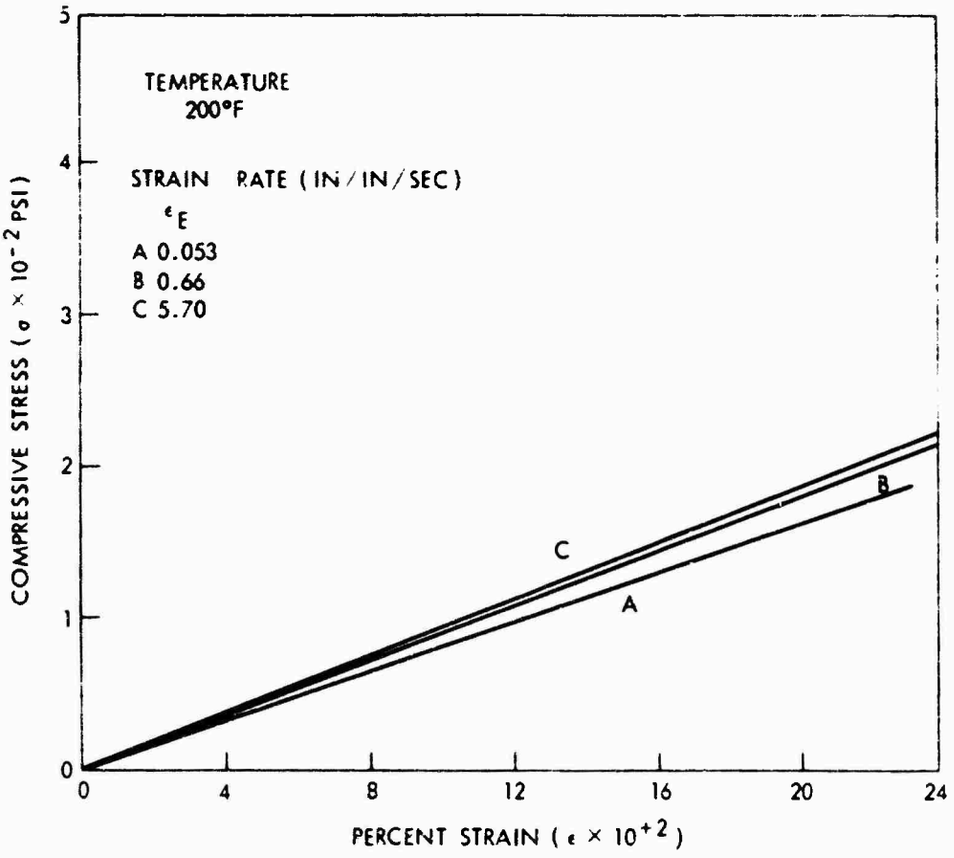

FIG. 16-b DYNAMIC STRESS-STRAIN RELATION OF RUBBER COMPOSITION WS-2822

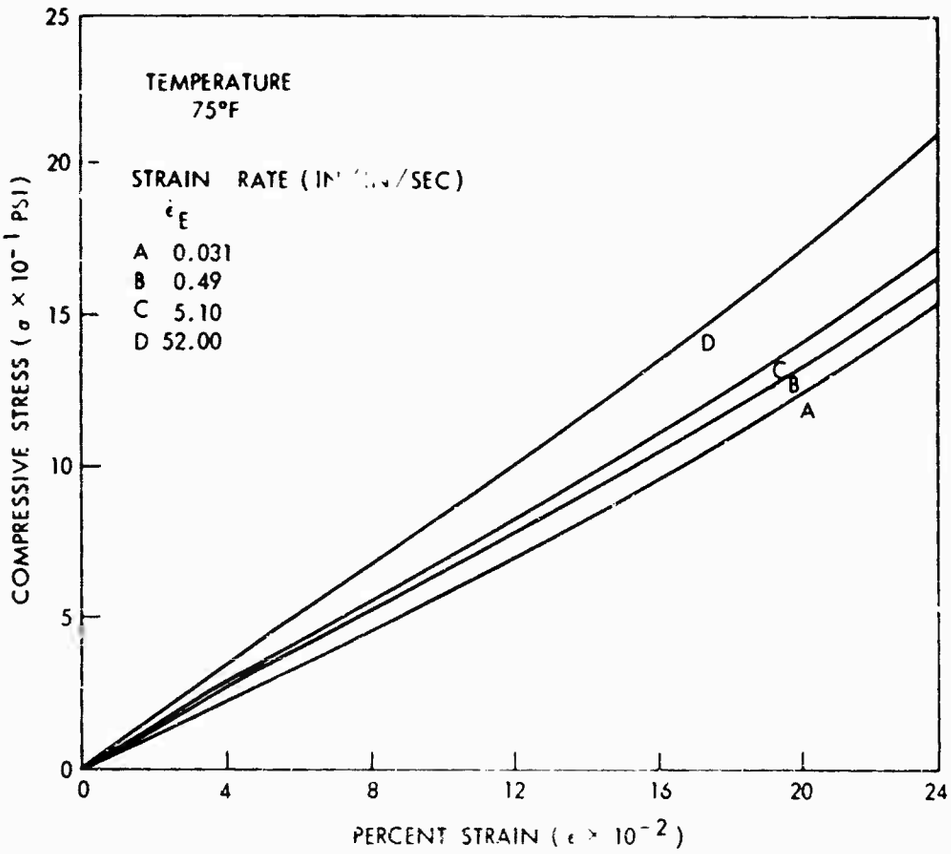

FIG. 17-a DYNAMIC STRESS-STRAIN RELATION OF RUBBER COMPOSITION UA-35

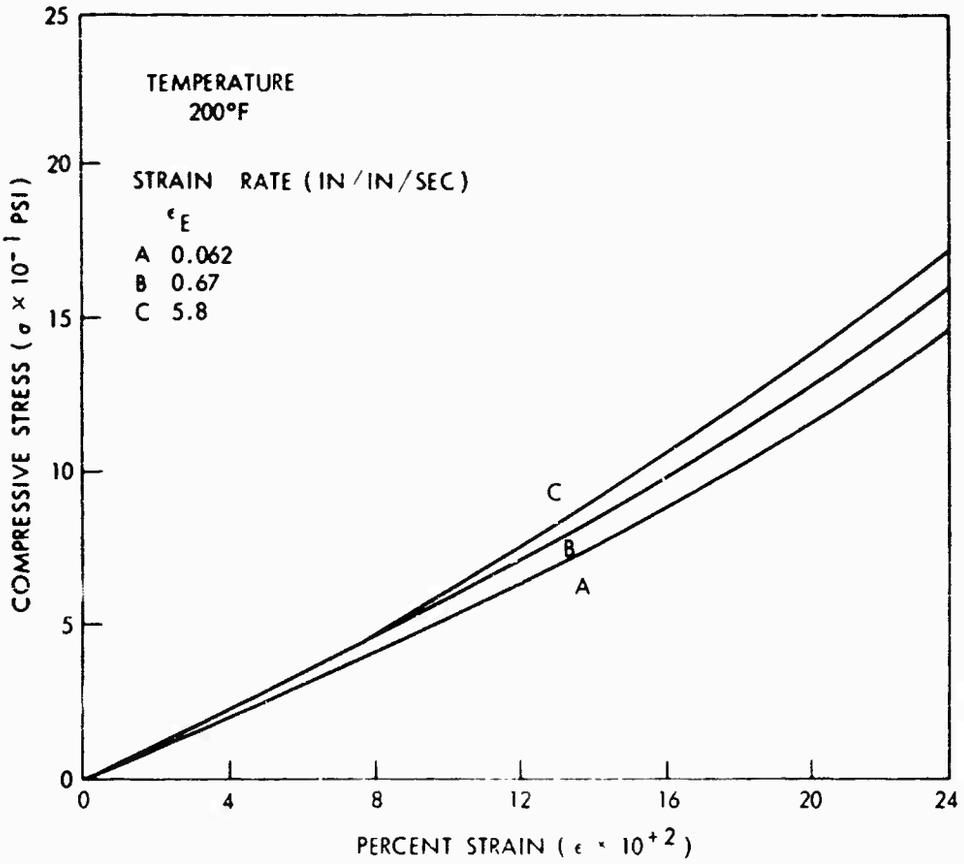

FIG. 17-b DYNAMIC STRESS-STRAIN RELATION OF RUBBER COMPOSITION UA-35

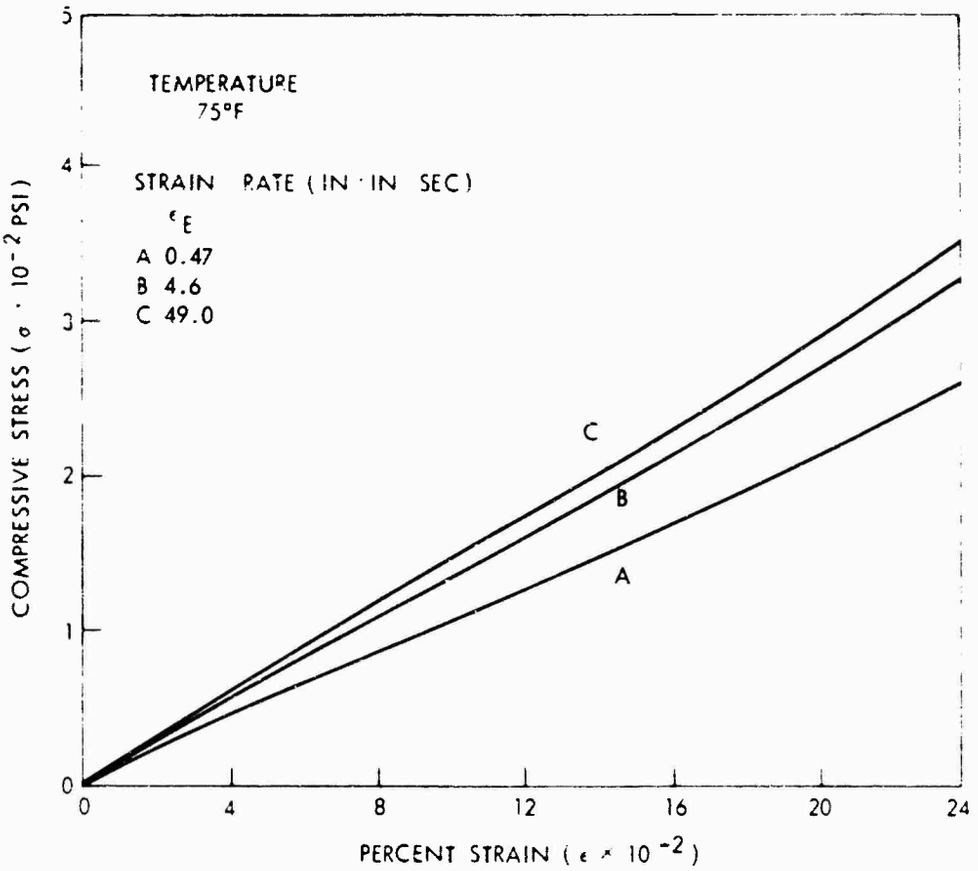

FIG. 18-a DYNAMIC STRESS-STRAIN RELATION OF RUBBER COMPOSITION SC-620

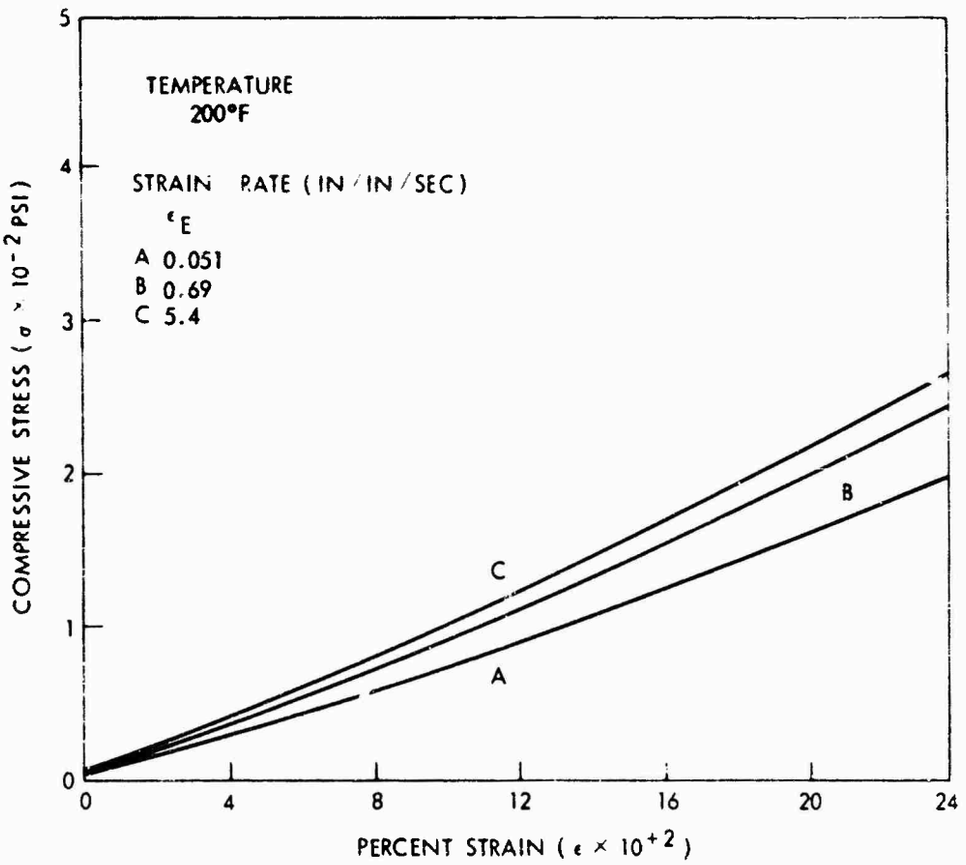

FIG. 18-b DYNAMIC STRESS-STRAIN RELATION OF RUBBER COMPOSITION SC-620

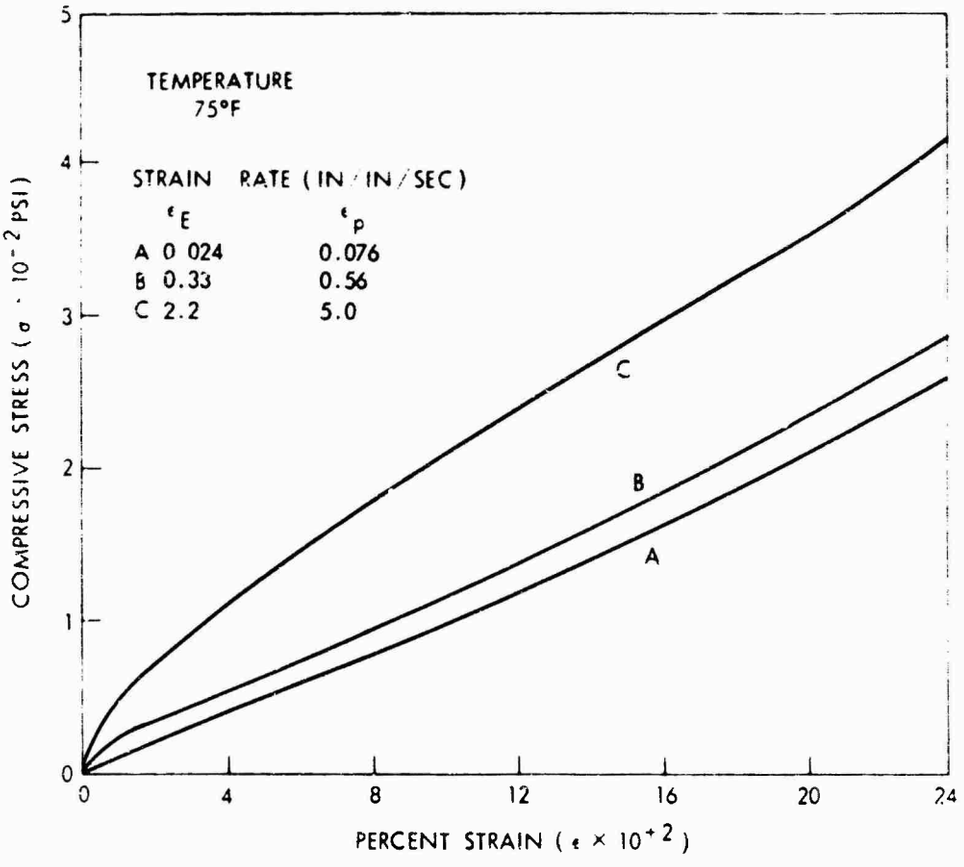

FIG. 19-a DYNAMIC STRESS-STRAIN RELATION OF RUBBER COMPOSITION PS-3

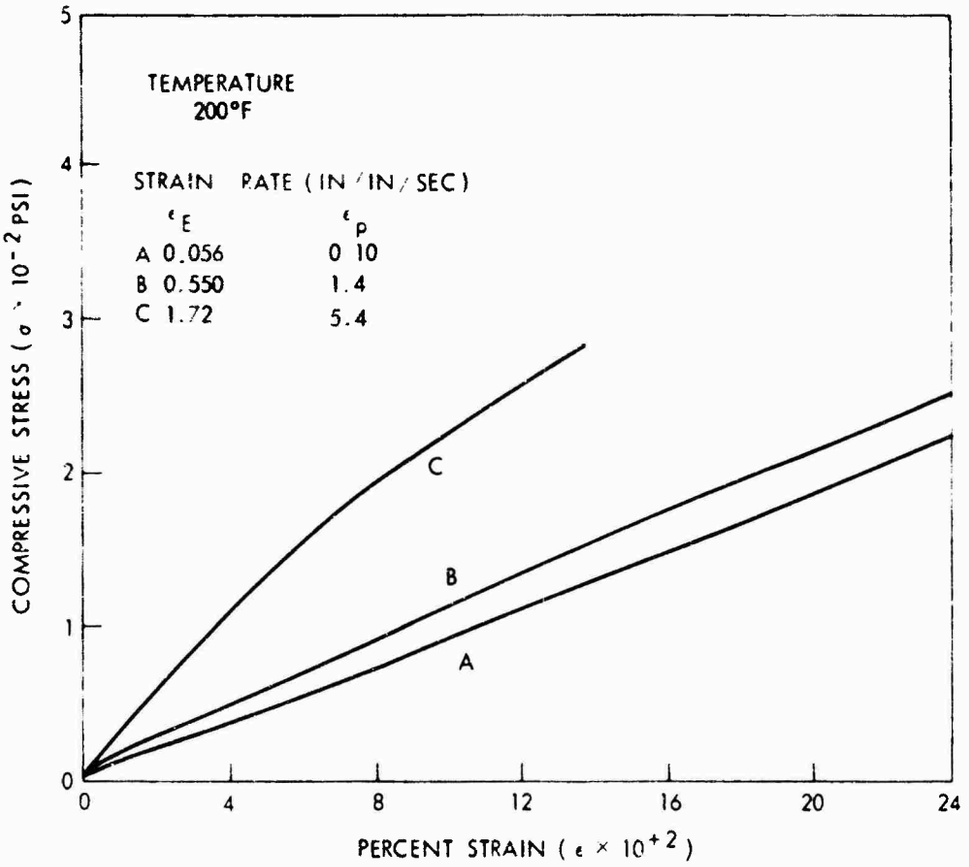

FIG. 19-b DYNAMIC STRESS-STRAIN RELATION OF RUBBER COMPOSITION PS-3

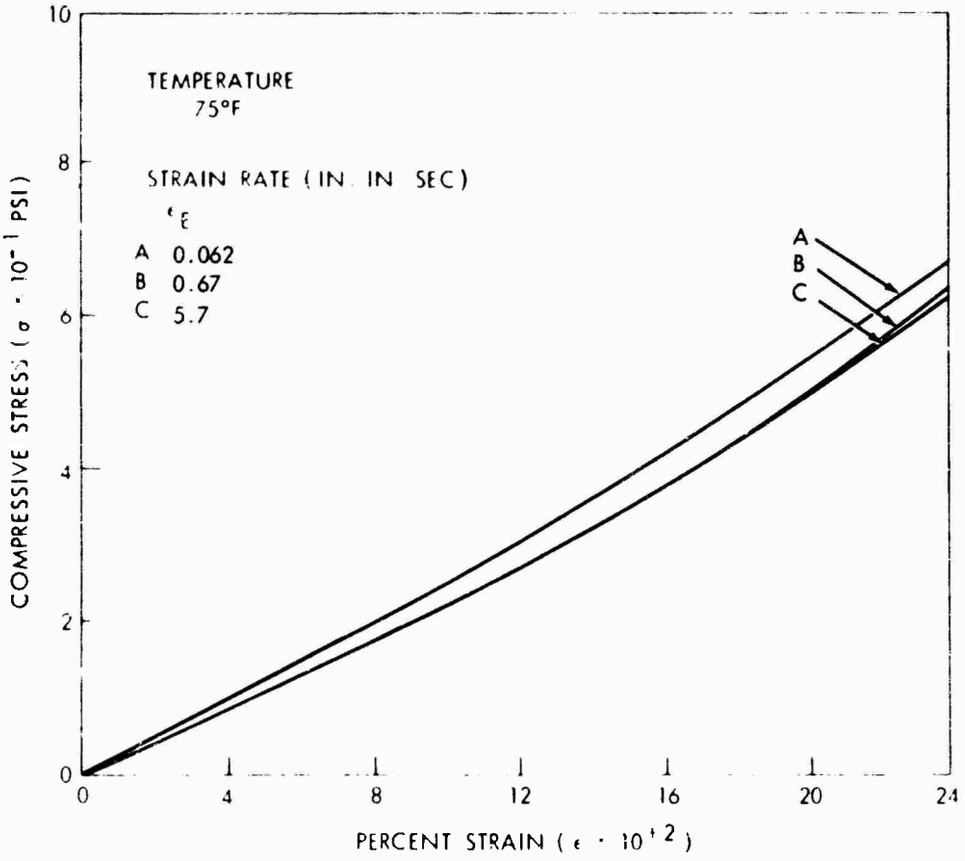

FIG. 20-a DYNAMIC STRESS-STRAIN RELATION OF RUBBER COMPOSITION GRI-218

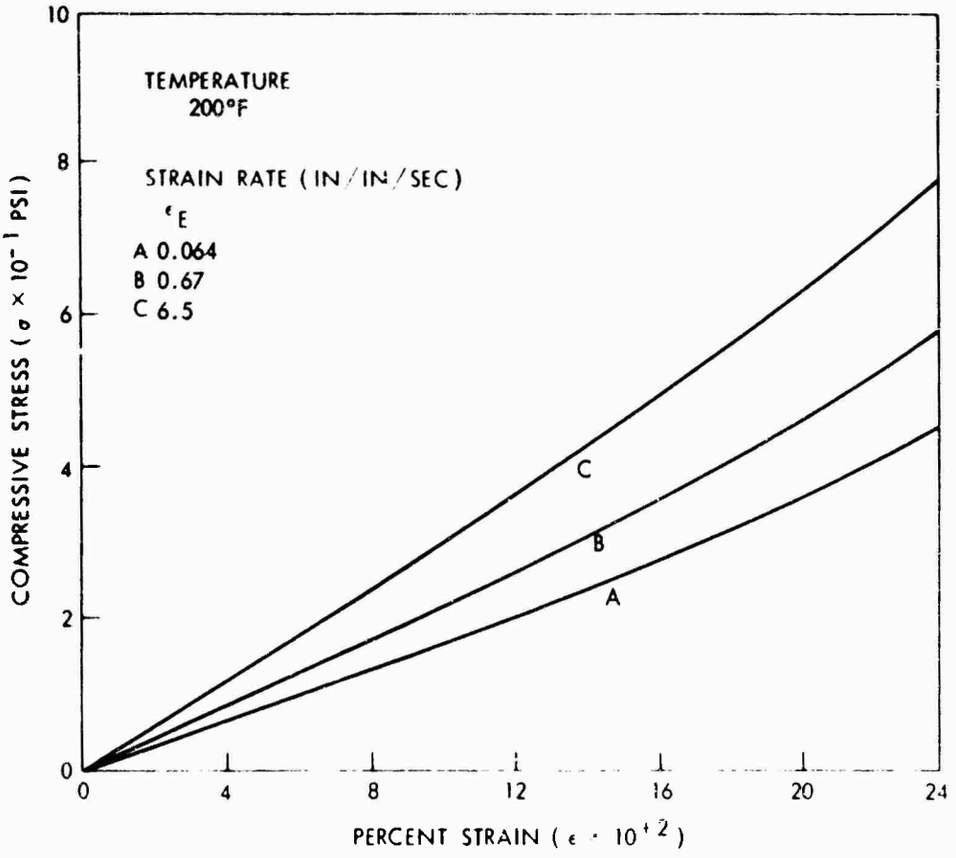

FIG. 20-b DYNAMIC STRESS-STRAIN RELATION OF RUBBER COMPOSITION GRI-218

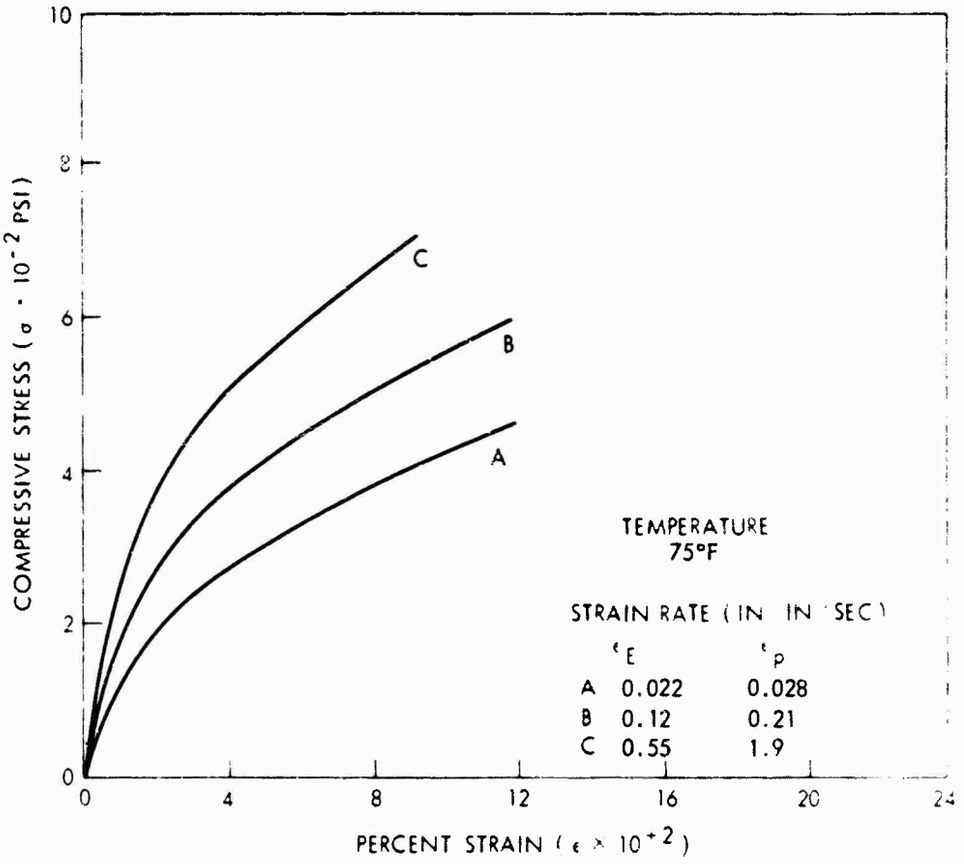

FIG. 21-a DYNAMIC STRESS-STRAIN RELATION OF RUBBER COMPOSITION FM-1

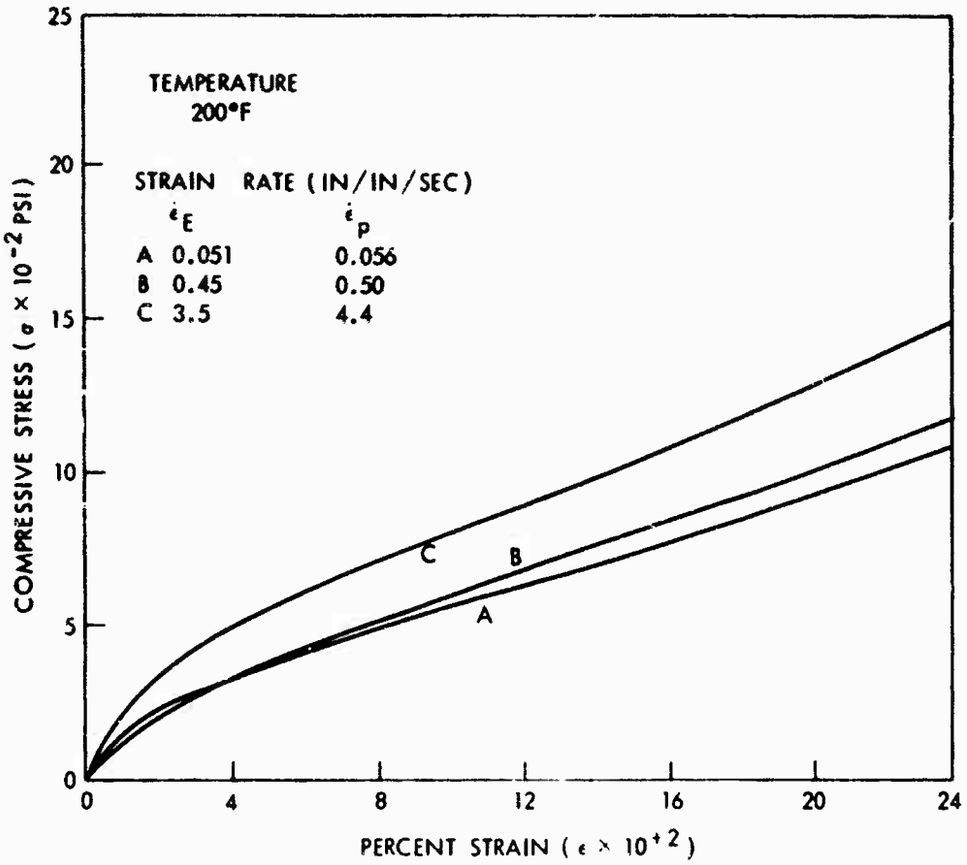

FIG. 21-b DYNAMIC STRESS-STRAIN RELATION OF RUBBER COMPOSITION FM-1

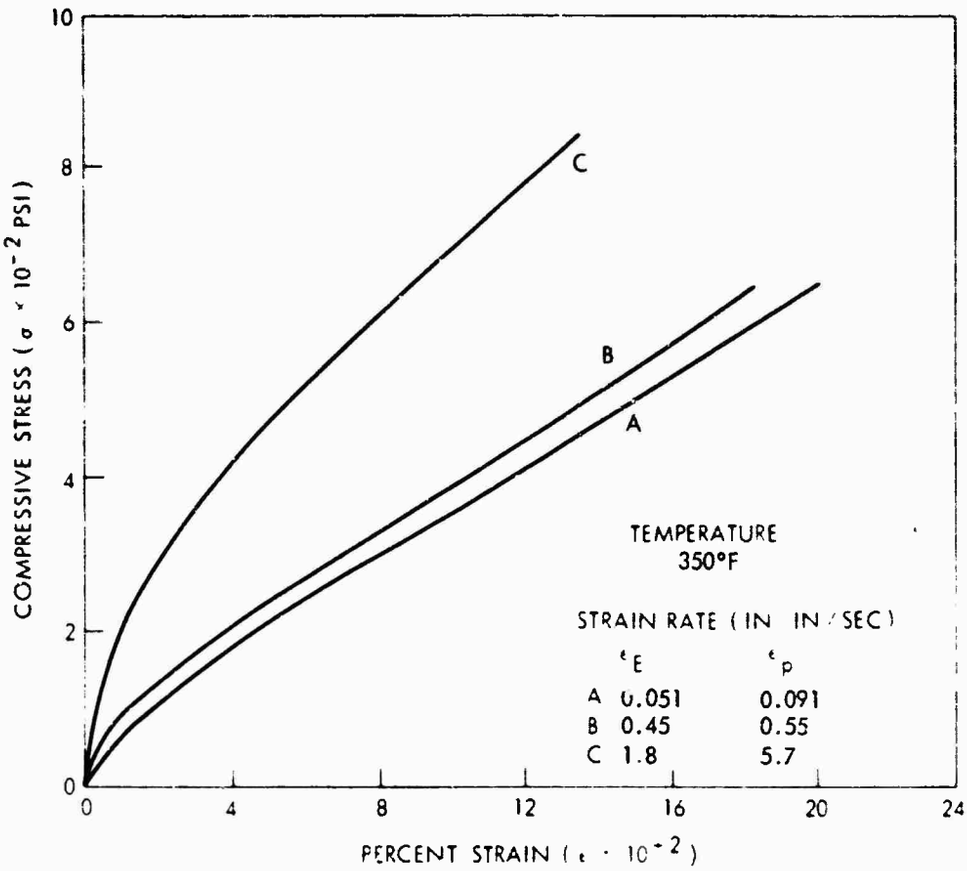

FIG. 2[illegible]-c DYNAMIC STRESS-STRAIN RELATION OF RUBBER COMPOSITION FM-1

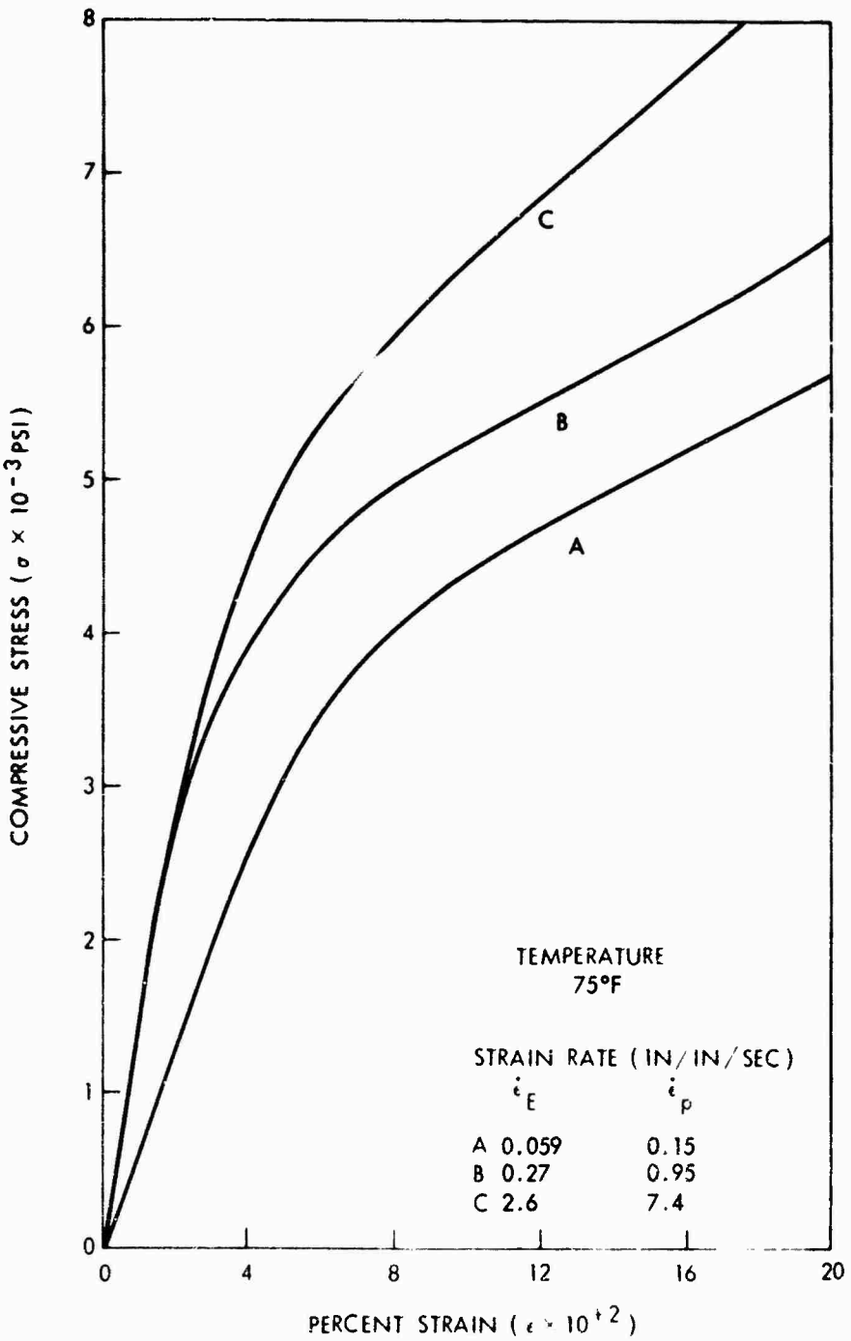

FIG. 22-a DYNAMIC STRESS-STRAIN RELATION OF ALATHON-7020

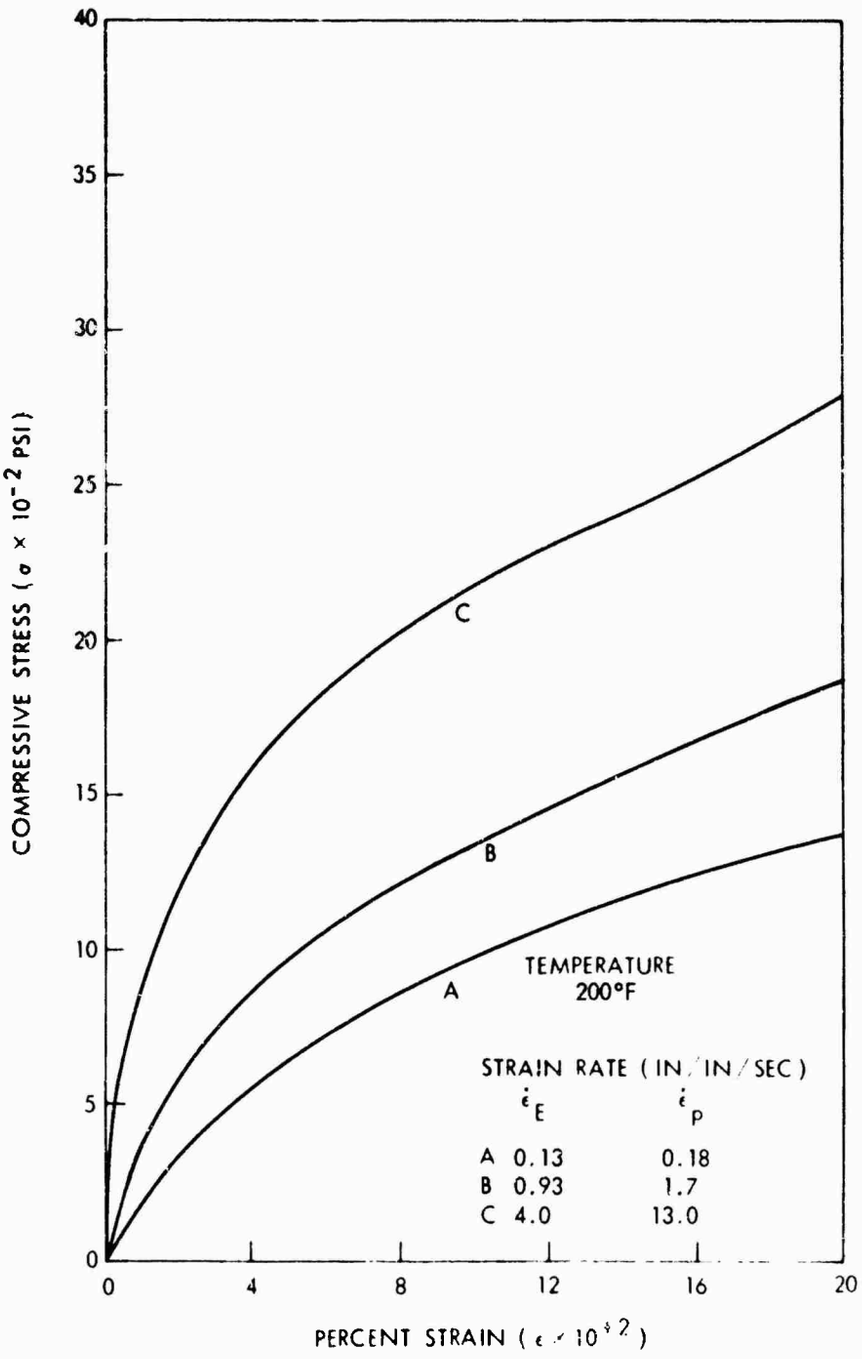

FIG. 22-b DYNAMIC STRESS-STRAIN RELATION OF ALATHON 7020

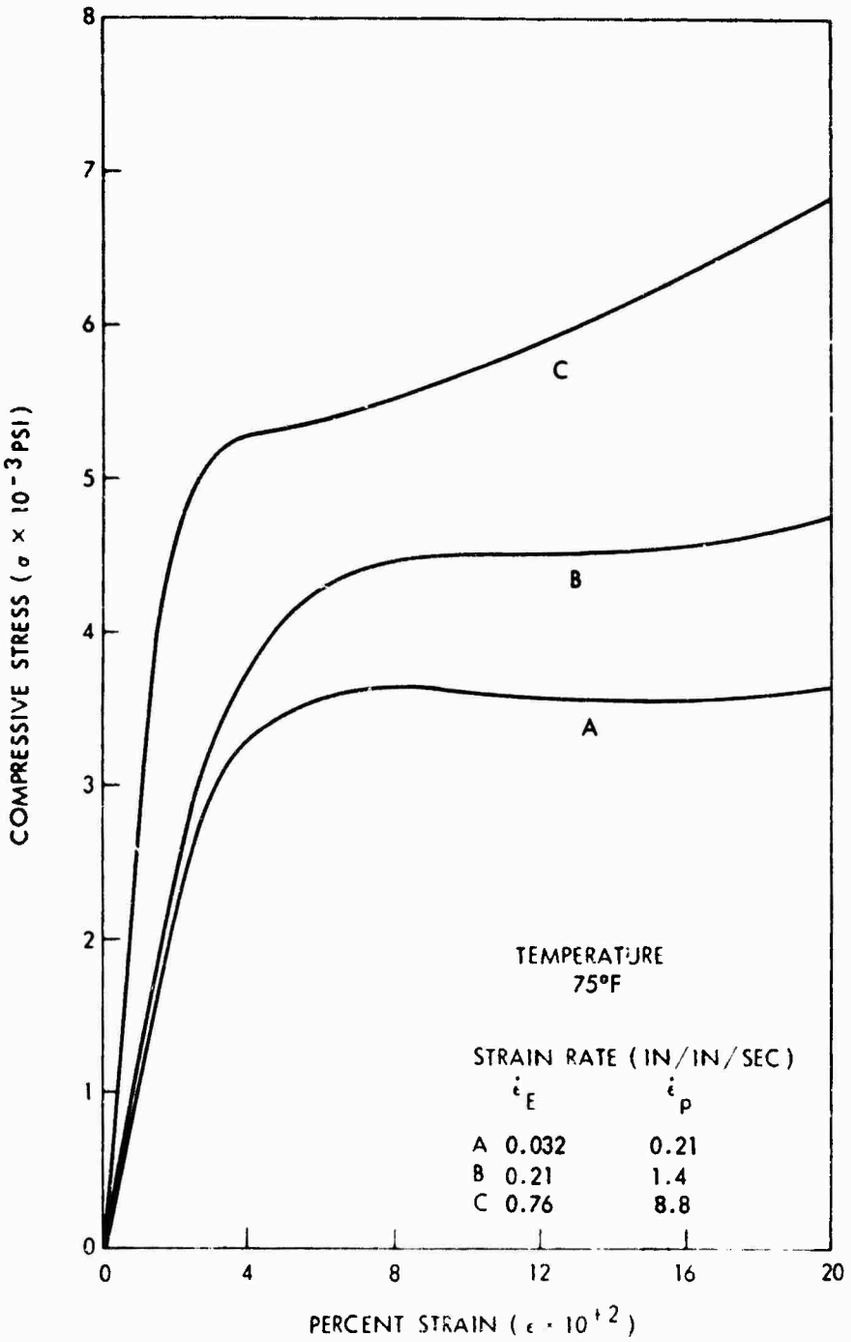

FIG. 23-a DYNAMIC STRESS-STRAIN RELATION OF TENITE 265A-372005

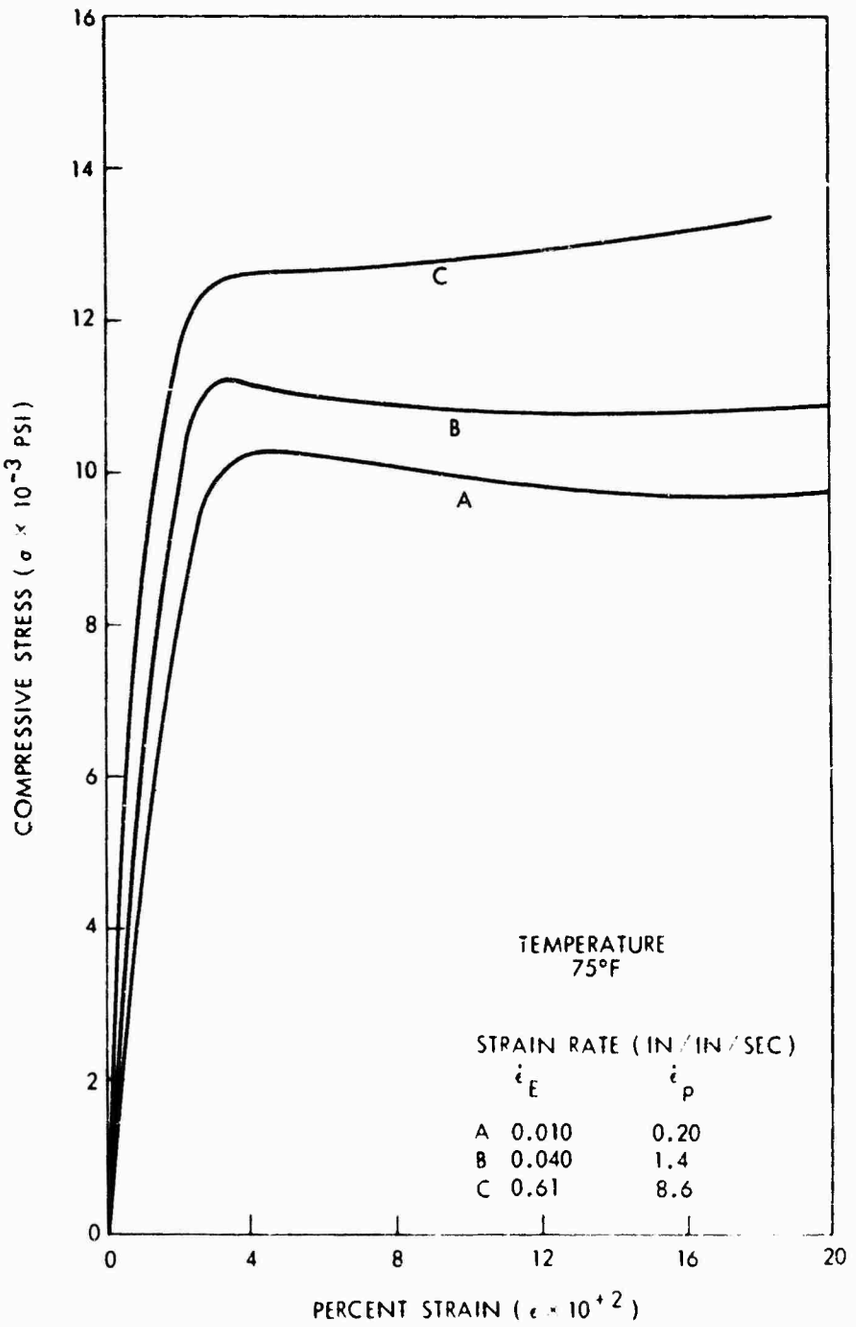

FIG. 24-a DYNAMIC STRESS-STRAIN RELATION OF CYCOLAC T-1000

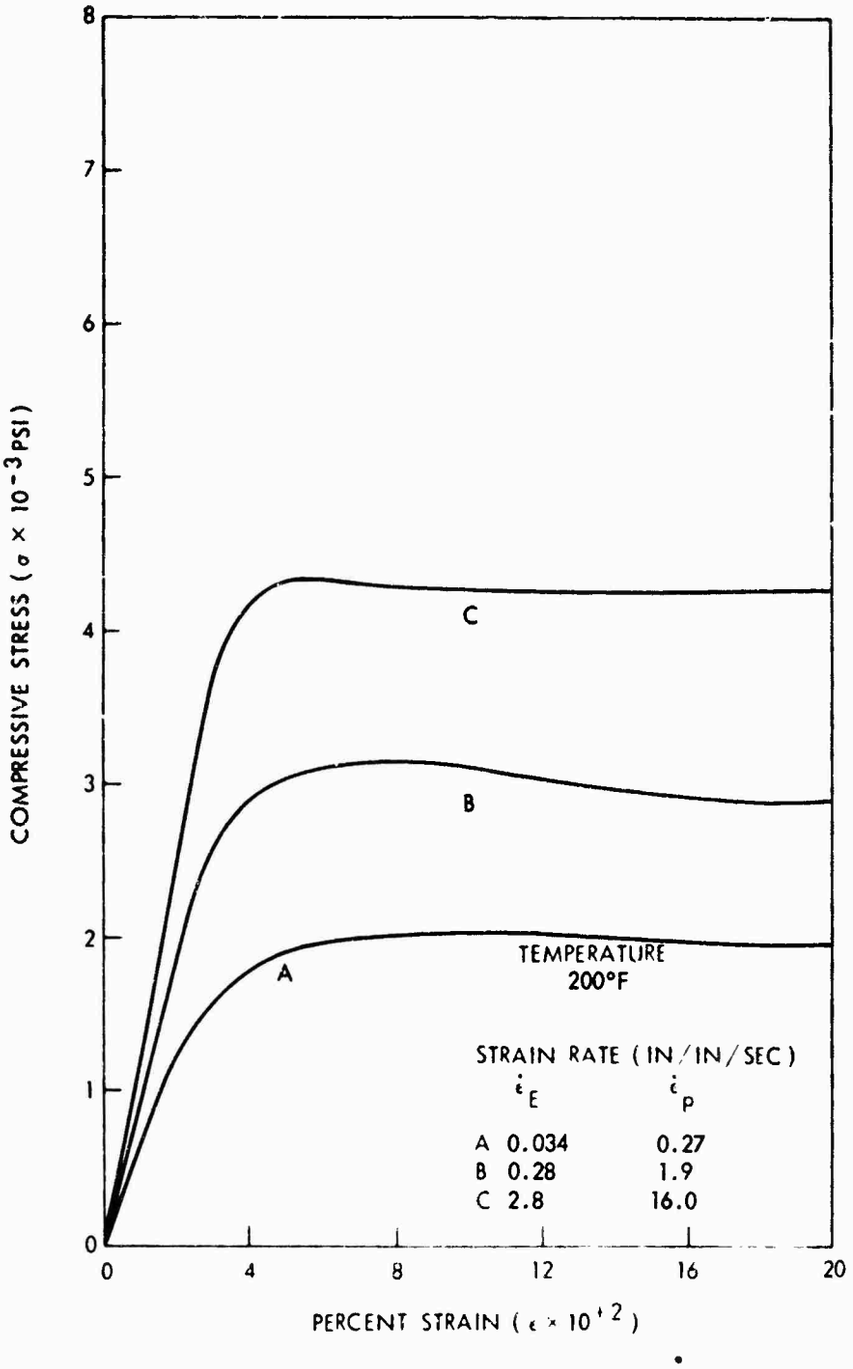

FIG. 24-b DYNAMIC STRESS-STRAIN RELATION OF CYCOLAC T-1000

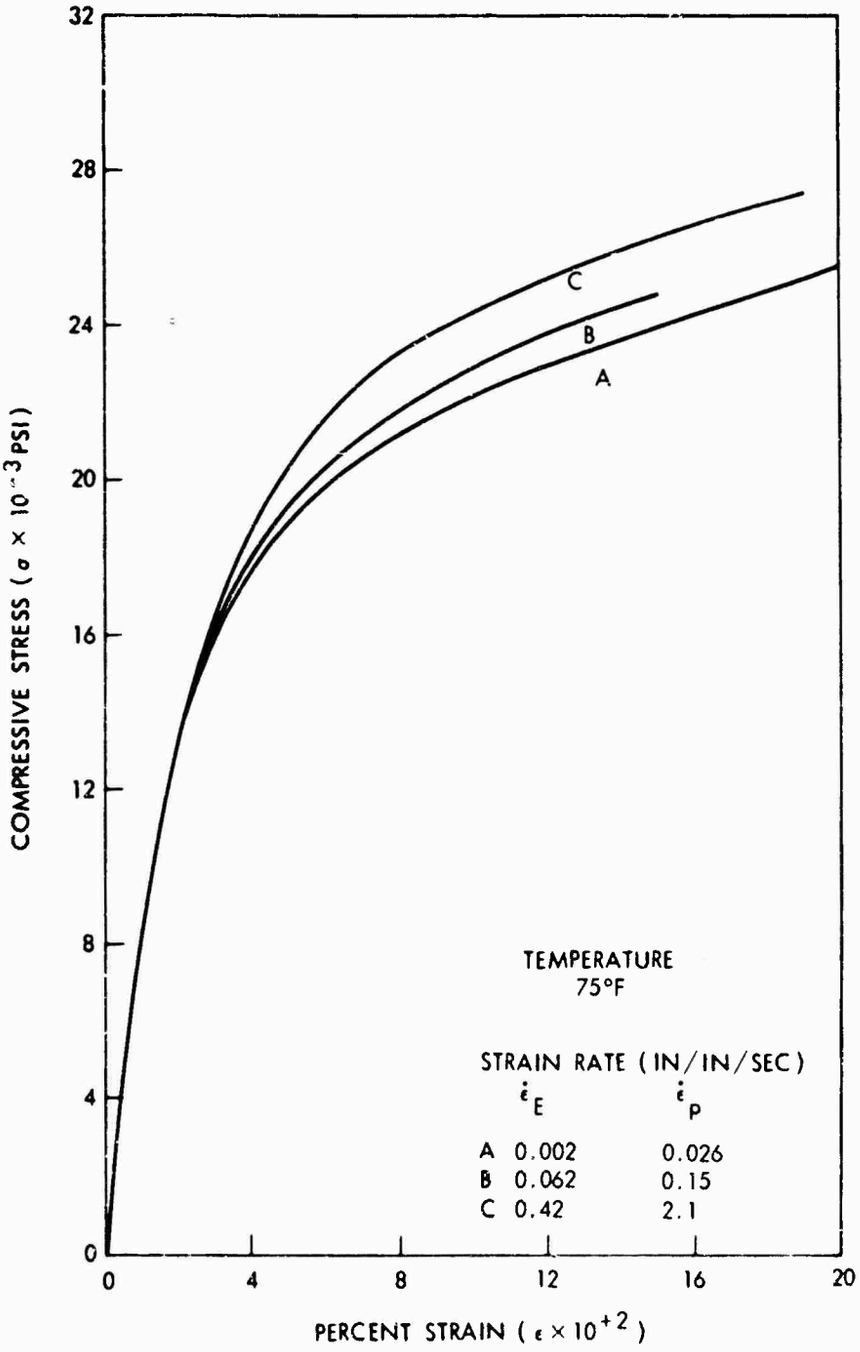

FIG. 25-a DYNAMIC STRESS-STRAIN RELATION OF DELRIN 500

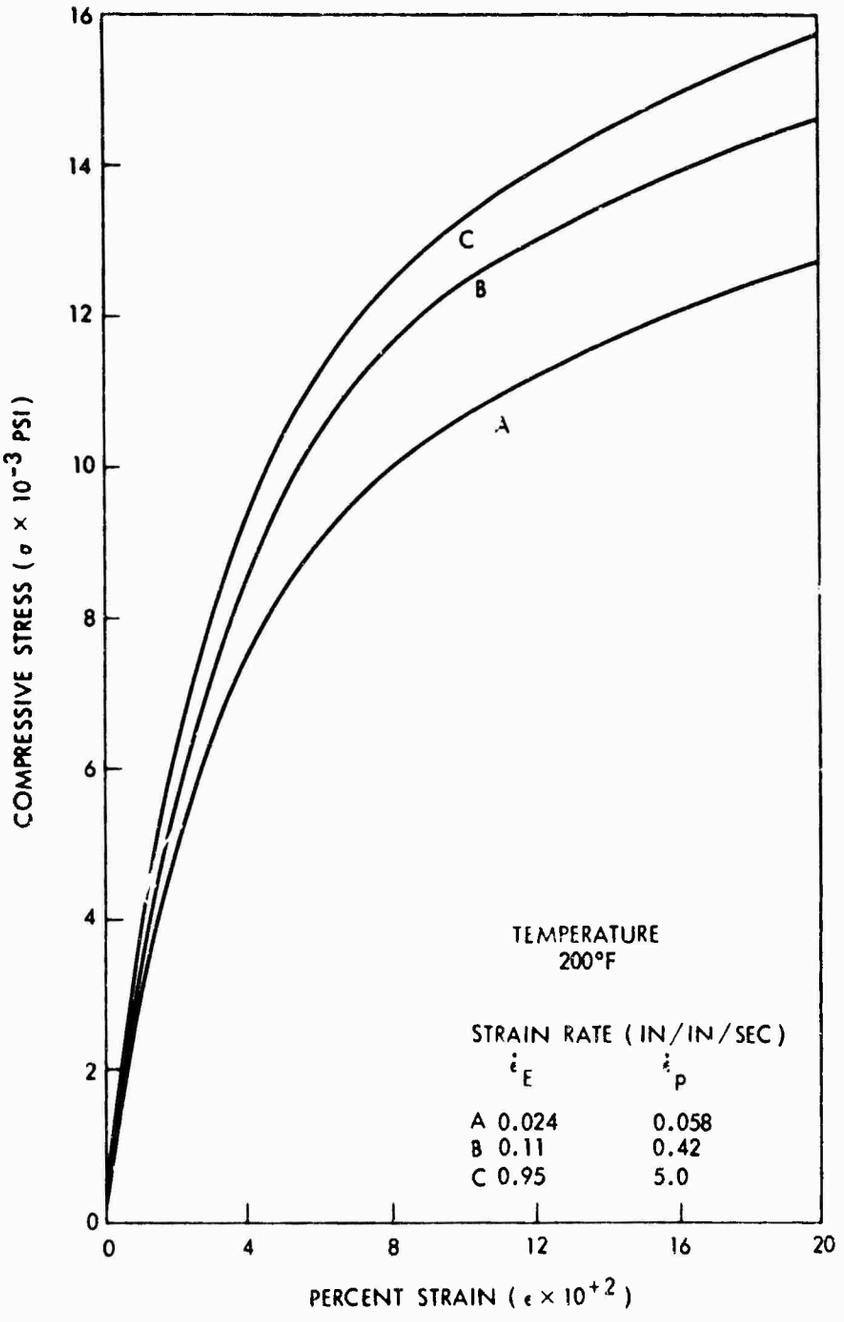

FIG. 25-b DYNAMIC STRESS-STRAIN RELATION OF DELRIN 500

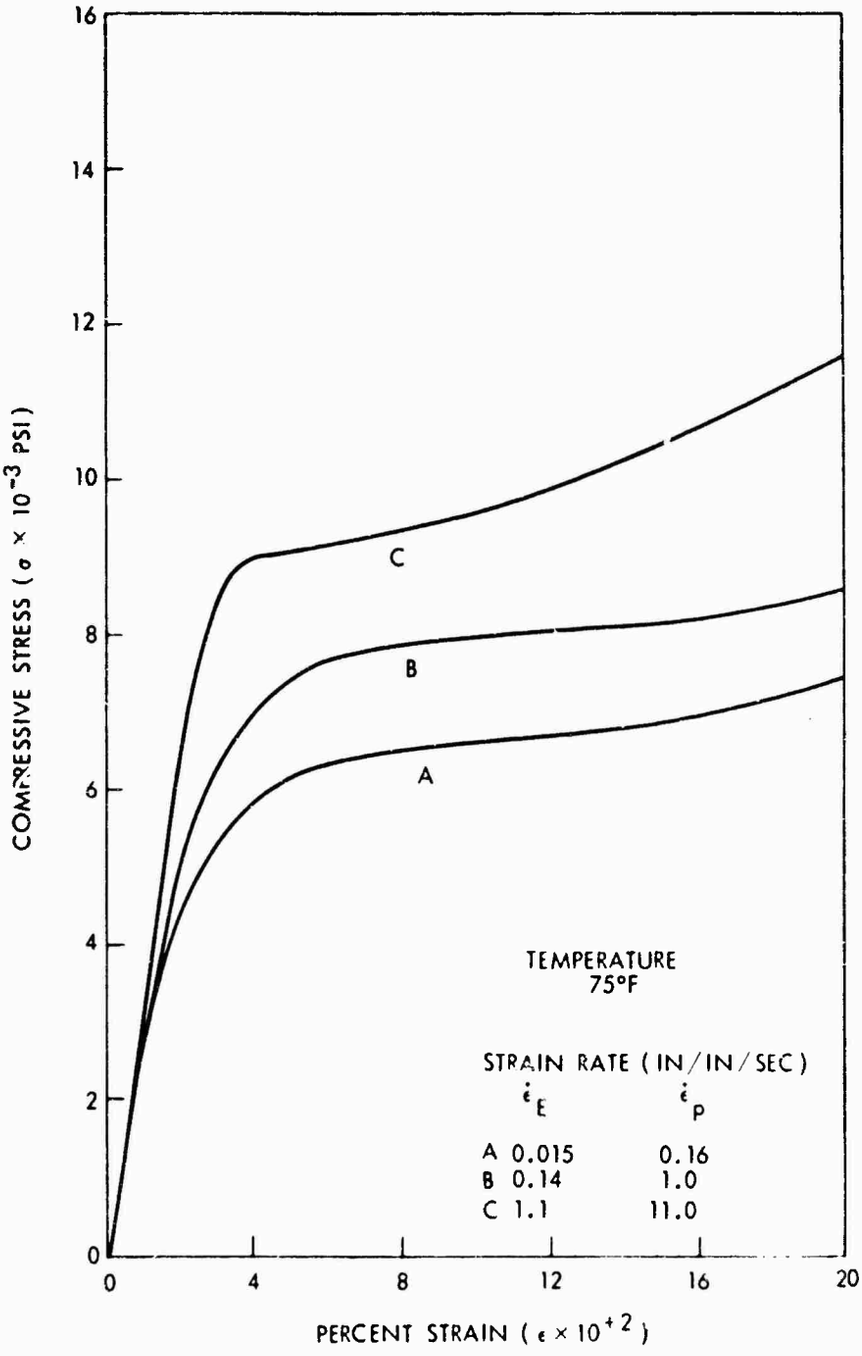

FIG. 26-a DYNAMIC STRESS-STRAIN RELATION OF ETHOCEL Q303.4

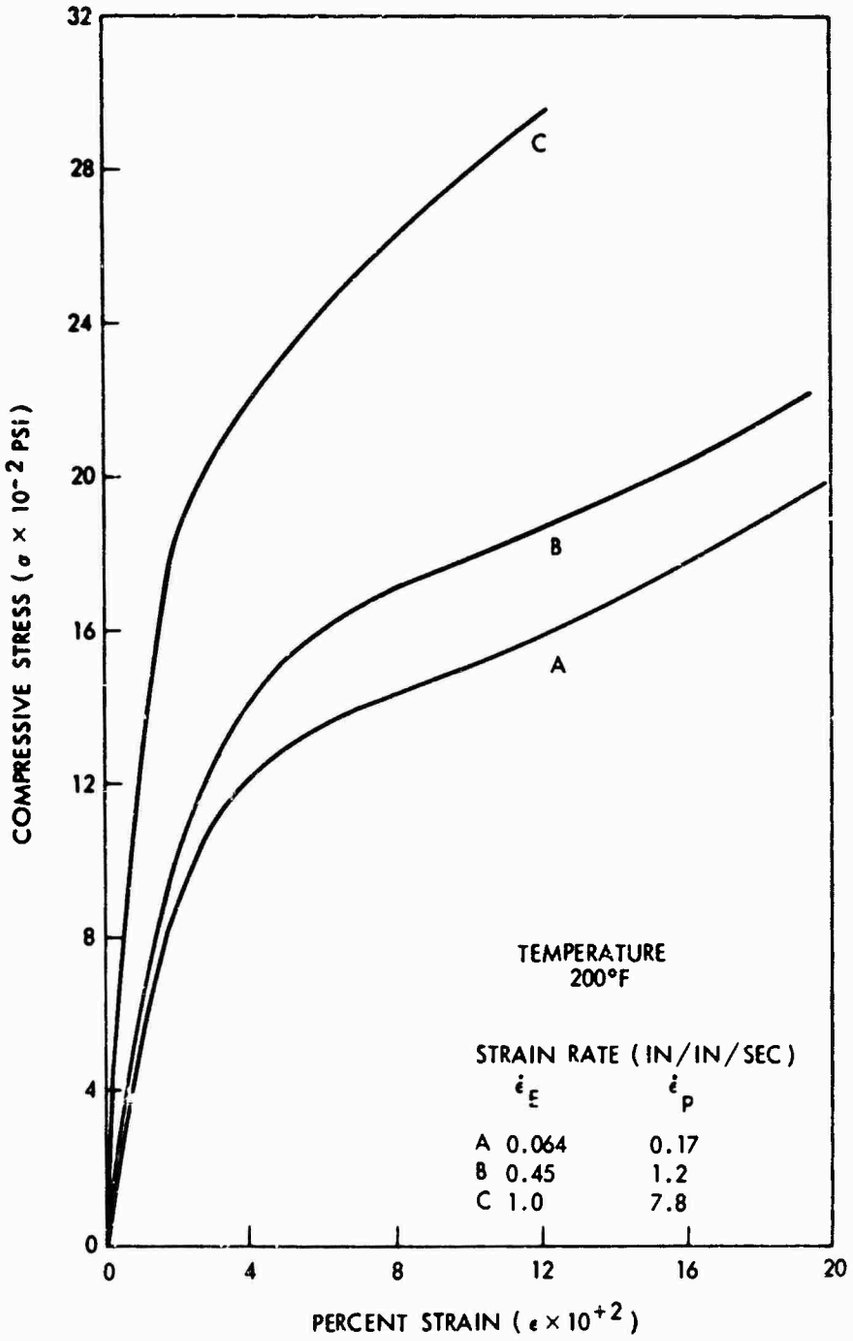

FIG. 26-b DYNAMIC STRESS-STRAIN RELATION OF ETHOCEL Q303.4

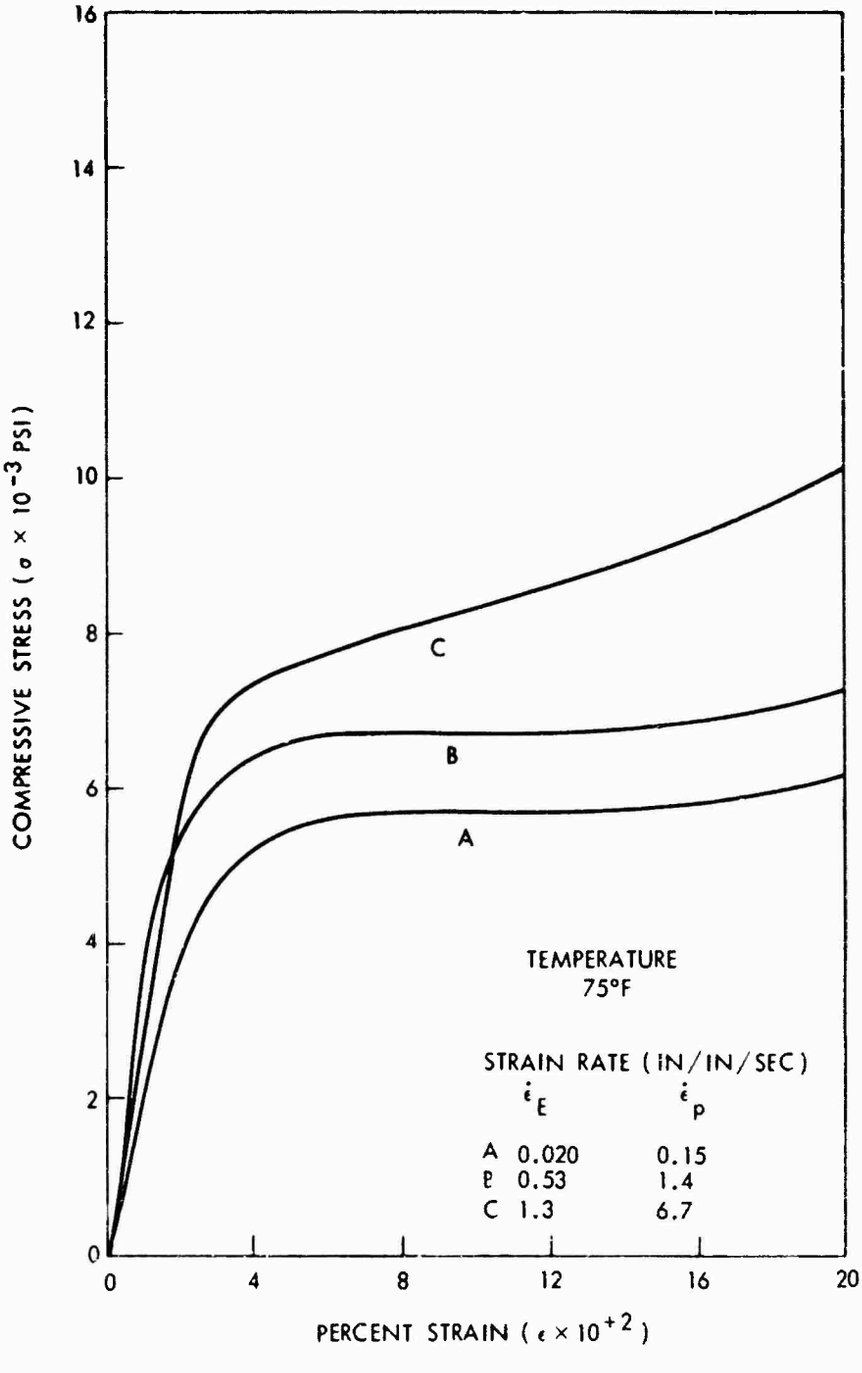

FIG. 27-a DYNAMIC STRESS-STRAIN RELATION OF ETHYLCELLULOSE

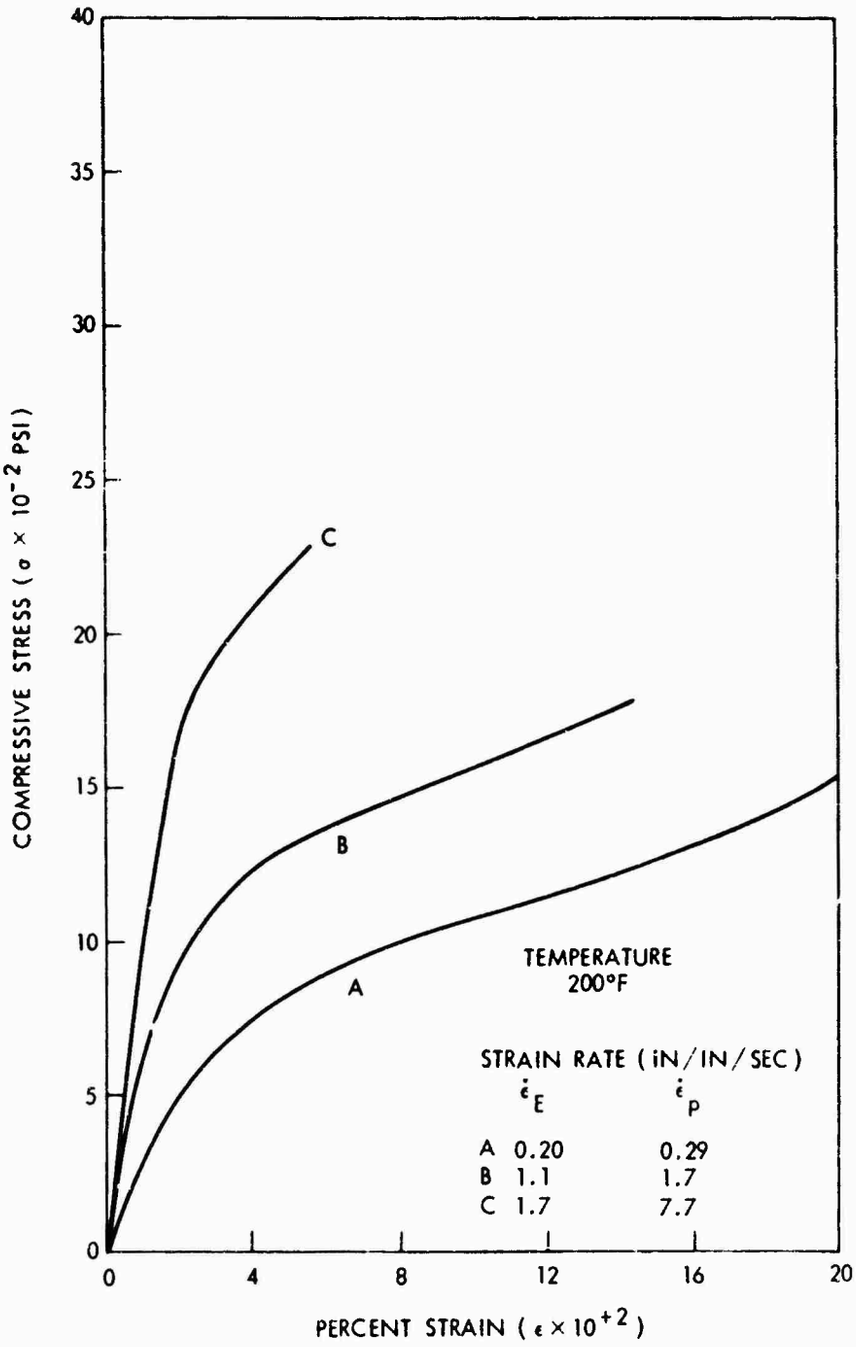

FIG. 27-b DYNAMIC STRESS-STRAIN RELATION OF ETHYLCELLULOSE

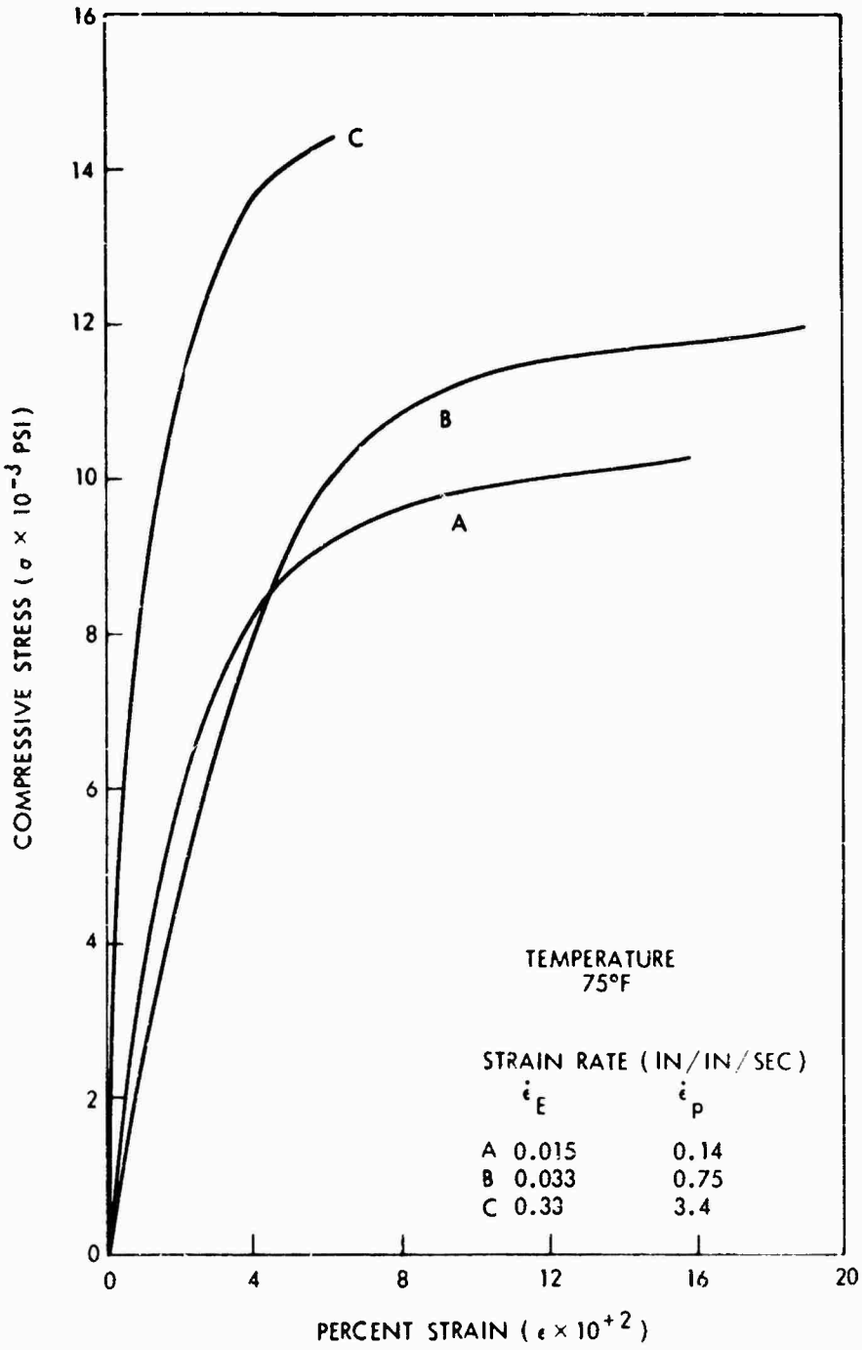

FIG. 28-a DYNAMIC STRESS-STRAIN RELATION OF KEL-F

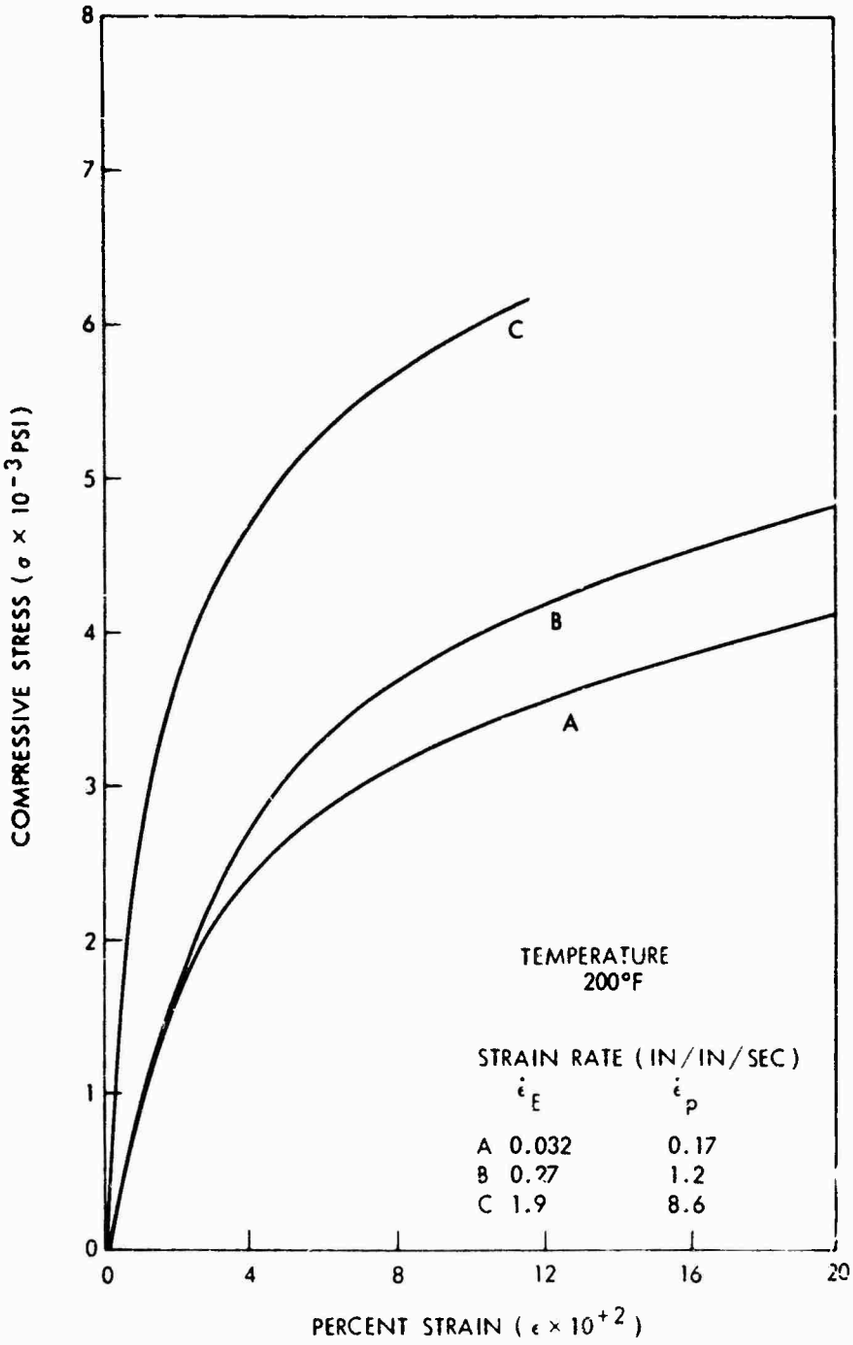

FIG. 28-b DYNAMIC STRESS-STRAIN RELATION OF KEL-F

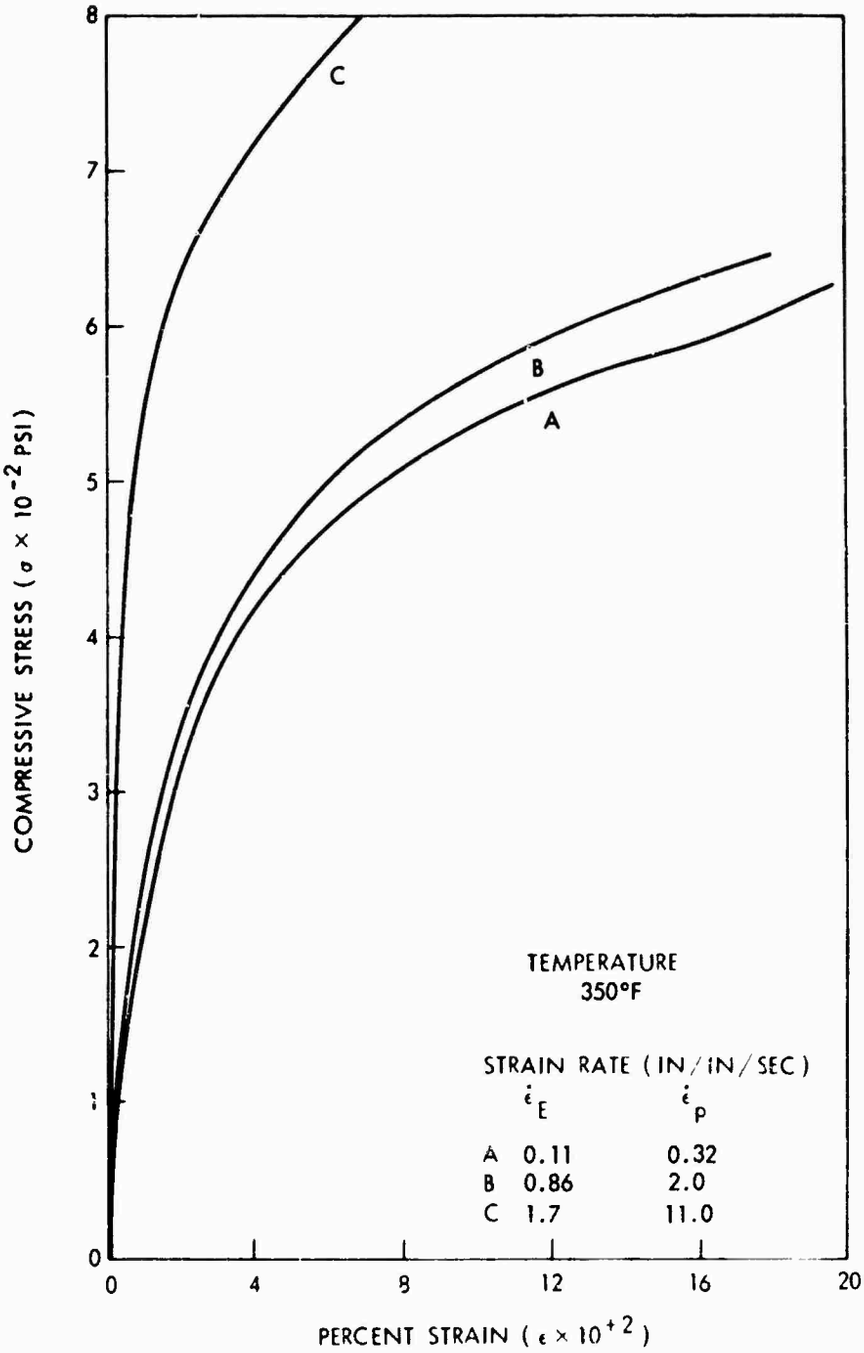

FIG. 28-c DYNAMIC STRESS-STRAIN RELATION OF KEL-F

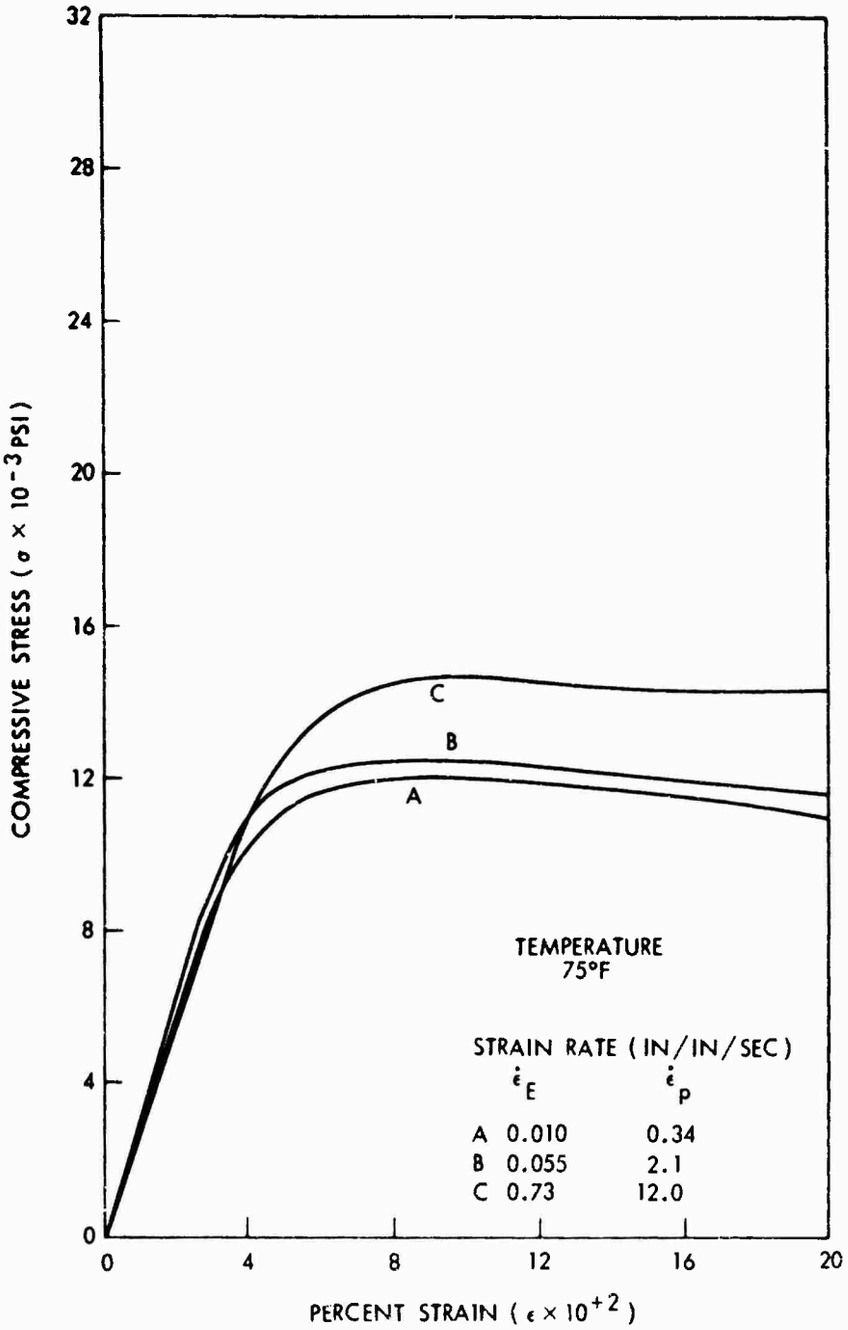

FIG. 29-a DYNAMIC STRESS-STRAIN RELATION OF LEXAN

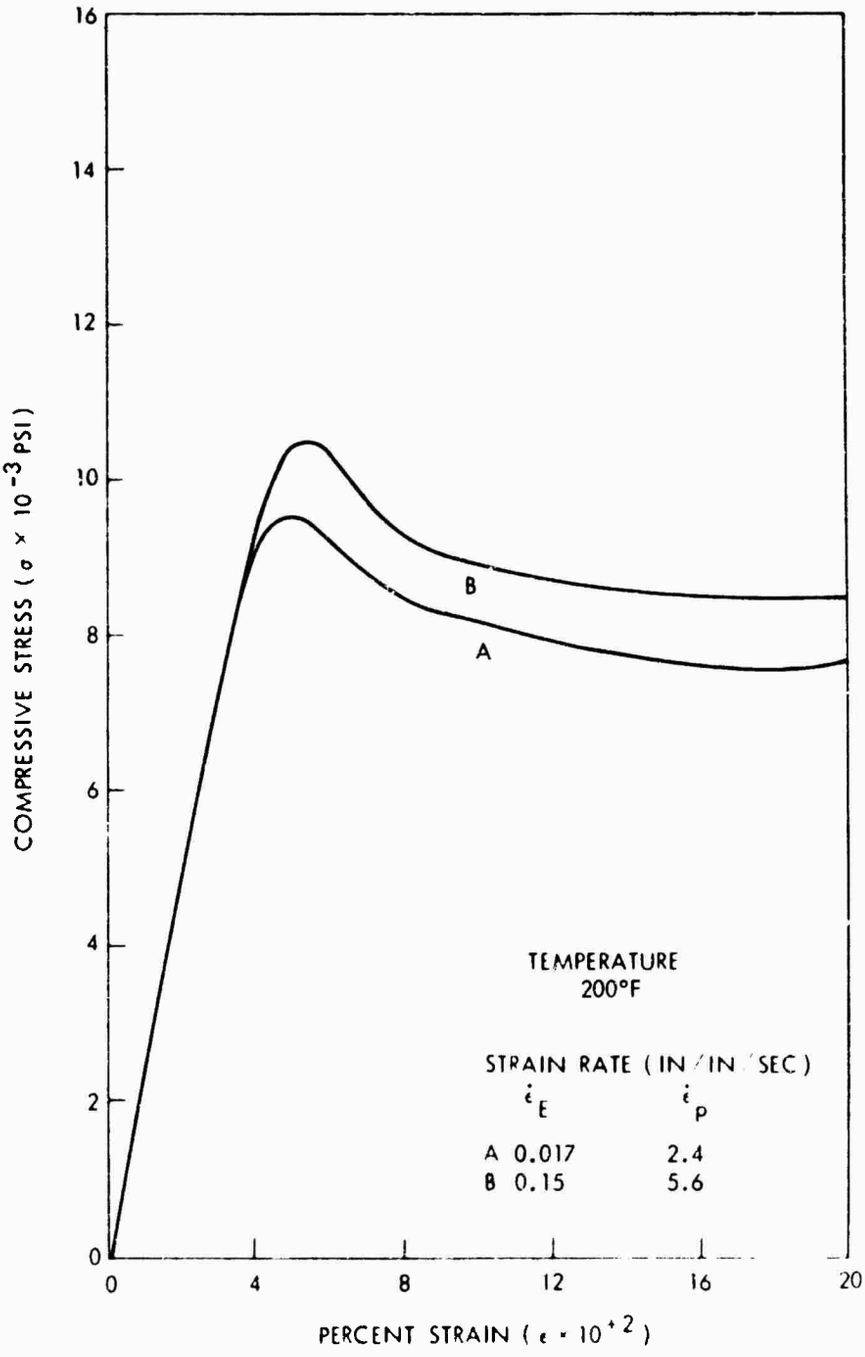

FIG. 29-b DYNAMIC STRESS-STRAIN RELATION OF LEXAN

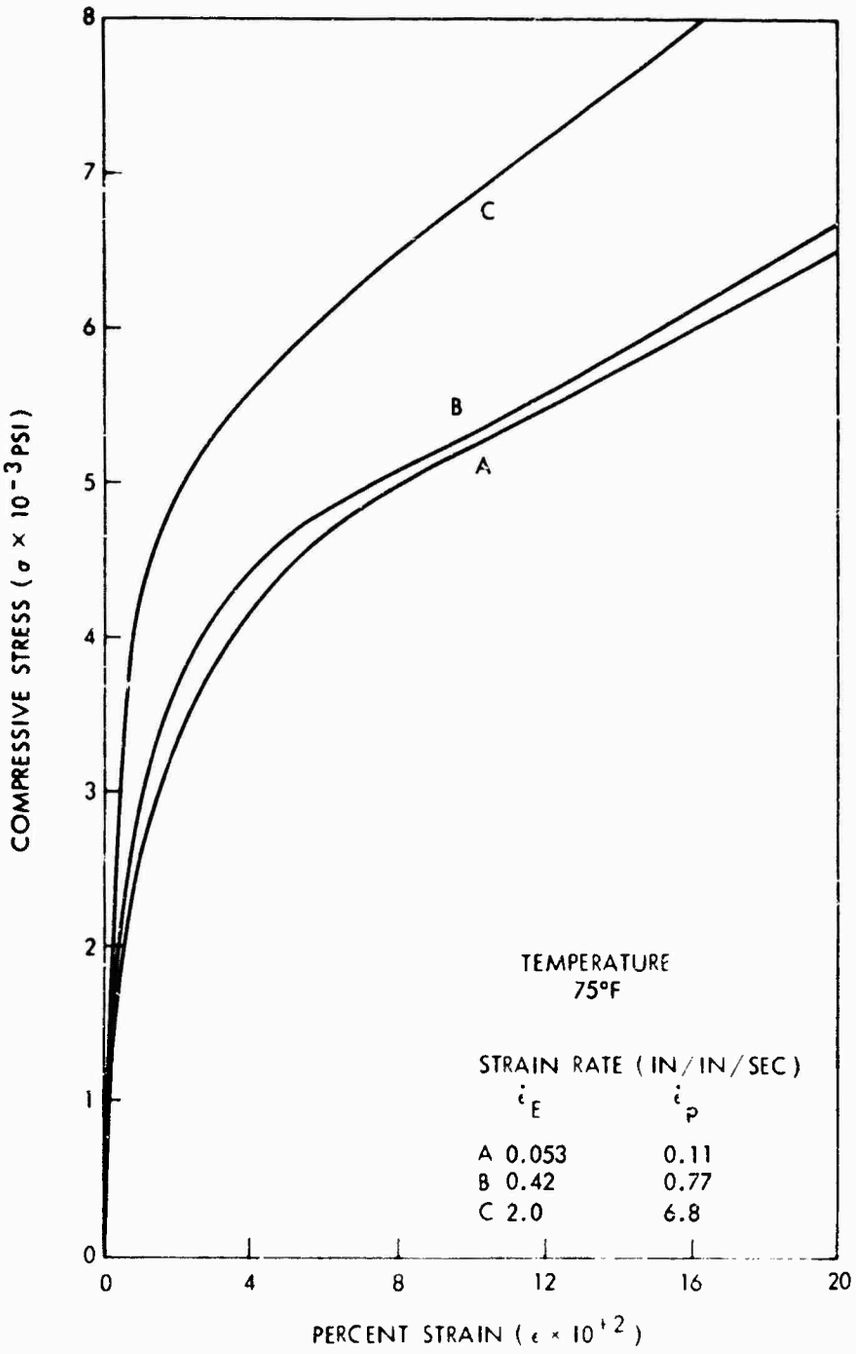

FIG. 30-a DYNAMIC STRESS-STRAIN RELATION OF MARLEX 5005

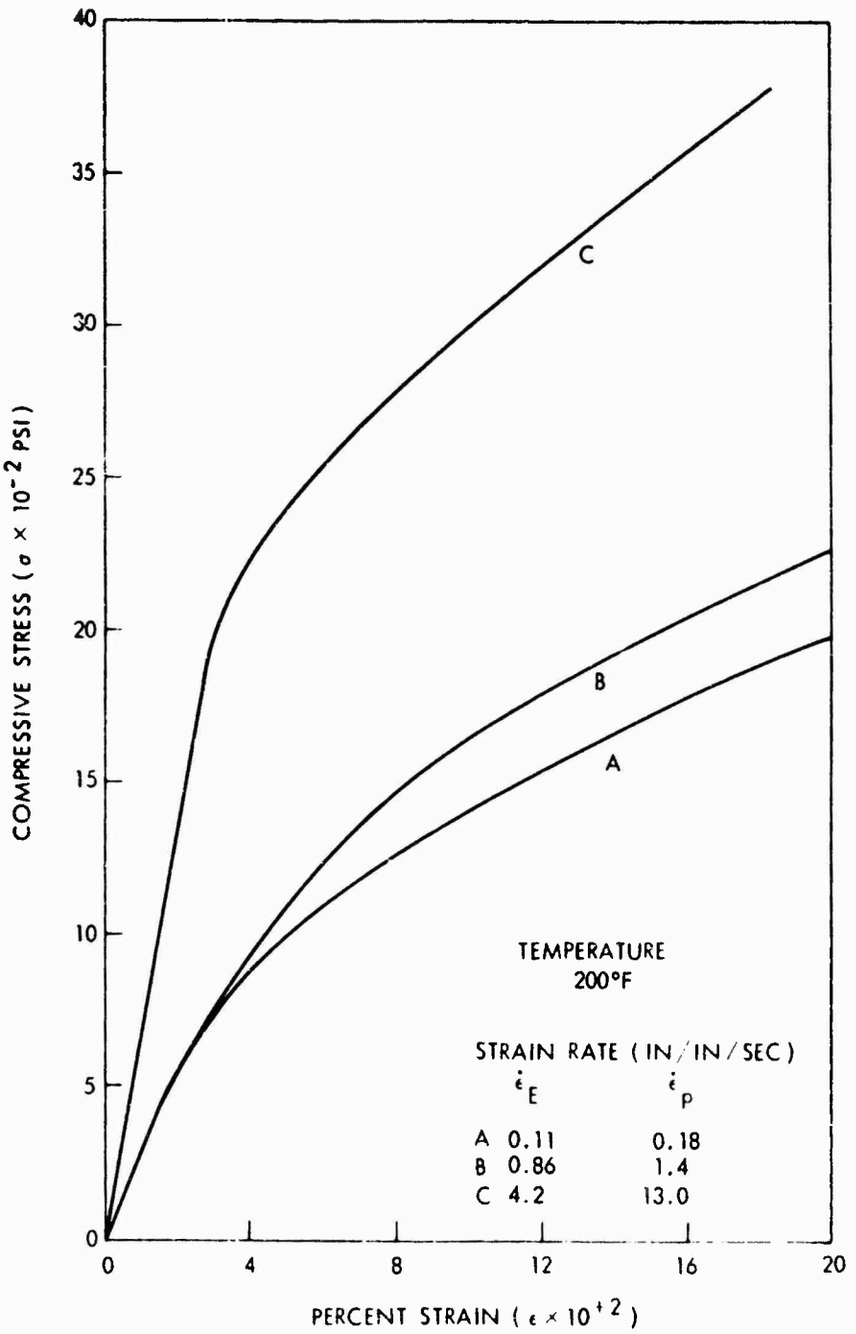

FIG. 30-b DYNAMIC STRESS-STRAIN RELATION OF MARLEX 5005

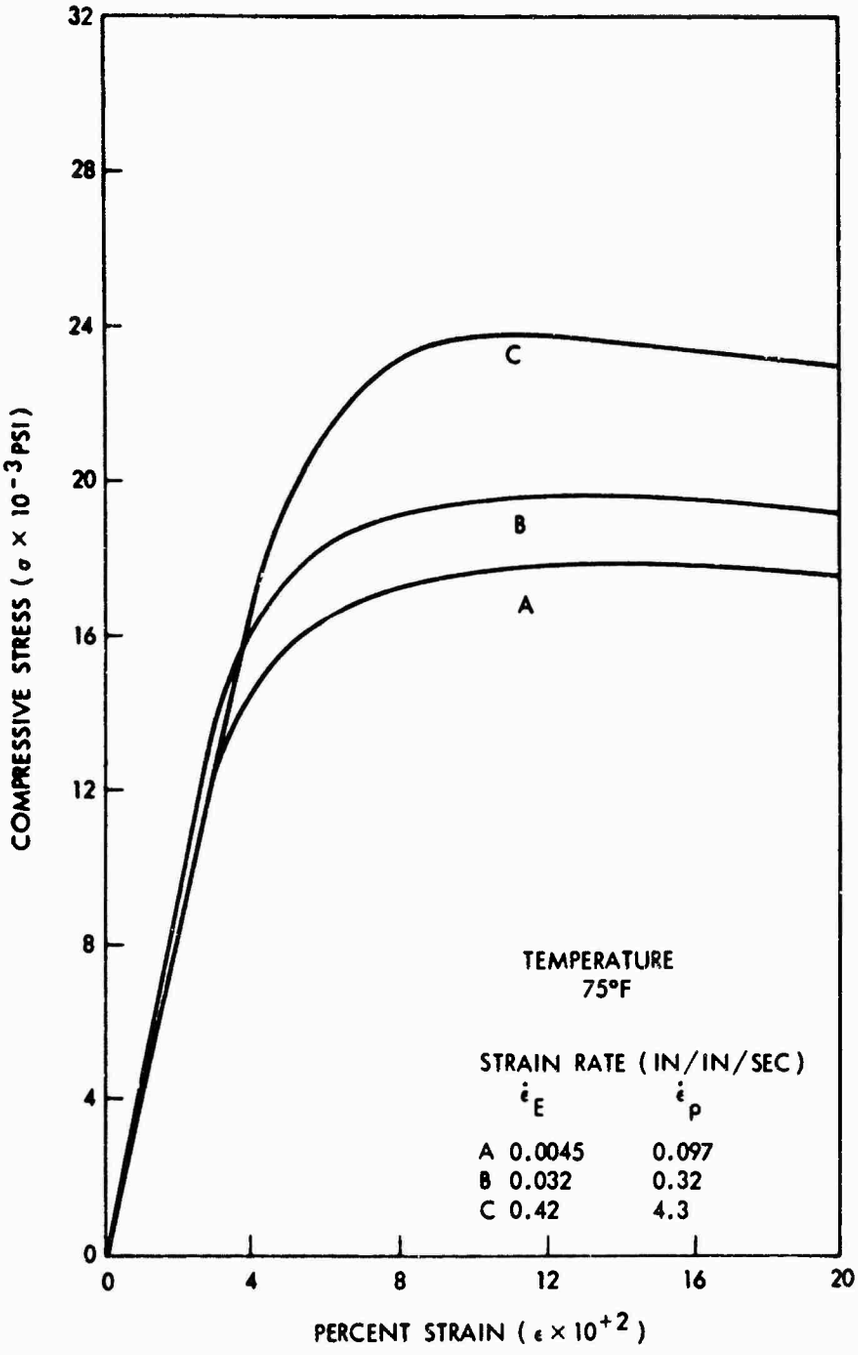

FIG. 31-a DYNAMIC STRESS-STRAIN RELATION OF PLEXIGLASS VS

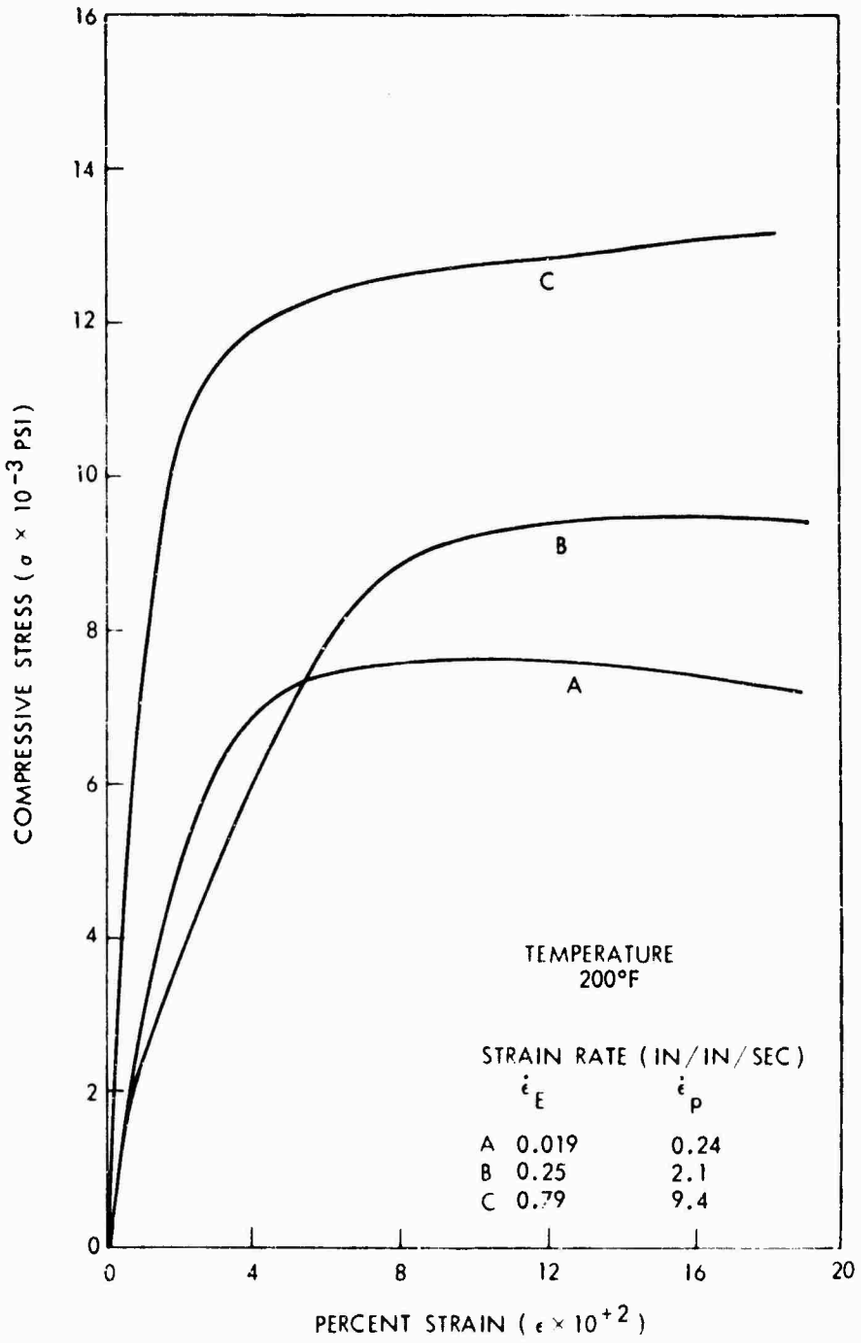

FIG. 31-b DYNAMIC STRESS-STRAIN RELATION OF PLEXIGLASS VS

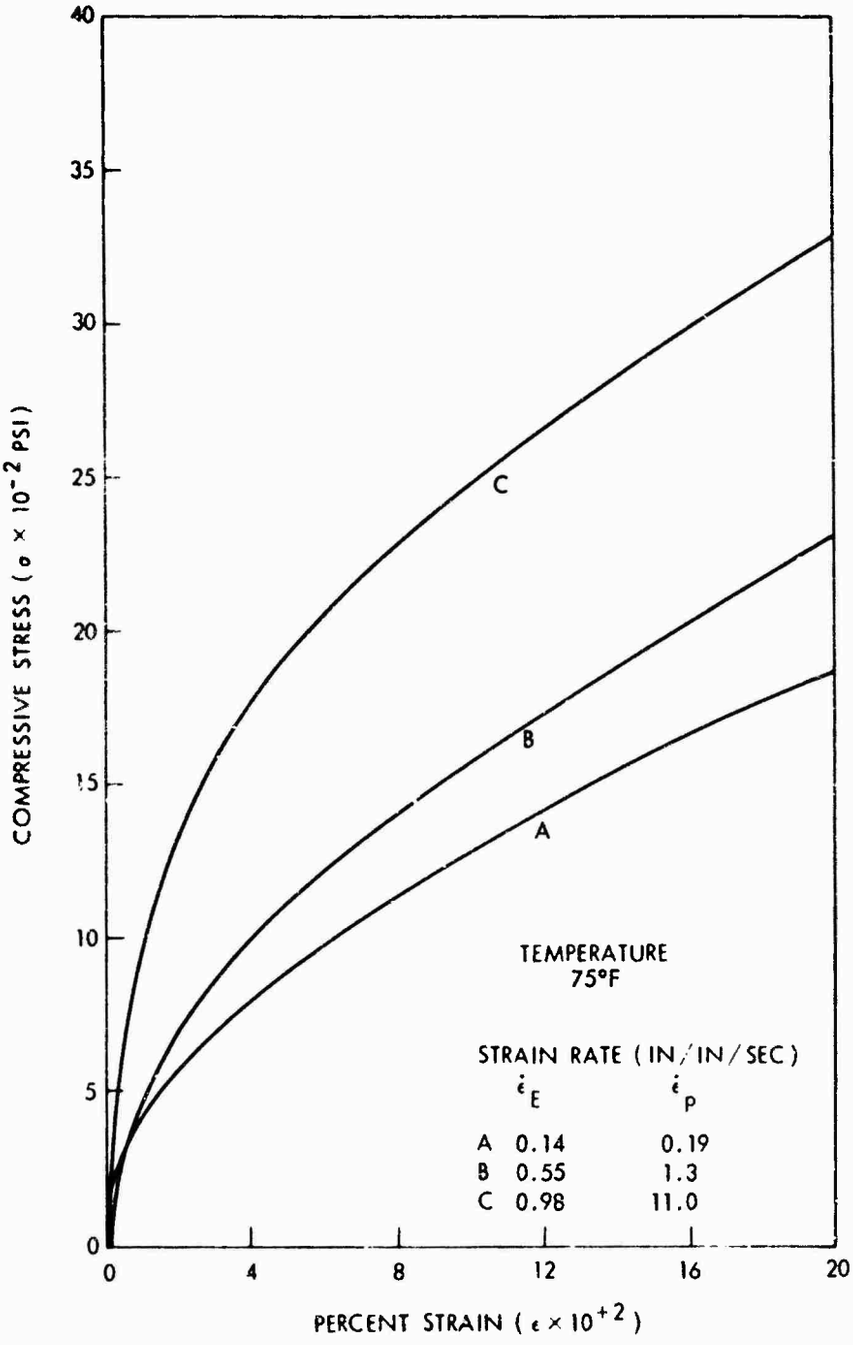

FIG. 32-a DYNAMIC STRESS-STRAIN RELATION OF POLYETHYLENE-DYLT

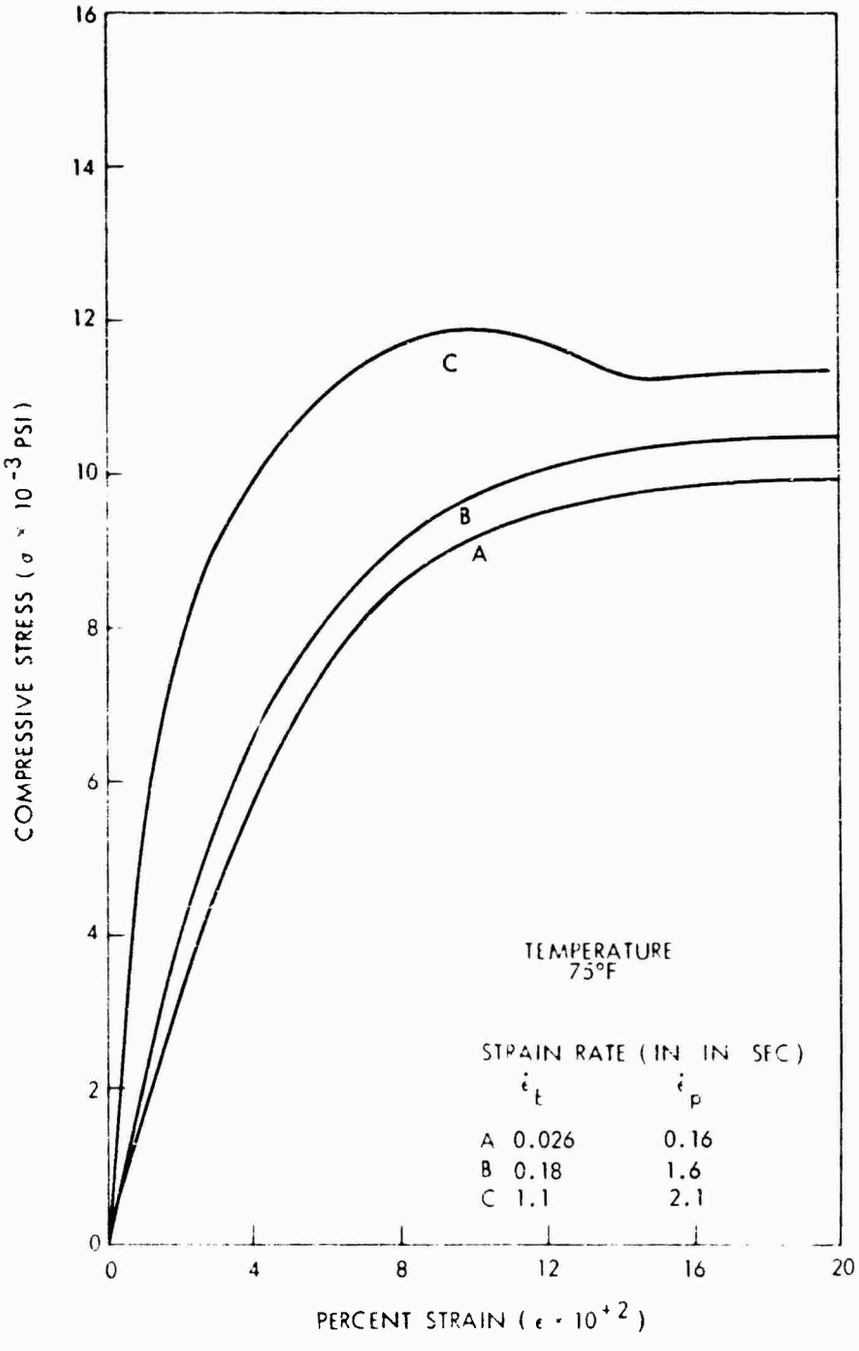

FIG. 33-a DYNAMIC STRESS-STRAIN RELATION OF POLYPROPYLENE 1014

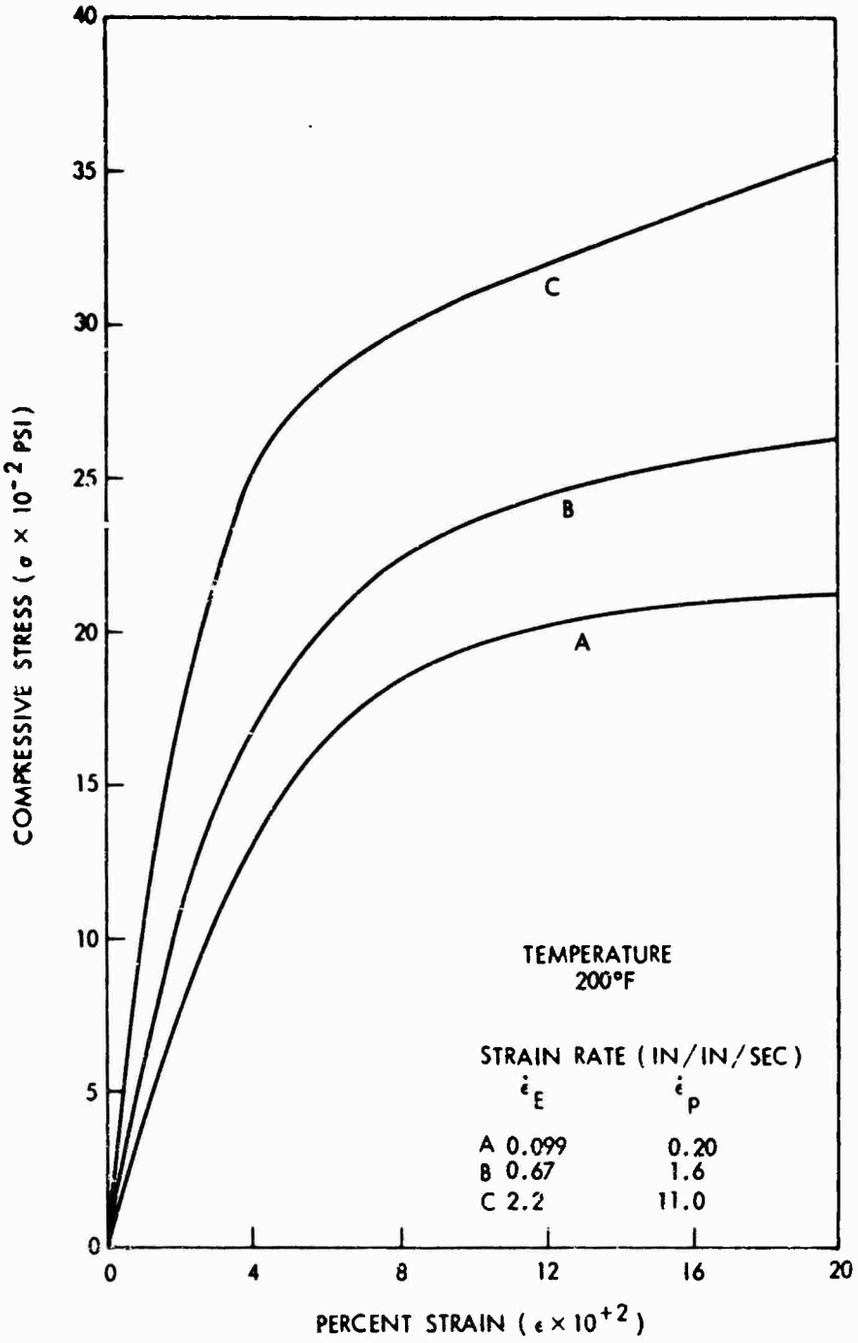

FIG. 33-b DYNAMIC STRESS-STRAIN RELATION OF POLYPROPYLENE 1014

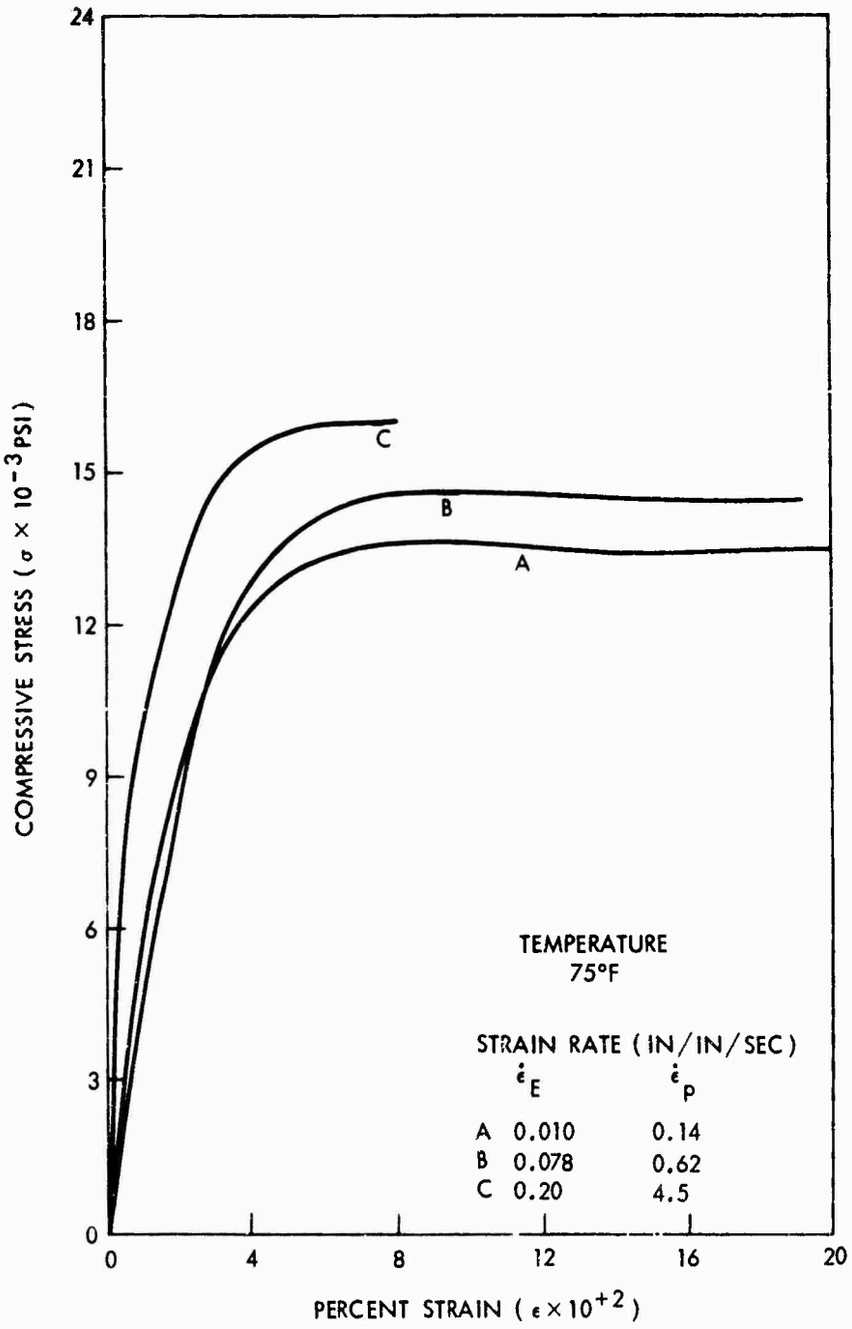

FIG. 34-a DYNAMIC STRESS-STRAIN RELATION OF PPO

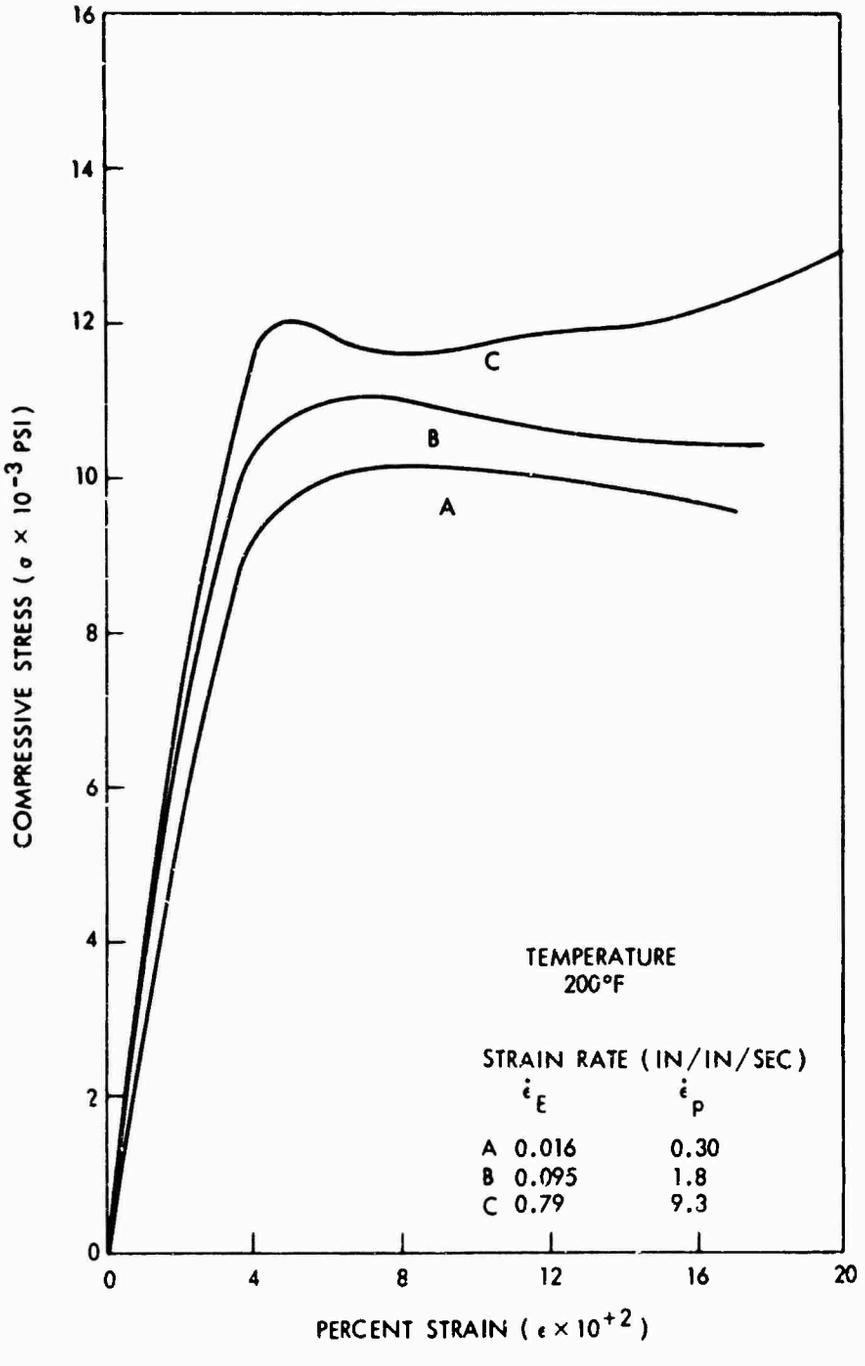

FIG. 34-b DYNAMIC STRESS-STRAIN RELATION OF PPO

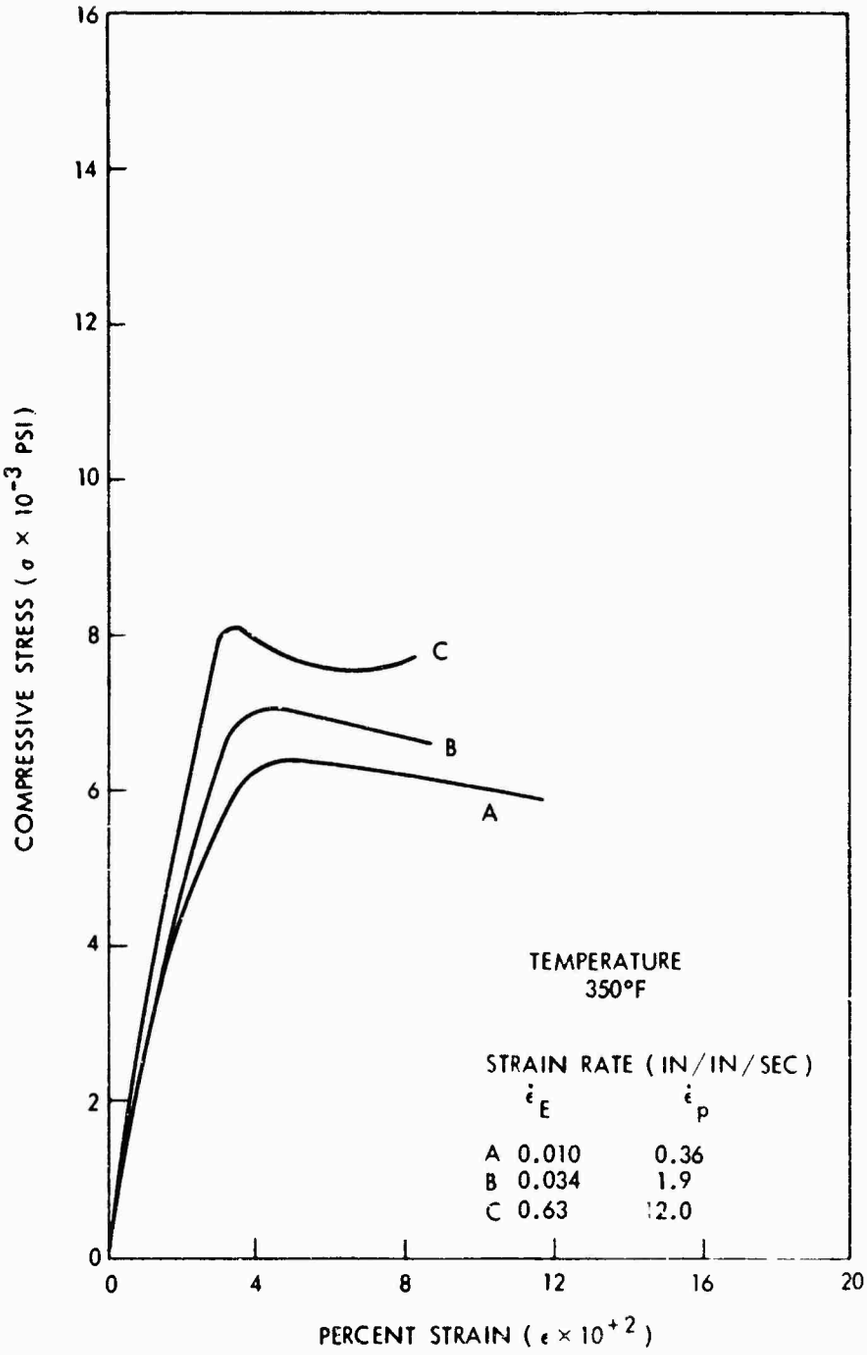

FIG. 34-c DYNAMIC STRESS-STRAIN RELATION OF PPO

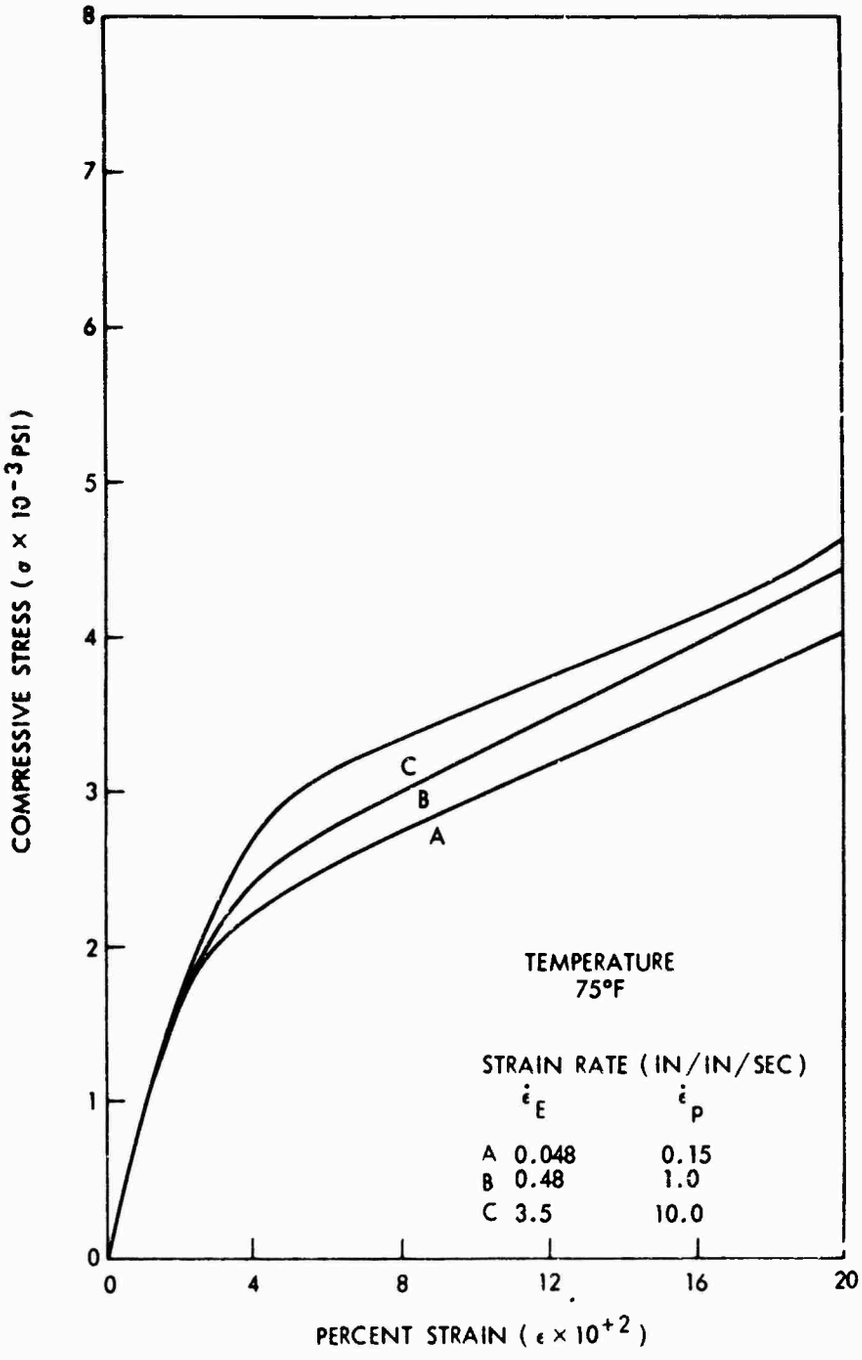

FIG. 35-a DYNAMIC STRESS-STRAIN RELATION OF TEFLON FEP100

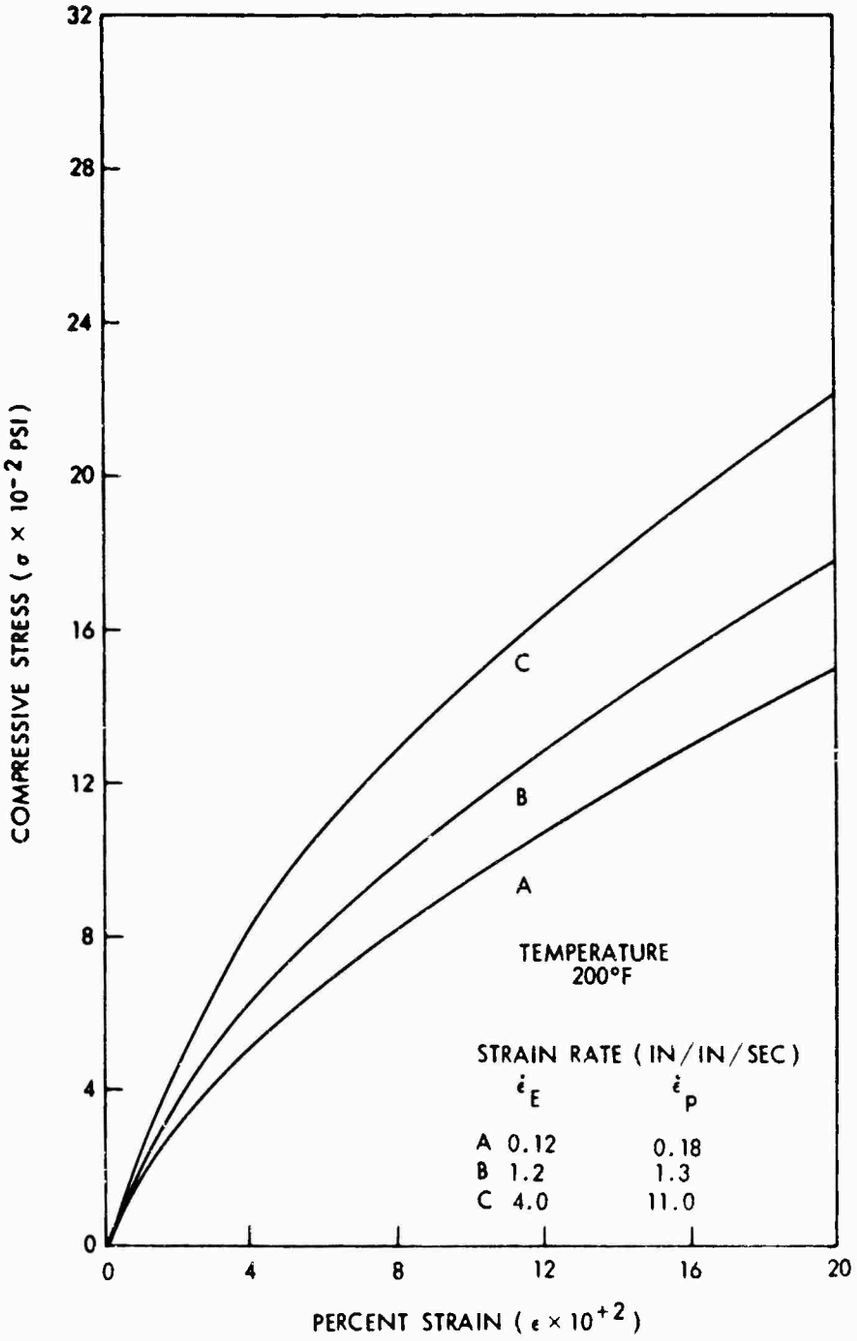

FIG. 35-b DYNAMIC STRESS-STRAIN RELATION OF TEFLON FEP100

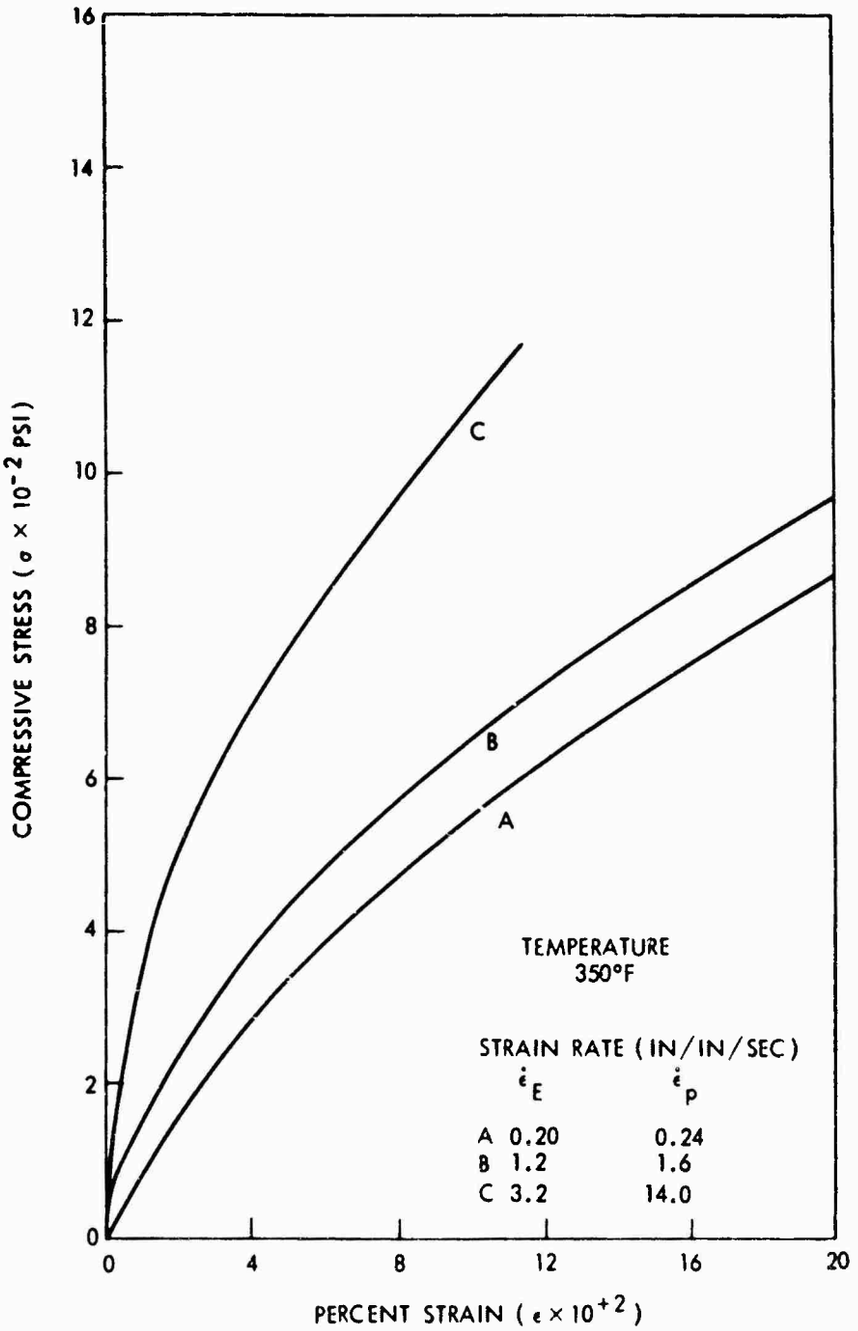

FIG. 35-c DYNAMIC STRESS-STRAIN RELATION OF TEFLON FEP100

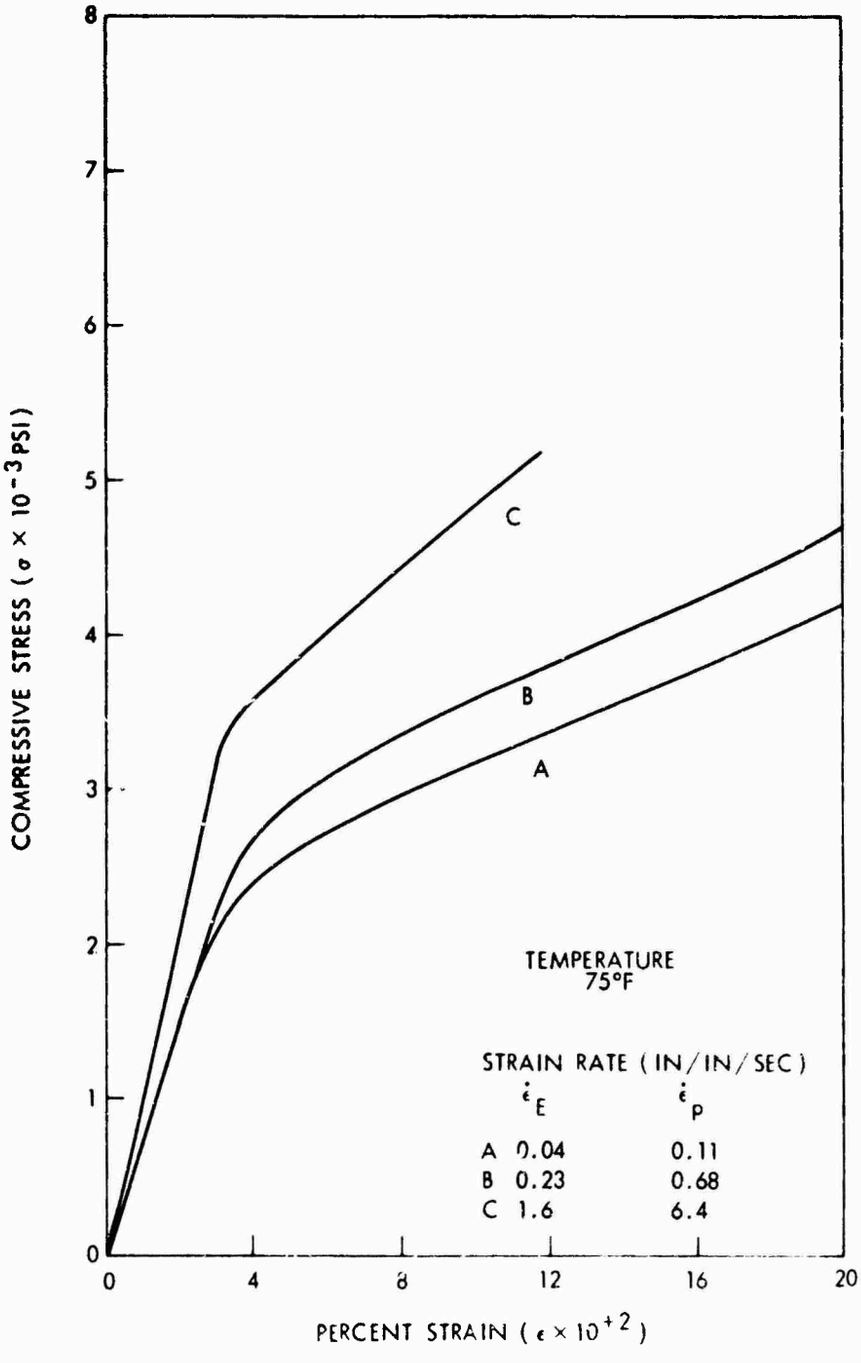

FIG. 36-a DYNAMIC STRESS-STRAIN RELATION OF TEFLON-TFE

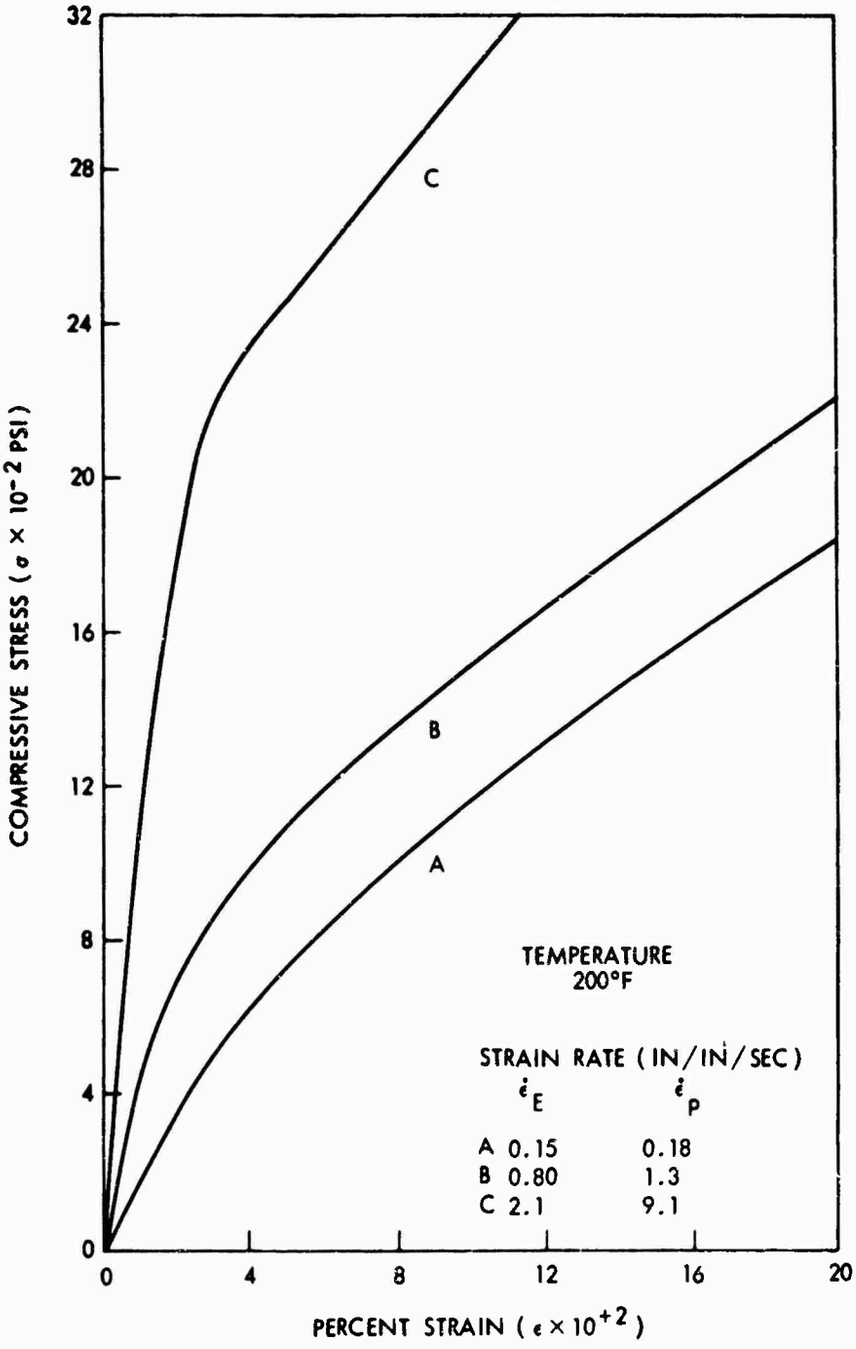

FIG. 36-b DYNAMIC STRESS-STRAIN RELATION OF TEFLON-TFE

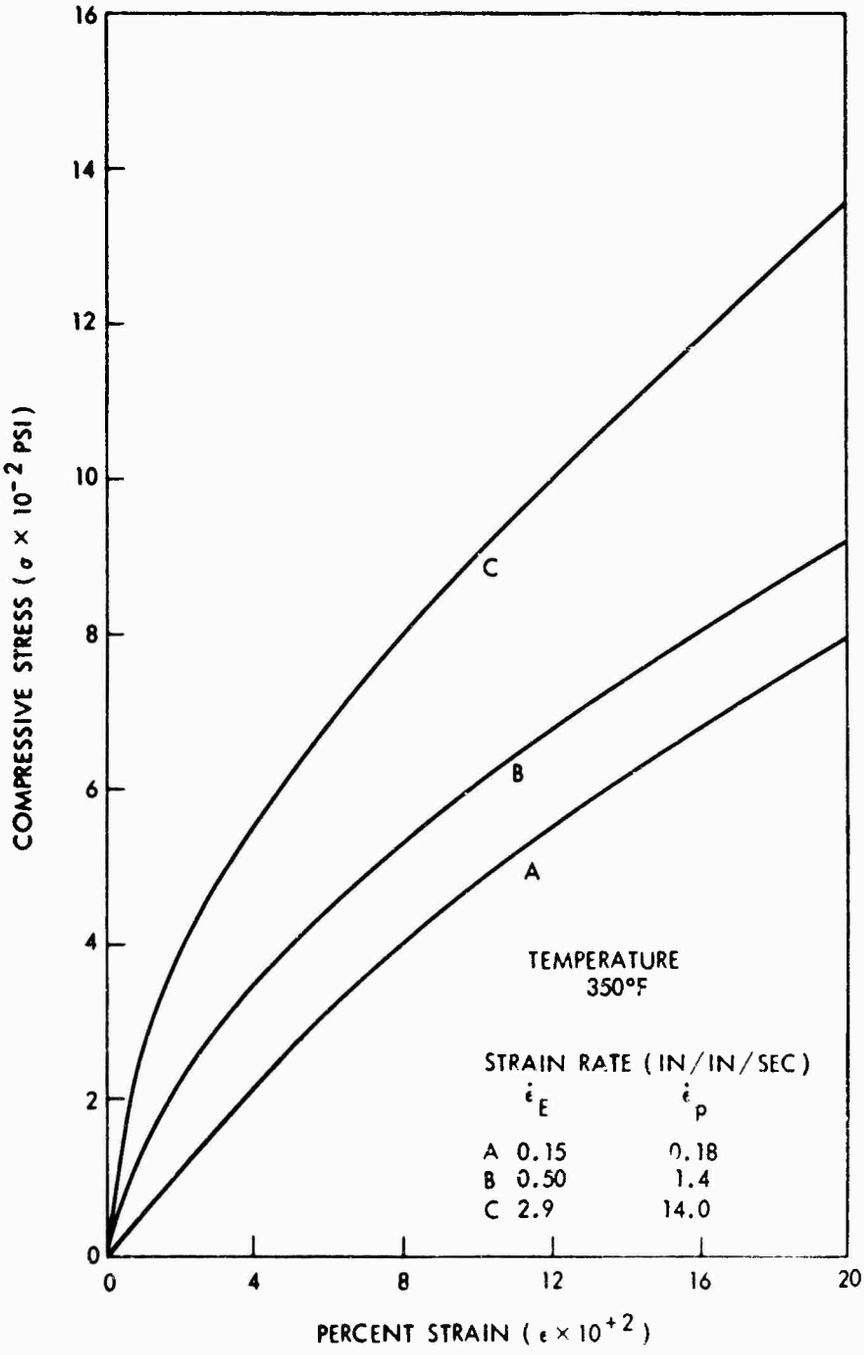

FIG. 36-c DYNAMIC STRESS-STRAIN RELATION OF TEFLON-TFE

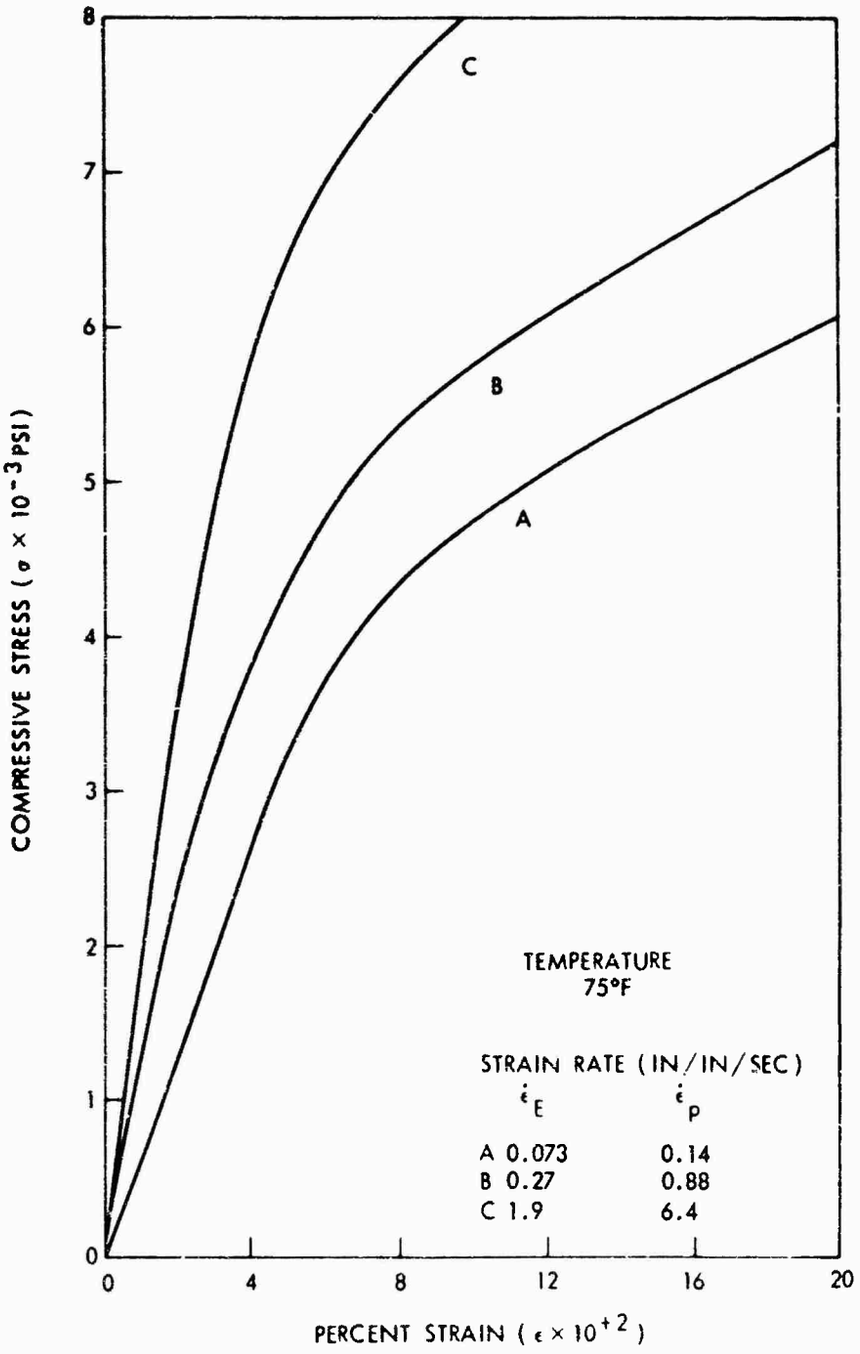

FIG. 37-a DYNAMIC STRESS-STRAIN RELATION OF ADIPRENE L-315

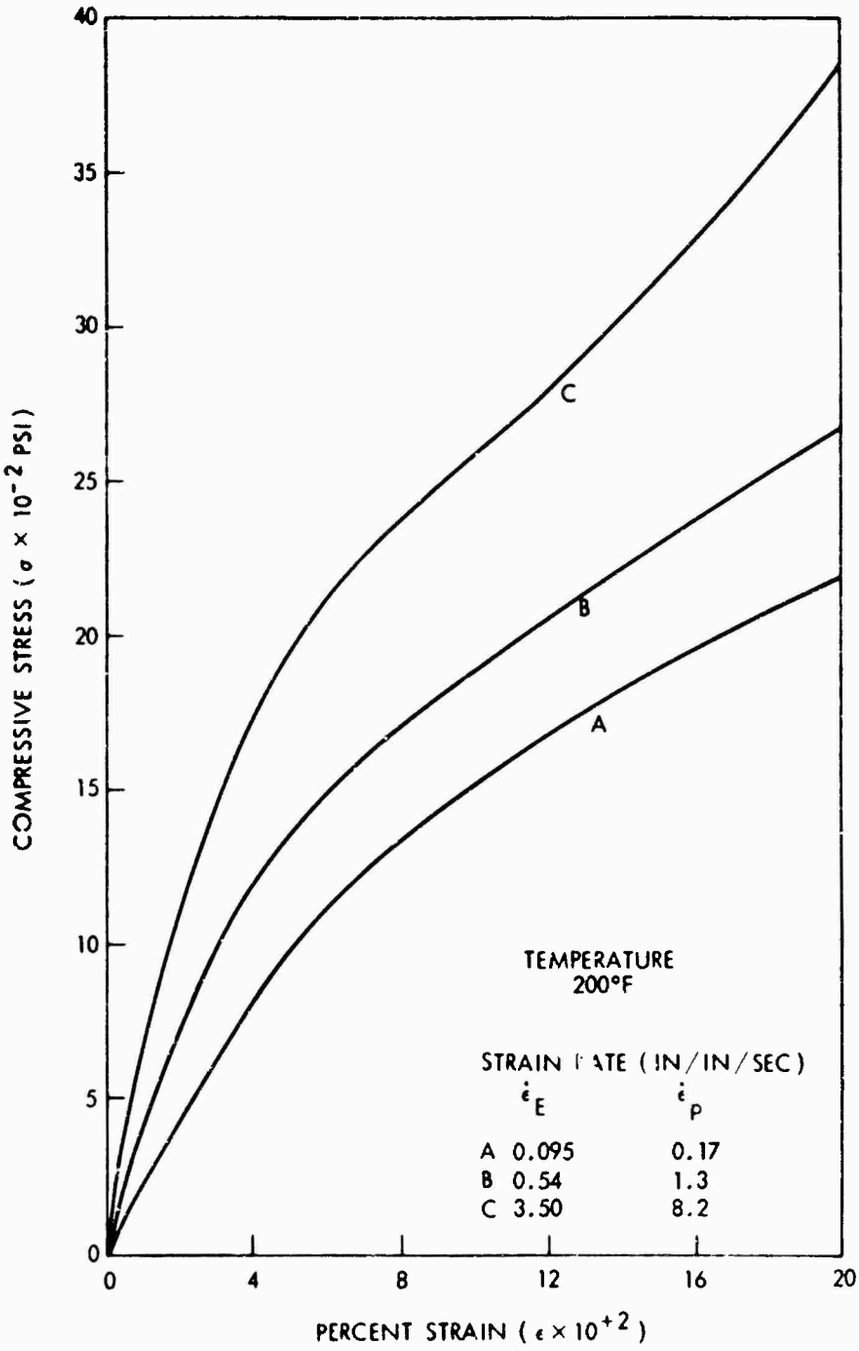

FIG. 37-b DYNAMIC STRESS-STRAIN RELATION OF ADIPRENE L-315

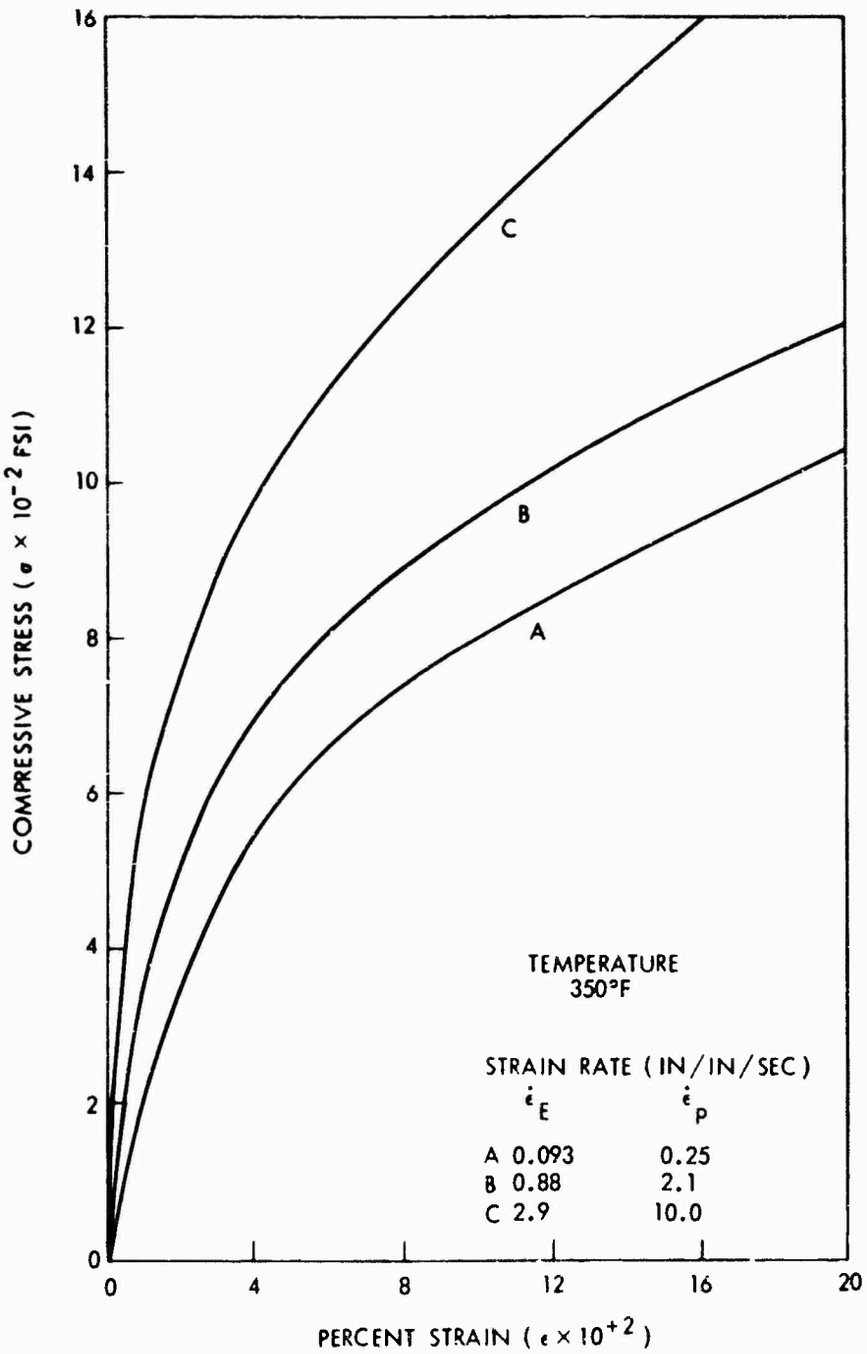

FIG. 37-c DYNAMIC STRESS-STRAIN RELATION OF ADIPRENE L-315

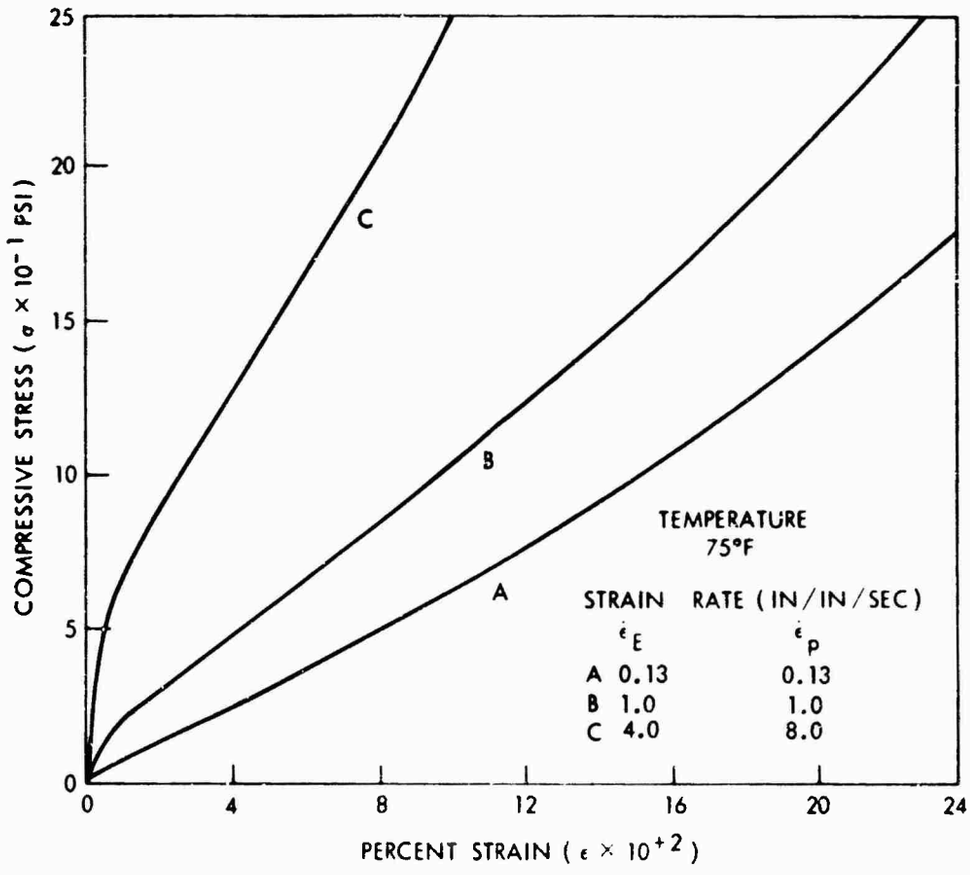

FIG. 38 - a DYNAMIC STRESS - STRAIN RELATION OF CONATHANE 2000

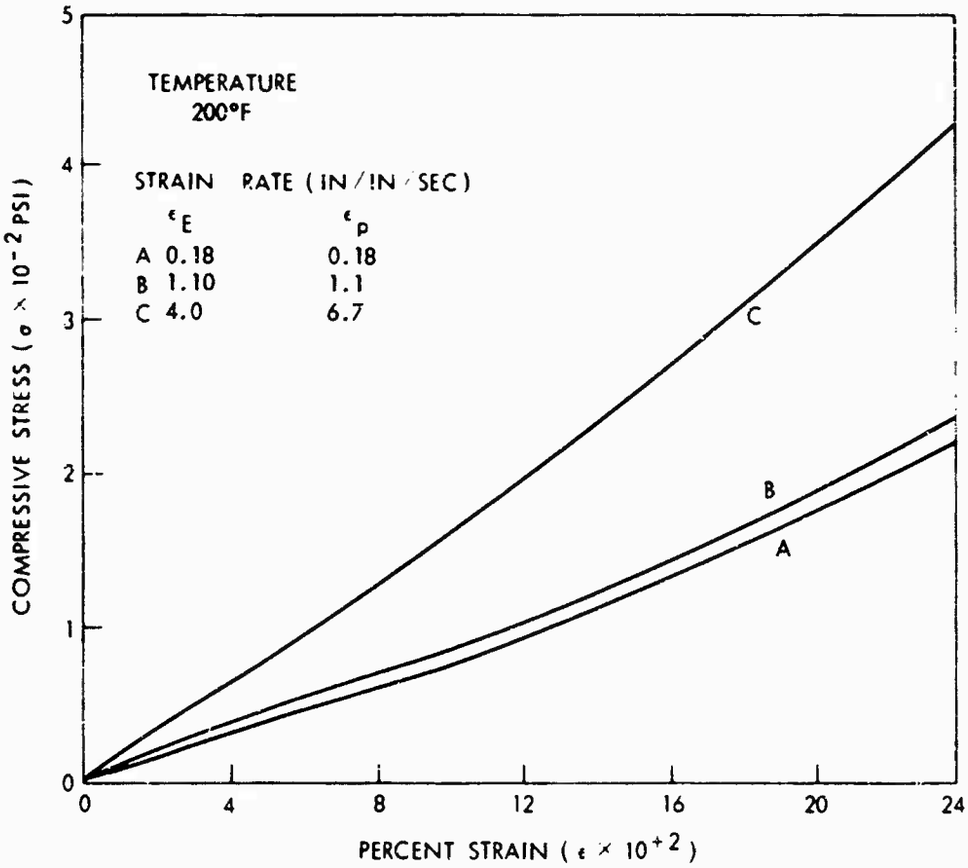

FIG. 38-b DYNAMIC STRESS-STRAIN RELATION OF CONATHANE 2000

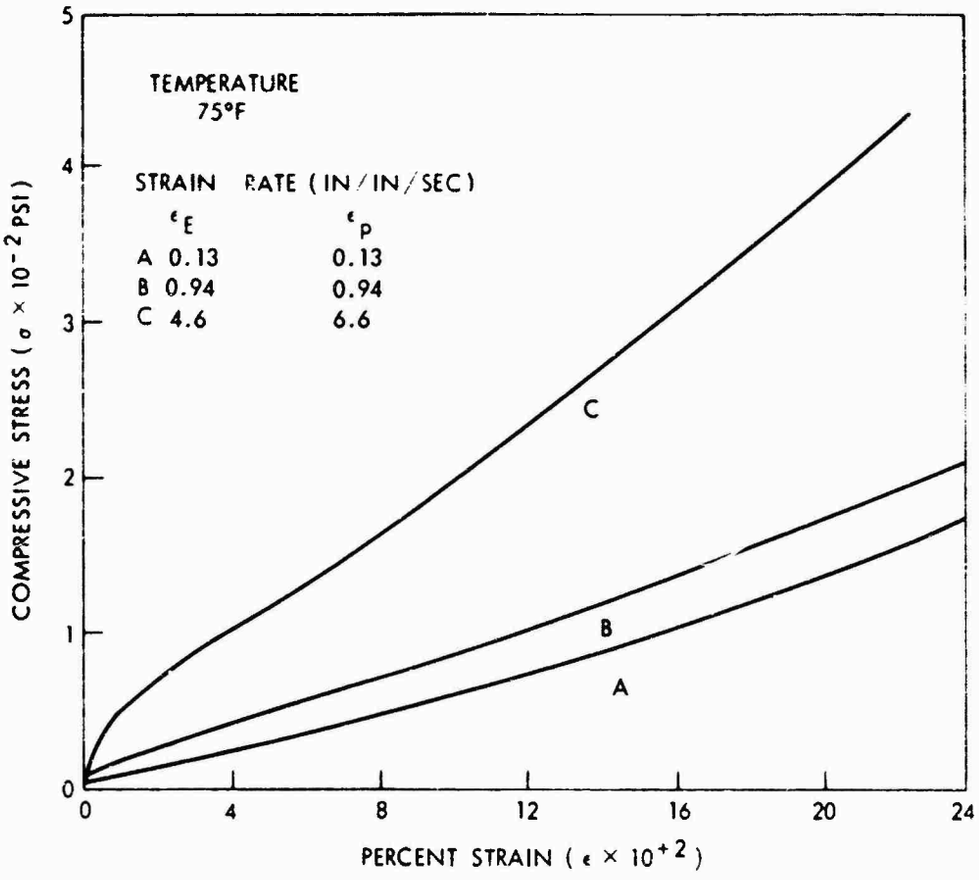

FIG. 39-a DYNAMIC STRESS-STRAIN RELATION OF SCOTCHCAST 221

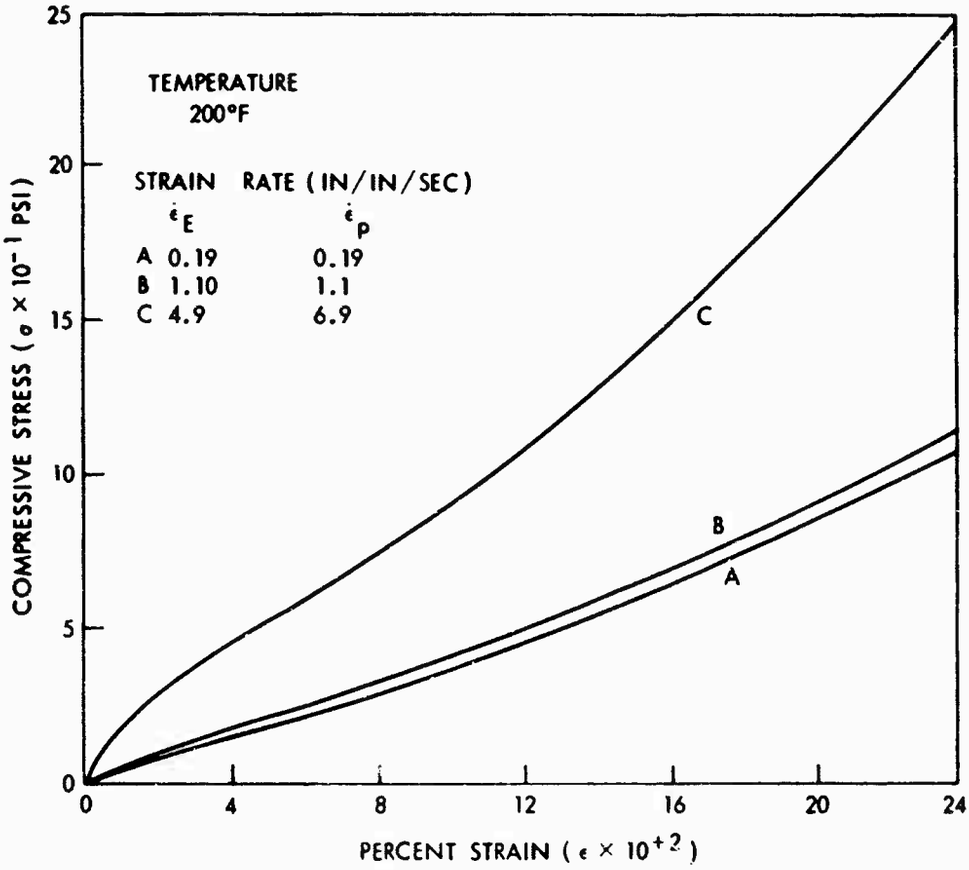

FIG. 39-b DYNAMIC STRESS-STRAIN RELATION OF SCOTCHCAST 221

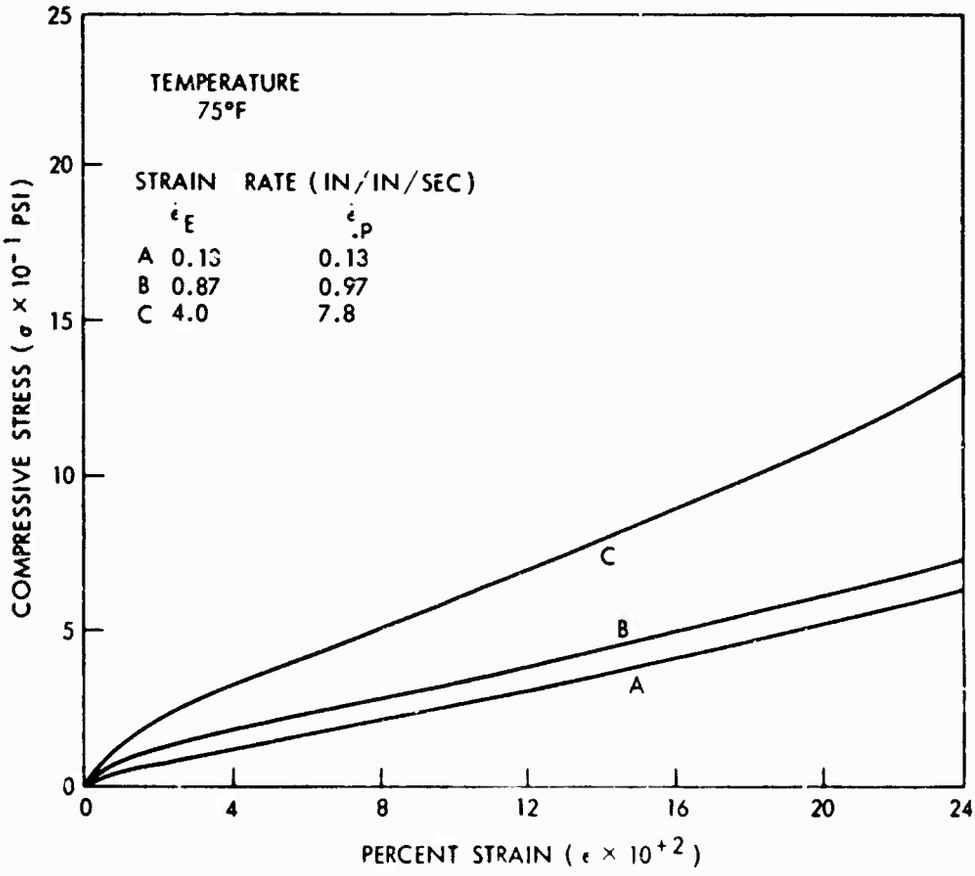

FIG. 40-a DYNAMIC STRESS-STRAIN RELATION OF SYLGARD 187

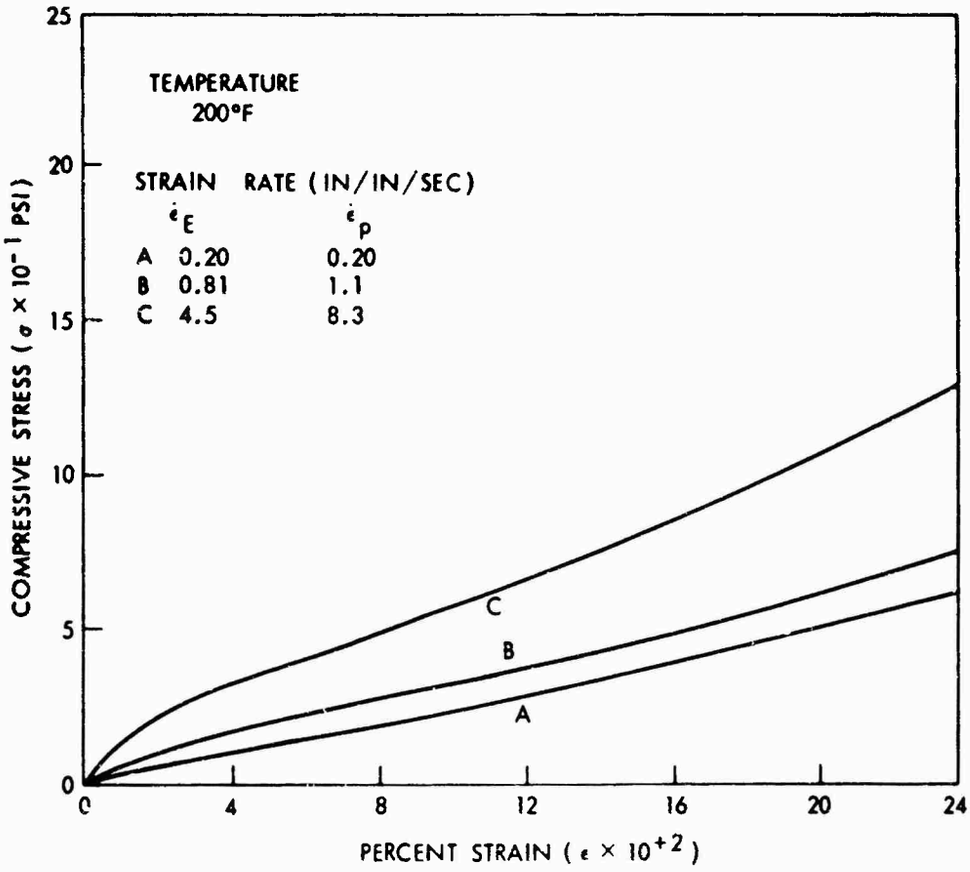

FIG 40-b DYNAMIC STRESS-STRAIN RELATION OF SYLGARD 187

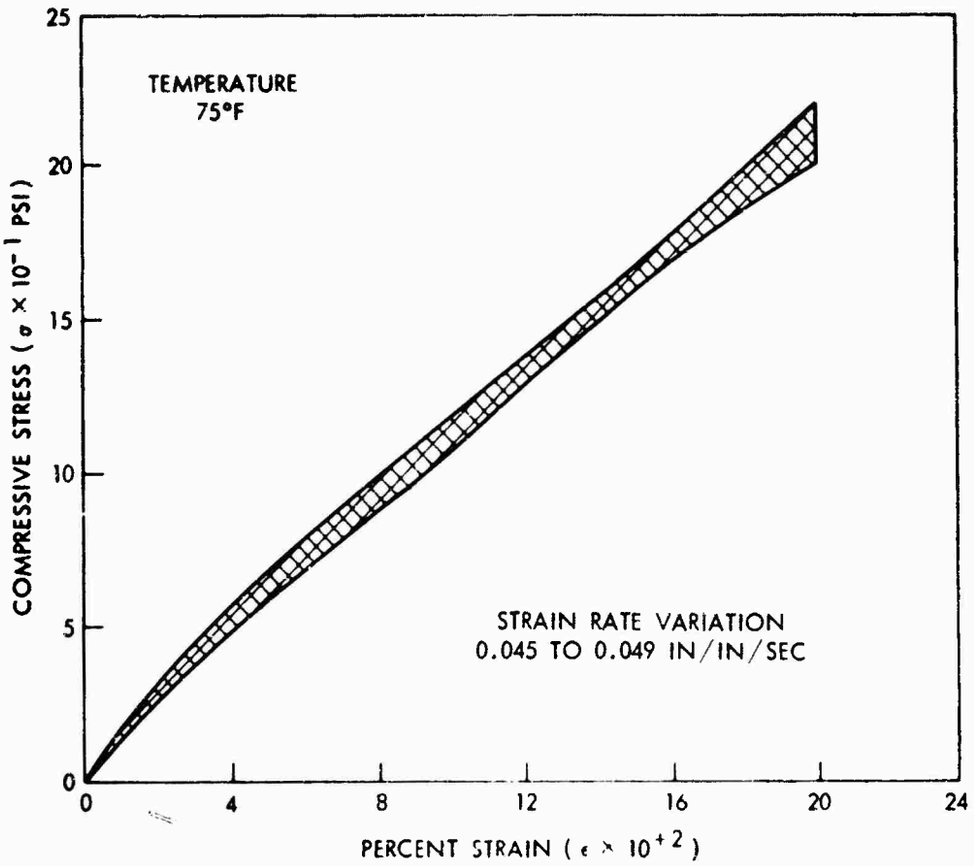

FIG. 41 VARIATION OF SIX STRESS-STRAIN CURVES FOR RUBBER COMPOSITION WS-2822

APPENDIX A

FREQUENCY ANALYSIS

The frequency response of the load cell system with the compression specimen was determined both theoretically and experimentally. The load cell system included the upper ball joint, the load cell, the thermal isolator, the compression cage, the lower ball joint, the platen, the piston rod and the piston.

The frequency was measured experimentally with an accelerometer, a variable band width filter and an oscilloscope with a polaroid camera. A specimen was placed in the compression cage and a constant load was applied to it. Next, the loaded system was excited. The harmonics were then filtered out and the fundamental frequency was recorded. The frequency response was determined for two cases, (1) with the thermal isolator and (2) without the thermal isolator. The frequency with the thermal isolator was 475 Hertz and without the thermal isolator was 500 Hertz. Evidently, removing the thermal isolator had little effect on the frequency response.

The theoretical analysis indicated that the load cell system and specimen could be considered as two series springs and one mass. The stiffnesses of the springs were the effective stiffness of the system and the stiffness of the specimen. The mass was the total of the system and the specimen.

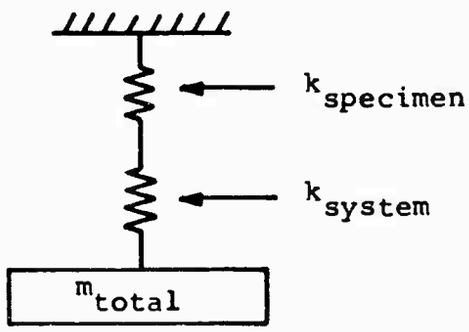

The system was divided into 37 springs and masses in series. The effective stiffness of the system with the thermal isolator was 11.8×10^4 lbs/in and without the thermal isolator was 17.2×10^4 lbs/in. The stiffness of the specimen used in the experimental determination was 7.35×10^4 lbs/in. The combined stiffness with thermal isolator was 4.4×10^4 lbs/in and without the thermal isolator was 5.1×10^4 lbs/in. The weight of the system was 13.8 pounds. The calculated fundamental frequency was 292 Hertz and 310 Hertz for cases 1 and 2, respectively. The specimen stiffness had a controlling effect on the frequency response, since it was less than the effective stiffness of the system. In fact, if the system were completely rigid and the weight remained at 13.8 pounds, then the frequency would be improved to 442 Hertz. Thus, any appreciable increase in the frequency response can only be accomplished by an appreciable decrease in the weight of the system which is not practical.

APPENDIX B

REFERENCES

1. Rand, J. L., and Hinckley, W. M., "Dynamic Compression Testing of Shock Mitigating Materials," NOLTR 66-39, Jan 1966

UNCLASSIFIED

DOCUMENT CONTROL DATA - R & D

U. S. Naval Ordnance Laboratory	UNCLASSIFIED --

MEDIUM STRAIN RATE, COMPRESSION TESTING OF SELECTED PLASTIC MATERIALS

William M. Hinckley
Frederick P. Stecher

23 December 1967	13	1

	NOLTR 67-173

Distribution of this document is unlimited.

Stress-strain relations have been obtained in compression at medium strain rates for selected plastic materials suitable for shock mitigation. Data have been acquired at room temperature, and at 200° F and 350° F for those materials capable of withstanding the elevated temperatures. Rates of strain between 0.004 in/in/sec and 60 in/in/sec have been obtained using a conventional high-speed testing machine. Most of the materials investigated have exhibited strain rate sensitivity over the range tested.

DD FORM 1473

UNCLASSIFIED

KEY WORDS	LINK A		LINK B		LINK C	
	ROLE	WT	ROLE	WT	ROLE	WT
stress						
strain						
testing						
medium strain rate						
compression						
temperature						
polymer						
resins						
rubber						
thermoplastics						
elastic						
plastic						